Response: We thank the two reviewers for the thoughtful suggestions and constructive criticism that have helped us to continue to improve our manuscript. Below we provide responses to referee comments and suggestions in blue font. All changes to the manuscript can be identified in the latest version submitted as well as in the marked-up manuscript at the end of this document.

Referee Comment: "An Aerosol Climatology via Remote Sensing over Metro Manila, Philippines"
Anonymous Referee #1
April 25, 2023

General Comments:

"Climatology" is generally referred to data over at least 30 years. In this study, the Authors present far fewer years, and these data are therefore considered long-term averages. The title needs to be changed. For example, it could be changed to "An Emerging Aerosol Climatology…" as inspired by Holben et al 2001. The Authors present a comprehensive analysis using several different aerosol and meteorological data sets to determine aerosol source partitioning over the Manila metropolitan region. The manuscript uses results from five clustered AERONET aerosol volume size distributions tied to MERRA-2 speciated AOD to determine the type of aerosol particles over the Manila region. At times, it is not clear how MERRA-2 data are being matched to AERONET data. As expected, Manila is dominated by coarse mode sea salt with fine mode pollution and sometimes cloud processed aerosols. Manila is impacted episodically by other aerosol sources such as smoke and pollution from other transboundary sources.

Overall, the manuscript is written and organized well; however, the data use and explanations resulted in several questions which are described below and may result in modifications to the data analysis. The questions below need to be clarified and changes supported by citations before publication.

Response: We thank the reviewer for this summarized perspective. As detailed below, we took actions to remedy some of these concerns. For instance, we did revise the title to now be "An Emerging Aerosol Climatology via Remote Sensing over Metro Manila, Philippines"

Detailed Comments:

Lines 24 and 25: Please combine these two sentences for a more complete statement. For example, "Aerosol particles…are challenging to characterize" due to "the diverse…"

Response: The two sentences have been combined: "Aerosol particles in Southeast Asia are challenging to characterize due to their complex life cycle within the diverse topography and weather in the region."

Line 26: Is it a climatology by definition? It seems more appropriate to name it a "long-term average" or perhaps "emerging climatology" as coined by Holben et al., 2001.

Response: The technical definition of climatology involves thirty years of data. The lack of long-term aerosol data does not make this possible yet for Metro Manila. However, some authors have

used the word climatology to describe analysis of data from 10 (Gui et al., 2022; Banerjee et al., 2021) to 20 years (Kinne, 2019). Others have referred to ten-year data analysis as "decadal climatology" (Tandule et al., 2020). To avoid confusion about the terminology, the word "emerging" was inserted before climatology.

Lines 27 to 30: These sentences should be combined and revised to produce a more complete statement.

Response: The sentences have been combined, and the timeframe of the high AOD values now include the months until October: "Aerosol optical depth (AOD) values were highest from August to October, partly from fine urban aerosol particles, including soot, coinciding with the burning season in Insular Southeast Asia when smoke is often transported to Metro Manila during the southwest monsoon."

Lines 30-37: MERRA-2 aerosol particle composition data are on the monthly basis (as discussed in Section 2.1.2) rather than determined for the nearest time to the AERONET size distribution retrieval in which the size distributions could change significantly in aerosol urban and transported plumes.   What is the difference between "fine polluted," "mixed polluted," "urban/industrial," and "cloud processed" since they are all in the fine mode.

Response: Hourly AOD data (M2T1NXAER) were used for comparison to the nearest AERONET volume size distribution data. The information in Section 2.1.2 (end of paragraph 1) was updated to include this dataset information: "; and M2T1NXAER Aerosol Diagnostics (1-hourly from 00:30 UTC time-averaged) for Total AOD and speciated AOD (Sulfate, Black Carbon (BC), Organic Carbon (OC), Dust, and Sea Salt)." Table 1 was likewise updated.

Fine polluted is the more general terminology. The first four mentioned air mass types in Table 2 are the most general (based on size fraction and clean or polluted conditions). More specific classifications based on aerosol particle sources are included after those four general ones. The urban/industrial air mass type here refers to local combustion along with long-range transported biomass burning. The terminology mixed/polluted has been dropped and replaced by a potential dust source (mixed dust). The cloud processed air mass is a more specific type of fine polluted air mass which has an accumulation mode peak that's slightly larger. This information has been added to the abstract, as shown here: "The following are the other particle sources over Metro Manila: fine polluted (20%), mixed dust (12%), urban/industrial (5%), and cloud processing (5%)."

Lines 114-116: Schuster reference is not very appropriate here. More appropriate is Dubovik and King, 2000, Dubovik et al. 2000, Dubovik et al. 2002, and Dubovik et al., 2006.

Response: The following references were used instead: (Dubovik and King, 2000; Dubovik et al., 2000; Dubovik et al., 2002; Dubovik et al., 2006).

Lines 132-151: Why not use the hourly MERRA-2 product (M2T1NXAER) to match up with AERONET?

Response: Yes, the hourly product (M2T1NXAER) was actually used, and it was just not indicated in the methodology previously. This information now has been included in this section: "; and M2T1NXAER Aerosol Diagnostics (1-hourly from 00:30 UTC time-averaged) for Total AOD and speciated AOD (Sulfate, Black Carbon (BC), Organic Carbon (OC), Dust, and Sea Salt)." Table 1 was also updated as shown below.

Parameter	Data Source	Spatial Coverage	Time Coverage
Aerosol Optical Depth (500 nm)	AERONET	14.635°N, 121.078°E	Jan 2009 - Oct 2018
Asymmetry Factor (440 nm - 1020 nm)	AERONET	14.635°N, 121.078°E	Jan 2009 - Oct 2018
Extinction Angstrom Exponent (440 nm -870 nm)	AERONET	14.635°N, 121.078°E	Jan 2009 - Oct 2018
Fine Mode Fraction	AERONET	14.635°N, 121.078°E	Jan 2009 - Oct 2018
Precipitable Water	AERONET	14.635°N, 121.078°E	Jan 2009 - Oct 2018
Single Scattering Albedo (440 nm - 1020 nm)	AERONET	14.635°N, 121.078°E	Jan 2009 - Oct 2018
Refractive Index (Real and Imaginary; 440 nm - 1020 nm)	AERONET	14.635°N, 121.078°E	Jan 2009 - Oct 2018
Volume Size Distribution	AERONET	14.635°N, 121.078°E	Jan 2009 - Oct 2018
Low Cloud Fraction (MODIS)	MERRA-2	14.3°N - 14.8°N, 120.75°E - 121.25°E	Jan 2009 - Dec 2018
Planetary Boundary Layer Height	MERRA-2	14.3°N - 14.8°N, 120.75°E - 121.25°E	Jan 2009 - Dec 2018
Relative Humidity (975 mb)	MERRA-2	14.3°N - 14.8°N, 120.75°E - 121.25°E	Jan 2009 - Dec 2018
Sea Level Pressure	MERRA-2	14.3°N - 14.8°N, 120.75°E - 121.25°E	Jan 2009 - Dec 2018
Temperature (975 mb)	MERRA-2	14.3°N - 14.8°N, 120.75°E - 121.25°E	Jan 2009 - Dec 2018
Wind (975 mb)	MERRA-2	14.3°N - 14.8°N, 120.75°E - 121.25°E	Jan 2009 - Dec 2018
Total Extinction Aerosol Optical Depth (550 nm)	MERRA-2	14.3°N - 14.8°N, 120.75°E - 121.25°E	Jan 2009 - Dec 2018
Sulfate, Black Carbon, Organic Carbon, Dust, and Sea Salt Extinction Aerosol Optical Depth (550 nm)	MERRA-2	14.3°N - 14.8°N, 120.75°E - 121.25°E	Jan 2009 - Dec 2018
Precipitation	PERSIANN	14.3°N - 14.8°N, 120.75°E - 121.25°E	Jan 2009 - Dec 2018

Line 152-161: It is important to state here that MISR retrievals are much fewer than other LEO and GEO sensors. How well do the monthly AOD averages from MISR represent the conditions over the Philippines in such a meteorological diverse environment?

Response: The large fraction of cirrus clouds overlapping with lower clouds, dominantly shallow cumuli, is significant in the CAMP^{2}Ex domain (Hong and Di Girolamo, 2020). This significantly impacts the number of Level 2 aerosol retrievals, not only for MISR, but all passive instruments, but more so for MISR because of its narrower swath. The sampling error is of course reduced by first computing monthly mean for individual 0.5° grid cells over 10 years of MISR data, followed by taking the mean over the 30°x30° region used here. This reduces the standard error in the mean AOD used in Figure 4 to values smaller than 0.002 for any month, which we now note in the text description. There is also the issue of representativeness of passive retrievals, such as MISR, MODIS, and VIIRS, as these are from clear sky only. This issue was directly addressed in Hong and Di Girolamo ((Hong and Di Girolamo, 2022)), where they used CALIPSO data to show that clear sky aerosol climatologies from passive sensors are also representative of all sky climatological conditions. The manuscript was edited also as noted

below to include notes on clear sky climatologies, clouds in the region, and MISR AOD as discussed.

1: "The overlapping of large fraction of cirrus clouds with lower clouds in the area (Hong and Di Girolamo, 2020) makes space-borne remote sensing of aerosol particles very challenging (Reid et al., 2013; Lin et al., 2014)."

2.1.1: "The AERONET observations were made during clear sky conditions, which has been shown (Hong and Di Girolamo, 2022) to be able to represent all sky conditions."

2.1.4: "Monthly 500 nm AOD data (Level 3 Global Aerosol: $0.5° \times 0.5°$ spatial resolution) from 2009 to 2018 are used from the Multi-angle Imaging SpectroRadiometer (MISR), (Diner et al., 2007; Garay et al., 2018) as regional (Southeast Asia) baseline remote sensing data to support the Manila Observatory AERONET data. The regional MISR data was used to confirm regional sources of aerosols that may be influencing the AOD over Metro Manila."

2.1.4: "Monthly mean AOD values were then calculated for each $0.5°$ grid point and then for the $30° \times 30°$ region, where the standard error in the monthly mean for the region is less than 0.002."

Lines 170-177: How were the NAAPS data products used? Where they used quantitatively or qualitatively?

Response: The maps of AOD and Surface Aerosol Concentrations for Southeast Asia were used qualitatively. This information is now more clearly indicated in the text (first paragraph of 2.1.5): "Archived maps of total and speciated optical depths and surface concentrations of sulfate, dust, and smoke for Southeast Asia are used from the Navy Aerosol Analysis and Prediction System (NAAPS: $1° \times 1°$ spatial resolution) (Lynch et al., 2016), and which are publicly available at https://www.nrlmry.navy.mil/aerosol/."

An additional sentence was added to the end of the section: "These maps help associate possible regional emission sources to extreme aerosol loading events in Manila Observatory."

Lines 178-181: Later discussion indicates use of other Worldview products. Please specify all products or images used.

Response: MODIS (Aqua and Terra) maps over Metro Manila and Southeast Asia were downloaded from Worldview. This information has been updated in the text." Archived maps of cloud fraction (Aqua MODIS and Terra MODIS) over Metro Manila and Southeast Asia were downloaded from NASA Worldview (*https://worldview.earthdata.nasa.gov)* for events of interest based on AERONET data."

Lines 184-185: The AERONET VSD is retrieved for discrete particle sizes and do not represent "bins" as mentioned here.

Response: The word "bins" has been changed to "discrete points". This is from 3.1 in https://aeronet.gsfc.nasa.gov/new_web/Documents/Inversion_products_for_V3.pdf.

Lines 193-194: The dust category can include mixed aerosols as well as dust. Lower FMF (<0.4 or <0.3) is more appropriate. Also, the desert dust AOD may not retain high aerosol loading over 1000s of kms. What wavelength is used for AOD, AE, and FMF in the table? For example, the dust case identified over Manila for March 24-25, 2018, does not reach 0.3 at Level 2.0 AOD 500nm. Which FMF wavelength is used? Please state in the caption. Overall, these threshold values for AOD, AE, and FMF are only estimates as they are not rigorous cutoffs for these air mass types and this should be discussed in the text referencing Table 2.

Response: This is true about the dust category being mixed with other aerosols, in the manuscript the air mass is renamed to mixed dust. The FMF values in Table 2 for the specific categories (clean marine, urban/industrial, biomass burning, and dust) were removed and the angstrom exponent values from literature (Kaskaoutis et al., 2009) were used. The wavelengths in Table 2 were indicated for those which had information about them, for example other studies just indicated the source of the data (MODIS).

The note about the lower AOD loading due to distance from the source has been added to the text in 3.4.2. "The AOD from both AERONET and MERRA-2 (Fig. 10b) are lower than 0.3 (the AOD threshold for dust in other studies, Table 2) because of the long distance from the source (thousands of kilometers)."

The text has been updated to indicate that these threshold values are estimates and that they can help in understanding aerosol sources as well as identify extreme cases. "The first four mentioned air mass types in Table 2 are the most general, four more classifications based on aerosol particle sources are included. The urban/industrial air mass type here refers to local combustion along with long-range transported biomass burning (Kaskaoutis et al., 2009). While these classifications are not rigid definitions of air masses, they help in understanding the sources that contribute to aerosols in Metro Manila and in identifying cases where certain sources are more influential than others."

Lines 214-219: When was the dust case identified? NAAPS itself is a model so how can it "confirm" the existence of dust over Manila? Also, HYSPLIT uses reanalysis data and it too depends on a model and a number of assumptions in which is provides a possible transport pathway for aerosols. Do you have surface based measurements confirming the dust reached Manila?

Response: The date for this case is 24 March 2018. The VSD for this case had a more dominant coarse contribution, which is the main reason for associating this as a dust case. We agree that these other sources of information (NAAPS and HYSPLIT) are not a ground truth to confirm the presence of an aerosol feature and are just supportive at most. In the first case study (Sect 2.3.1) we modified the text to be softer (changed "identify" to "provide support for" to reflect this reviewer comment: "were used to **provide support for** the likely source and transport pathway for the smoke cases".

Lines 224-225: How were the NASA Worldview images used for verification? For example, NASA Worldview provides many products. Authors, need to use caution and understand the

uncertainties related to MERRA-2 in regards to data assimilation, modeling, and determination of aerosol species. The MERRA-2 data set should not be treated as a measurement.

Response: The sentence was improved to state more clearly that it was MODIS and not MERRA-2 that was used to "verify" clouds: "The presence of clouds was verified qualitatively with MODIS (Aqua and Terra) imagery from NASA Worldview in the path of air parcels reaching Metro Manila based on HYSPLIT back-trajectories."

Lines 252-253: Where is the plot?

Response: The maps described here are in Figure 12 (b to d). The sentence was edited. "From the linear regression equation, the regression coefficient per grid was calculated. Each grid on the Southeast Asia map was colored based on the calculated regression coefficient value."

Line 278-279: AERONET data at Manila are considerably under-sampled during the months during the Summer Southwest Monsoon between May and October. For example, some years during this period, very few data were collected (e.g., 2013) due to the weather and the changing of the instrument. State in the text or in the figure the total number of observations used for each monthly average.

Response: The following was inserted into the main text: "(from available AERONET data of 513 points in August, 4015 points in February, and 5049 points in March)". The counts per month were also inserted into the figure caption. "(h) precipitable water (data counts per month Jan: 2131, Feb: 4015, Mar: 5049, Apr: 5844, May: 3448, Jun: 1696, Jul: 652, Aug: 513, Sep: 753, Oct: 1700, Nov: 2084, Dec: 1449);"

Line 284-288: Which level are temperature, relative humidity? It should be indicated that low-cloud fraction is from MERRA-2 with cloud top pressure > 680hPa. How is the distinction made between precipitating and non-precipitating clouds? It is very likely aerosols are washed out in precipitating clouds so partitioning by precipitating and non-precipitating clouds is important in the cloud processing assessment. Also, the cloud processing is difficult to determine monthly as these processes occur on the sub day temporal grid.

Response: Both temperature and relative humidity values are for 975 mb. This value has been indicated in the results text and the figure caption. "(a) temperature at 975 mb, (b) relative humidity at 975 mb,"

The text "(cloud top pressure > 680 hPa)" was inserted in the figure caption. There is no distinction made between precipitating and non-precipitating clouds in this study, however.

For this study we identified possible cloud processing for one date based on the AERONET volume size distribution and MERRA-2 data.

Line 308: What are the values in the legend and why is the scale so small (i.e., 10^-7)?

Response: The values in the legend are the density value contributions to calculated cumulative probability distribution surfaces, where the red areas have the greatest number of trajectories within a 100 km radius. The text of the caption was edited as follows. The legend was not included to avoid confusion.

"Density plots of HYSPLIT trajectories reaching Manila Observatory per month from 2009 to 2018. Red denotes areas with the greatest number of back trajectories within a 100 km radius. The colors represent density value contributions to Matlab-calculated cumulative probability distribution surfaces (100 km radius) from coordinates of three-day back trajectories of the specific months."

Line 334-342 (Figure 3): In Figure 3c, specify that these data are the SDA retrievals. What are the total number of observations and/or days for each monthly averages presented? The total number may explain some of the variations in the plots due to low sampling of AERONET data and quality controls. The Figures 3d and 3e are not clear on which data whisker plots refer to which wavelengths; please specify them on the plot. In Figure 3h, the blue line the ratio of RI between 440nm and 675nm but the red line is the ratio of RI between 440nm to the RI average of 670-1020nm. It seems either the wavelength should be 670nm or 675 consistently through the document.

Response: FMF has been specified as an SDA retrieval. "(c) spectral de-convolution algorithm (SDA) retrievals of fine mode fraction (FMF, 500nm)"

The total numbers per month have been indicated in the figure caption." Monthly characteristics of AERONET aerosol particle parameters: (a) aerosol optical depth (AOD, 500nm) with counts (Jan: 2107, Feb: 3931, Mar: 4923, Apr: 5755, May: 3389, Jun: 1653, Jul: 637, Aug: 483, Sep: 718, Oct: 1555, Nov: 2001, Dec: 1386) (b) extinction angstrom exponent (EAE, 440-870 nm) with counts (Jan: 102, Feb: 248, Mar: 312, Apr: 309, May: 137, Jun: 53, Jul: 14, Aug: 18, Sep: 18, Oct: 79, Nov: 77, Dec: 52), (c) spectral de-convolution algorithm (SDA) retrievals of fine mode fraction (FMF, 500nm) with the same counts as AOD, (d) single scattering albedo (SSA) from 440 nm (leftmost boxplot) to 1020 nm (rightmost boxplot) with counts (Jan: 6, Feb: 31, Mar: 62, Apr: 50, May: 29, Jun: 8, Aug: 3, Sep: 5, Oct: 17, Dec: 3), (e) asymmetry factor (AF) from 440 nm (leftmost boxplot) to 1020 nm (rightmost boxplot) with the same counts as EAE, (f) real and (g) imaginary refractive index (RI) values (440 nm) with the same counts as SSA,"

The wavelengths have been specified in the caption for Figures 3d and 3e as indicated in the text in the previous sentence.

The wavelength should be 675 nm in the caption for Figure 3h. This has been updated.

Line 350-351- MISR monthly averages are based on more limited data per month due to its orbit and measurement technique. Also, MISR over pass is in the afternoon so these data are biased to the afternoon clouds. Does MERRA-2 have the same constraint? Therefore, is MISR the appropriate instrument to compare monthly AOD? Why not use MODIS, VIIRS, or possibly Himawari AOD?

Response: The reviewer is incorrect: MISR is in a morning orbit (10:30 AM ECT descending branch), not an afternoon orbit. The morning orbit has a significant advantage over the afternoon orbit because cirrus coverage is at a minimum, thus allowing for more valid retrievals to occur. This, in part, is why we chose MISR. But there are other great reasons. MISR and MODIS AOD have extensive validation, more than any other passive AOD product. Unlike MODIS, MISR also includes an assessment of the impact of small cumulus (typical of the CAMP2Ex domain) contamination on aerosol retrievals, which was shown to have a negligible impact on MISR AOD and particle properties (Zhao et al., 2009). MISR also compares better with AERONET than MODIS, as cited in the original manuscript. MISR also provides particle size and particle shape segregated AOD, which no other passive sensor provides. As noted earlier, sampling noise for the large domain, 10-year monthly mean value is small relative to the seasonal signal that we are examining with the data. So, the choice to use MISR was logical. Not using other satellite data does not invalidate our use of MISR. The MERRA-2 reanalysis AOD product includes data assimilation from MODIS (Terra: 10:30 AM, Aqua: 1:30 PM), AVHRR (~ 1:30 AM, 9:30 AM, 1:30 PM, 9:30 PM), and MISR (10:30 AM) and are therefore constrained by these sensors. Studies in Asia (Xiao et al., 2009; Qi et al., 2013; Choi et al., 2019) show relatively higher MODIS AOD compared to MISR AOD and which could affect the MERRA-2 AOD. The subsection on MISR regional AOD was moved to 2.1.4 after all the datasets (i.e., MODIS is 2.1.2) that were used primarily for Metro Manila.

2.1.2: "The aerosol reanalysis data includes data assimilation of AOD from the Moderate Resolution Imaging Spectroradiometer (MODIS: Terra, 2000 to present and Aqua, 2002 to present), Advanced Very High Resolution Radiometer (AVHRR, 1979-2002), and Multiangle Imaging SpectroRadiometer (MISR, 2000-2014) (Buchard et al., 2017; Rizza et al., 2019)."

2.1.4: "Monthly 500 nm AOD data (Level 3 Global Aerosol: 0.5° × 0.5° spatial resolution) from 2009 to 2018 are used from the Multi-angle Imaging SpectroRadiometer (MISR), (Diner et al., 2007; Garay et al., 2018) as regional (Southeast Asia) baseline remote sensing data to support the Manila Observatory AERONET data. The regional MISR data was used to confirm regional sources of aerosols that may be influencing the AOD over Metro Manila. Level 3 MISR products are global maps of parameters available in Level 2 (measurements derived from the instrument data) products. MISR is ideal for remote sensing in the CAMP[2]Ex region because it has an overpass at 10:30 AM ECT (descending mode) (when cirrus is minimal) and its retrievals have been shown to be unimpacted by small cumulus (Zhao et al., 2009), which are typical in the region. MISR has relatively more accurate AOD and agrees better with AERONET data compared to other satellite products due to its multi-angle measurements (Choi et al., 2019; Kuttippurath and Raj, 2021). The MISR sampling noise is relatively small due to the large domain and seasonal averages that are considered in this study. MISR is also the only passive sensor that speciates aerosol particle size and shape. All these factors led to the choice of using regional MISR data to associate long-range sources influencing AERONET data in Manila Observatory."

3.2.1: "Regional AOD (550 nm) over the larger Southeast Asia domain from MISR and MERRA-2 (Fig. 4) had a similarly large peak around the same time beginning in September until October which, however, was second only in magnitude to a March peak, which is influenced by biomass burning in Peninsular Southeast Asia (PSEA) (Gautam et al., 2013; Hyer et al., 2013;

Dong and Fu, 2015; Wang et al., 2015; Yang et al., 2022). This is consistent with the peak in speciated AOD due to fine (radii <0.7 µm), spherical, and absorbing aerosols that were observed by MISR from March to April (Fig. S1)."

3.2.1: "This dip was also observed in the regional AOD data (MISR and MERRA-2, Fig. 4). This is most probably due to the decrease in the AOD contribution from fine (radii <0.7 µm) and spherical particles based on size speciated MISR AOD (Fig. S1). Larger and non-spherical particle contributions to AOD increase in November in the Southeast Asia region. The MERRA-2 AOD is relatively higher than the MISR AOD probably due to assimilation of MODIS data into MERRA-2. Studies in Asia (Xiao et al., 2009; Qi et al., 2013; Choi et al., 2019) have observed relatively higher MODIS AOD compared to MISR AOD."

3.2.2: "The high EAE over Manila Observatory from July to September is probably regional in nature based on the MISR data showing increased EAE with increased AOD from fine, spherical, and absorptive particles (Fig. S1) in Southeast Asia during the same months."

3.2.2" "The lowest EAE values (0.08) and thus the largest particles were observed in December, which again may be regional in nature with MISR EAE also lowest during this time with increased AOD from larger and non-spherical particles (Fig. S1)."

Line 360-362: "0 for particles as large as cloud drops" – the desert dust aerosols can also generate EAE near and below zero. This statement "except for when the coarse mode has a large impact on the angstrom exponent" is not clear and needs revision.

Response: A reference for desert dust and sea salt has been added. And the statement referred to in the second sentence of this comment has been removed. "The EAE is usually greater for smaller particles (> 2 for small particles, ~4 for very small particles that undergo Rayleigh scattering, < 1 for large particles like sea salt and dust, and 0 for particles as large as cloud drops) (Schuster et al., 2006; Bergstrom et al., 2007)."

Line 371: EAE values less than 0.8 EAE are less likely to be fine mode dominated and/or impacted by optically thin cirrus clouds (especially in the Southeast Asia/Philippines region).

Response: The text was edited to indicate that most of the EAE values were greater than 0.8. "Of the high loading cases (AOD >1), the EAE values were mostly greater than 0.8 indicating fine mode particles (Che et al., 2015)."

Lines 458-461: However, Sinyuk et al. 2020 (https://amt.copernicus.org/articles/13/3375/2020/) showed that the AERONET real part of the refractive index is correlated to the fine mode size distribution contribution which makes is a less robust parameter.

Response: The following text was included in the mentioned section. "For the case of the AERONET data, which include refractive index values that are insensitive to coarse particles (Sinyuk et al., 2020), the focus of the discussion will be for fine mode particles and may be limited when coarse particles are involved."

Line 465-466: The Authors have presented SSA at four wavelengths from AERONET and not just one. AERONET SSA is computed using the four standard wavelengths (440, 670, 870, 1020nm) (e.g., Dubovik and King, 2000, Dubovik, et al. 2002).

Response: Thanks for pointing this out. We revised the text to not make this incorrect connection between wavelengths and SSA: "For this study, we examine refractive index values at 440 nm wavelength."

Line 545 (Figure 5): Very interesting plot showing the variations of the size distributions from AERONET at Manila. Can you please provide the related VSD properties (effective radius, median radius, standard deviation, peak radius of volume concentration) for each mode (fine and coarse) in a table or plot in the manuscript or supplementary? Also, what is the average AOD and FMF related to each VSD?

Response: The VSD properties and AOD and FMF values were tabulated and added to the supplementary section. The table is shown below. The text was edited as well to refer to Table 1. "The fine mode median values peaked in the accumulation mode at 0.148 µm particle radius while the coarse mode median values peaked at 3.857 µm (Fig. 5a and Table S1). The median coarse mode amplitudes and volume concentrations were higher than the fine mode amplitudes and volume concentrations for most of the year (DJF, MAM, and SON, Fig. 5b and Table S1), except during the southwest monsoon (JJA) when the fine mode amplitude and volume concentration was higher."

Table S1: Median aerosol properties associated with the volume size distribution data for the total, fine, and coarse fractions. The volume concentration (C_v) has units of $\mu m^3 \ \mu m^{-2}$. The following parameters have units of µm: radius at peak volume concentration (r_{peak}), effective radius (r_{eff}), volume mean radius (r_v), and standard deviation (σ).

Time Frame	AOD	C_v	FMF	Fine AOD	Fine C_v	Fine r_{peak}	Fine r_{eff}	Fine r_v	Fine σ	Coarse AOD	Coarse C_v	Coarse r_{peak}	Coarse r_{eff}	Coarse r_v	Coarse σ
ALL	0.1674	0.0610	0.6514	0.1086	0.0220	0.1482	0.1450	0.1630	0.4890	0.0524	0.0360	3.8575	1.9690	2.6410	0.7330
DJF	0.1507	0.0590	0.6215	0.0907	0.0190	0.1482	0.1475	0.1640	0.4960	0.0557	0.0390	3.8575	2.0410	2.7300	0.7335
MAM	0.1791	0.0630	0.6774	0.1240	0.0235	0.1482	0.1430	0.1600	0.4820	0.0522	0.0360	3.8575	1.9435	2.5995	0.7330
JJA	0.1708	0.0520	0.7700	0.1400	0.0310	0.1482	0.1460	0.1670	0.5080	0.0360	0.0220	2.9400	2.1680	2.7520	0.6670
SON	0.1479	0.0575	0.5733	0.0869	0.0170	0.1482	0.1480	0.1665	0.5035	0.0570	0.0370	2.9400	1.9290	2.5640	0.7505

| AM | 0.1654 | 0.0600 | 0.6443 | 0.1067 | 0.0210 | 0.1482 | 0.1460 | 0.1640 | 0.4950 | 0.0518 | 0.0350 | 3.8575 | 1.9494 | 2.5925 | 0.7360 |
| PM | 0.1850 | 0.0575 | 0.6847 | 0.1264 | 0.0260 | 0.1482 | 0.1410 | 0.1550 | 0.4590 | 0.0555 | 0.0390 | 3.8575 | 2.2070 | 2.8850 | 0.7190 |

Lines 551-570: The discussion of the VSD peaks needs further clarification. For example, instead of "The average coarse mode peak (0.04 um3/um2) was the highest…," you could say, "The average coarse mode peak for the volume concentration (0.04 um3/um2) was the highest…" Several other sentences in this paragraph are similarly vague and should be revised.

Response: The words "volume concentration" were added whenever the VSD magnitude and peaks were mentioned. An example is noted below:

3.2.6: "The median coarse mode amplitudes and volume concentrations were higher than the fine mode amplitudes and volume concentrations for most of the year (DJF, MAM, and SON, Fig. 5b and Table S1), except during the southwest monsoon (JJA) when the fine mode amplitude and volume concentration was higher."

Line 597-600: What are the total number of AERONET measurements in each cluster? Figure 6 indicates that a total of 1345 VSDs were used for the cluster averaging. How were the corresponding parameters correlated to each of these clusters? Previous plots show mainly monthly averages however individual VSD retrievals and even VSD clusters are not explicitly tied to a month. How are the corresponding parameters in Figure 7 grouped into the clusters? The SDA FMF is not within inversion product so what timing threshold is used to link to the inversion data? Also, the AOD 500nm is measured at a different time than the retrieval unless you are taking the AE and computing AOD 500nm between 440nm and 675nm.

Response: The number of AERONET measurements per cluster and the corresponding MERRA-2 data is the same as in Figure 6 (total of 1419). Figure 7 caption has been edited to include the counts. "Average compositional contributions to aerosol optical depth (AOD) from MERRA-2 per identified cluster (counts per cluster from 1 to 5: 830, 284, 166, 74, 65)." The corresponding AERONET and MERRA-2 parameters that were closest in time to the VSD date and time were considered for the plots in Figure 7. All the corresponding data were plotted as boxplots in Figure 7. We just associated the AOD 500 nm, EAE, and FMF data that was available that were closest in date and time to the VSD data date and time.

Line 668: Figure 8b, how well does the total AOD from MERRA-2 compare to AERONET AOD at the same time? What wavelength is used for MERRA-2 data in the plot? Please indicate this information in Figure 8b. Also, if this is 500nm AOD then it appears underestimated at the specified times. Figure 8d back trajectory analysis only shows for three days so it is difficult to determine the source region. The Back trajectory analysis should be used between 5 and 7 days to better show the source region.

Response: The total AOD from MERRA-2 (550 nm) is slightly smaller for all the cases compared to the AERONET AOD (500 nm), except for the dust case (almost the same as the AERONET AOD at 500 nm). For comparison, the AOD from AERONET has been plotted alongside the compositional AOD from MERRA-2. The back trajectory analysis has been extended to 7 days for all the cases noted. The updated plot and caption are found below.
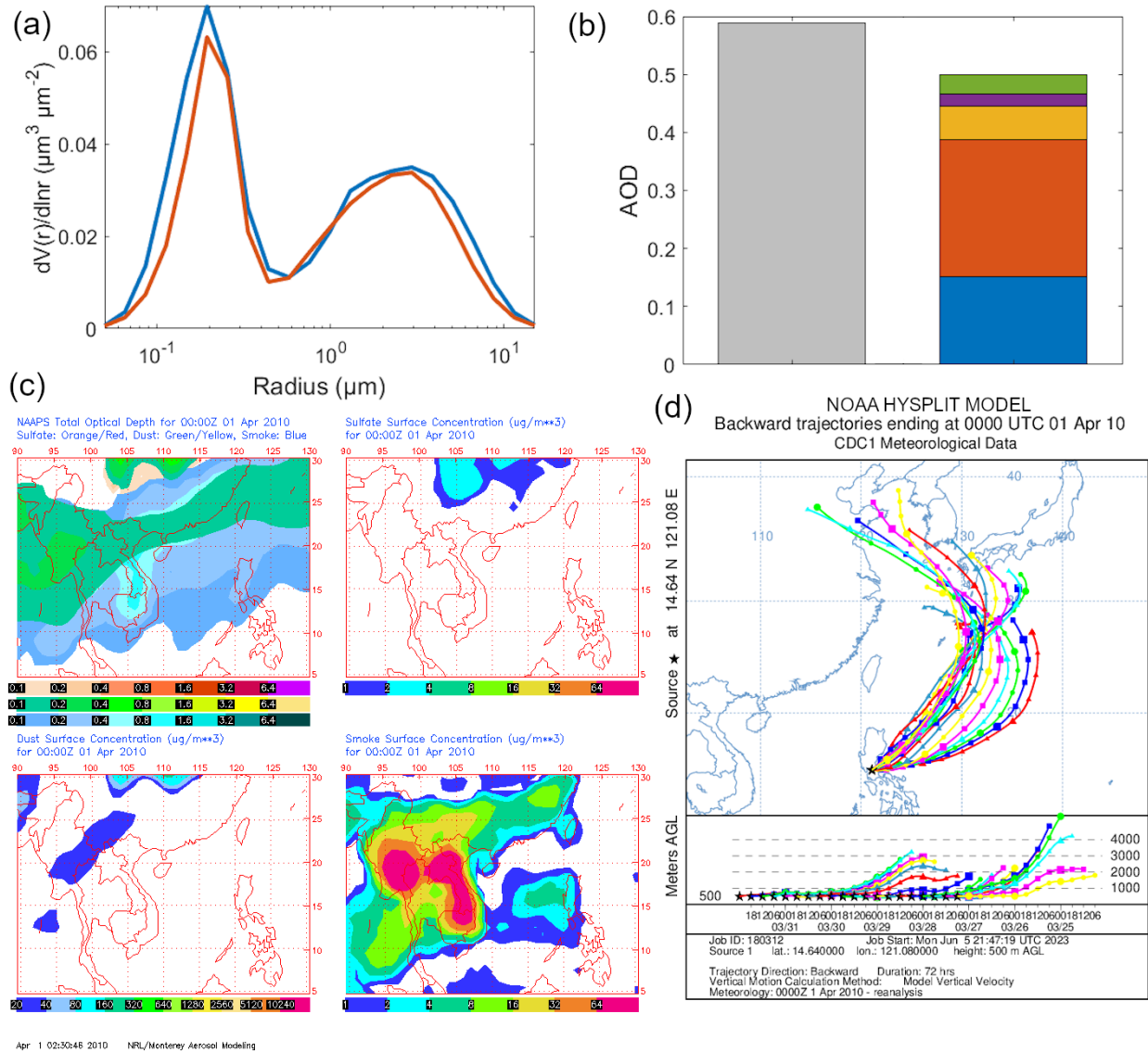
Figure 8: Case study of long-range transport (smoke – East Asia) around 1 April 2010. (a) AERONET VSDs at (blue) 00:01 and (red) 00:26 UTC, (b) AOD from AERONET (gray: median AOD at 500 nm) and MERRA-2 hourly (green: black carbon, violet: dust, yellow: sea salt, orange: organic carbon, blue: sulfate) compositional contributions to AOD (550 nm) closest in time to 00:01 UTC, (c) NAAPS maps of total and compositional hourly AOD (orange/red: sulfate, green/yellow: dust, blue: smoke) and sulfate, dust, and smoke surface concentrations at 00:00 UTC, and (d) HYSPLIT seven-day back-trajectories arriving at Manila Observatory at 00:00 UTC.

Line 697: Same as Figure 8 comments.

Response: Figure 9 and its captions have been updated as noted in the response to comments above for Figure 8.

Line 716: Same as Figure 8 comments.

Response: Figure 10 and its captions have been updated as noted in the response to comments above for Figure 8.

Line 741: Same as Figure 8 comments.

Response: Figure 11 and its captions have been updated as noted in the response to comments above for Figure 8.

Line 748: Section 3.6 seems out of place and perhaps should be part of Section 2.4, 2.5, or new 2.6.

Response: We thought hard about this but still think its current placement is suitable for how we feel the information can be presented.

References:

Banerjee, T., Shitole, A., Mhawish, A., Anand, A., Ranjan, R., Khan, M. F., Srithawirat, T., Latif, M. T., and Mall, R.: Aerosol climatology over South and Southeast Asia: Aerosol types, vertical profile, and source fields, Journal of Geophysical Research: Atmospheres, 126, e2020JD033554, 2021.
Bergstrom, R. W., Pilewskie, P., Russell, P. B., Redemann, J., Bond, T. C., Quinn, P. K., and Sierau, B.: Spectral absorption properties of atmospheric aerosols, Atmos. Chem. Phys., 7, 5937-5943, https://doi.org/10.5194/acp-7-5937-2007, 2007.
Buchard, V., Randles, C., Da Silva, A., Darmenov, A., Colarco, P., Govindaraju, R., Ferrare, R., Hair, J., Beyersdorf, A., and Ziemba, L.: The MERRA-2 aerosol reanalysis, 1980 onward. Part II: Evaluation and case studies, Journal of Climate, 30, 6851-6872, https://doi.org/10.1175/JCLI-D-16-0613.1, 2017.
Che, H., Xia, X., Zhu, J., Wang, H., Wang, Y., Sun, J., Zhang, X., and Shi, G.: Aerosol optical properties under the condition of heavy haze over an urban site of Beijing, China, Environ. Sci. Pollut. R., 22, 1043-1053, https://doi.org/10.1007/s11356-014-3415-5, 2015.
Choi, M., Lim, H., Kim, J., Lee, S., Eck, T. F., Holben, B. N., Garay, M. J., Hyer, E. J., Saide, P. E., and Liu, H.: Validation, comparison, and integration of GOCI, AHI, MODIS, MISR, and VIIRS aerosol optical depth over East Asia during the 2016 KORUS-AQ campaign, Atmos. Meas. Tech., 12, 4619-4641, https://doi.org/10.5194/amt-12-4619-2019, 2019.
Diner, D. J., Di Girolamo, L., and Nolin, A.: Preface to the MISR special issue, Remote Sens. Environ., 107, 1, https://doi.org/10.1016/j.rse.2006.11.001, 2007.
Dong, X., and Fu, J. S.: Understanding interannual variations of biomass burning from Peninsular Southeast Asia, part II: Variability and different influences in lower and higher atmosphere levels, Atmospheric Environment, 115, 9-18, https://doi.org/10.1016/j.atmosenv.2015.05.052, 2015.

Dubovik, O., and King, M. D.: A flexible inversion algorithm for retrieval of aerosol optical properties from Sun and sky radiance measurements, J. Geophys. Res.- Atmos., 105, 20673-20696, https://doi.org/10.1029/2000JD900282, 2000.

Dubovik, O., Smirnov, A., Holben, B., King, M., Kaufman, Y., Eck, T., and Slutsker, I.: Accuracy assessments of aerosol optical properties retrieved from Aerosol Robotic Network (AERONET) Sun and sky radiance measurements, Journal of Geophysical Research: Atmospheres, 105, 9791-9806, https://doi.org/10.1029/2000JD900040, 2000.

Dubovik, O., Holben, B., Lapyonok, T., Sinyuk, A., Mishchenko, M., Yang, P., and Slutsker, I.: Non-spherical aerosol retrieval method employing light scattering by spheroids, Geophysical Research Letters, 29, 54-51-54-54, https://doi.org/10.1029/2001GL014506, 2002.

Dubovik, O., Sinyuk, A., Lapyonok, T., Holben, B. N., Mishchenko, M., Yang, P., Eck, T. F., Volten, H., Munoz, O., and Veihelmann, B.: Application of spheroid models to account for aerosol particle nonsphericity in remote sensing of desert dust, Journal of Geophysical Research: Atmospheres, 111, https://doi.org/10.1029/2005JD006619, 2006.

Garay, M. J., Bull, M. A., Nastan, A. M., Witek, M. L., Seidel, F. C., Diner, D. J., Kahn, R. A., Limbacher, J. A., and Kalashnikova, O. V.: Data Product Specification for the MISR Level 2 Aerosol Product, Jet Propulsion Laboratory, California Institute of Technology. JPL D-100649. https://asdc.larc.nasa.gov/documents/misr/DPS_AEROSOL_V023.20180125.pdf, 2018.

Gautam, R., Hsu, N. C., Eck, T. F., Holben, B. N., Janjai, S., Jantarach, T., Tsay, S.-C., and Lau, W. K.: Characterization of aerosols over the Indochina peninsula from satellite-surface observations during biomass burning pre-monsoon season, Atmos. Environ., 78, 51-59, https://doi.org/10.1016/j.atmosenv.2012.05.038, 2013.

Gui, L., Tao, M., Wang, Y., Wang, L., Chen, L., Lin, C., Tao, J., Wang, J., and Yu, C.: Climatology of aerosol types and their vertical distribution over East Asia based on CALIPSO lidar measurements, International journal of climatology, 42, 6042-6054, 2022.

Hong, Y., and Di Girolamo, L.: Cloud phase characteristics over Southeast Asia from A-Train satellite observations, Atmos. Chem. Phys., 20, 8267-8291, https://doi.org/10.5194/acp-20-8267-2020, 2020.

Hong, Y., and Di Girolamo, L.: An overview of aerosol properties in clear and cloudy sky based on CALIPSO observations, Earth and Space Science, 9, e2022EA002287, https://doi.org/10.1029/2022EA002287, 2022.

Hyer, E. J., Reid, J. S., Prins, E. M., Hoffman, J. P., Schmidt, C. C., Miettinen, J. I., and Giglio, L.: Patterns of fire activity over Indonesia and Malaysia from polar and geostationary satellite observations, Atmos. Res., 122, 504-519, https://doi.org/10.1016/j.atmosres.2012.06.011, 2013.

Kaskaoutis, D., Badarinath, K., Kumar Kharol, S., Rani Sharma, A., and Kambezidis, H.: Variations in the aerosol optical properties and types over the tropical urban site of Hyderabad, India, Journal of Geophysical Research: Atmospheres, 114, https://doi.org/10.1029/2009JD012423, 2009.

Kinne, S.: The MACv2 aerosol climatology, Tellus B: Chemical and Physical Meteorology, 71, 1-21, 2019.

Kuttippurath, J., and Raj, S.: Two decades of aerosol observations by AATSR, MISR, MODIS and MERRA-2 over India and Indian Ocean, Remote Sens. Environ., 257, 112363, https://doi.org/10.1016/j.rse.2021.112363, 2021.

Lin, N.-H., Sayer, A. M., Wang, S.-H., Loftus, A. M., Hsiao, T.-C., Sheu, G.-R., Hsu, N. C., Tsay, S.-C., and Chantara, S.: Interactions between biomass-burning aerosols and clouds over

Southeast Asia: Current status, challenges, and perspectives, Environ. Pollut., 195, 292-307, https://doi.org/10.1016/j.envpol.2014.06.036, 2014.

Lynch, P., Reid, J. S., Westphal, D. L., Zhang, J., Hogan, T. F., Hyer, E. J., Curtis, C. A., Hegg, D. A., Shi, Y., and Campbell, J. R.: An 11-year global gridded aerosol optical thickness reanalysis (v1. 0) for atmospheric and climate sciences, Geosci. Model Dev., 9, https://doi.org/10.5194/gmd-9-1489-2016, 2016.

Qi, Y., Ge, J., and Huang, J.: Spatial and temporal distribution of MODIS and MISR aerosol optical depth over northern China and comparison with AERONET, Chinese science bulletin, 58, 2497-2506, https://doi.org/10.1007/s11434-013-5678-5, 2013.

Reid, J. S., Hyer, E. J., Johnson, R. S., Holben, B. N., Yokelson, R. J., Zhang, J., Campbell, J. R., Christopher, S. A., Di Girolamo, L., and Giglio, L.: Observing and understanding the Southeast Asian aerosol system by remote sensing: An initial review and analysis for the Seven Southeast Asian Studies (7SEAS) program, Atmos. Res., 122, 403-468, https://doi.org/10.1016/j.atmosres.2012.06.005, 2013.

Rizza, U., Mancinelli, E., Morichetti, M., Passerini, G., and Virgili, S.: Aerosol optical depth of the main aerosol species over Italian cities based on the NASA/MERRA-2 model reanalysis, Atmosphere, 10, 709, https://doi.org/10.3390/atmos10110709, 2019.

Schuster, G. L., Dubovik, O., and Holben, B. N.: Angstrom exponent and bimodal aerosol size distributions, J. Geophys. Res.- Atmos., 111, https://doi.org/10.1029/2005JD006328, 2006.

Sinyuk, A., Holben, B. N., Eck, T. F., Giles, D. M., Slutsker, I., Korkin, S., Schafer, J. S., Smirnov, A., Sorokin, M., and Lyapustin, A.: The AERONET Version 3 aerosol retrieval algorithm, associated uncertainties and comparisons to Version 2, Atmospheric Measurement Techniques, 13, 3375-3411, https://doi.org/10.5194/amt-13-3375-2020, 2020.

Tandule, C. R., Kalluri, R. O. R., Gugamsetty, B., Kotalo, R. G., Thotli, L. R., Rajuru, R. R., and Vaddin, S.: Decadal climatology of the spatial and vertical distributions of tropospheric aerosol over the Arabian Sea based on satellite observations, International Journal of Climatology, 40, 4676-4689, 2020.

Wang, S.-H., Welton, E. J., Holben, B. N., Tsay, S.-C., Lin, N.-H., Giles, D., Stewart, S. A., Janjai, S., Nguyen, X. A., and Hsiao, T.-C.: Vertical distribution and columnar optical properties of springtime biomass-burning aerosols over Northern Indochina during 2014 7-SEAS campaign, Aerosol and Air Quality Research, 15, 2037-2050, https://doi.org/10.4209/aaqr.2015.05.0310, 2015.

Xiao, N., Shi, T., Calder, C. A., Munroe, D. K., Berrett, C., Wolfinbarger, S., and Li, D.: Spatial characteristics of the difference between MISR and MODIS aerosol optical depth retrievals over mainland Southeast Asia, Remote Sensing of Environment, 113, 1-9, https://doi.org/10.1016/j.rse.2008.07.011, 2009.

Yang, S., Lau, W. K., Ji, Z., Dong, W., and Yang, S.: Impacts of radiative effect of pre-monsoon biomass burning aerosols on atmospheric circulation and rainfall over Southeast Asia and southern China, Climate Dynamics, 59, 417-432, https://doi.org/10.1007/s00382-021-06135-7, 2022.

Zhao, G., Di Girolamo, L., Dey, S., Jones, A. L., and Bull, M.: Examination of direct cumulus contamination on MISR-retrieved aerosol optical depth and angstrom coefficient over ocean, Geophysical Research Letters, 36, https://doi.org/10.1029/2009GL038549, 2009.

Referee Comment: "An Aerosol Climatology via Remote Sensing over Metro Manila, Philippines"
Anonymous Referee #2
May 23, 2023

Lorenzo et al. have explored aerosol climatology over Manila using AERONET database. Besides, MISR AOD was considered with MERRA-2 data and other met. data to explain aerosol type and aerosol movement through wind. The manuscript in most cases lost direction and lack critical analysis, as too many datasets were used without much detail interpretation. Writing of the text also needs improvement.

General comments:

1. The manuscript lack of novelty. Aerosol climatology has not been constituted with long term database. Authors have explored too many aerosols dataset without being conclusive on any of these. Determination of aerosol type lacks more analysis and improvement of hypothesis.

   Response: Thank you for the critical feedback as it is helpful to see one side of a perspective on our work. The other side is that the analysis and results help to better understand aerosol characteristics in a climate-sensitive region of the world where aerosol measurements are very difficult to do. The AERONET database is in fact the longest continuous aerosol column database in the Philippines to date. We feel strongly that our analysis sheds important light on aerosol characteristics in a way that has not been done before, with the foundation being the AERONET dataset whose long-term nature has yet to be exploited in the way we did in this study. We have analyzed aerosol parameters besides AOD: which was the focus of other recent studies on columnar aerosol in the Philippines and in Metro Manila. The comparison of the Metro Manila data to regional Southeast Asia AOD shows a unique characteristic of Metro Manila that is affected by the West Pacific as well as the monsoon trough, that is not necessarily a Southeast Asian region-wide phenomena. Therefore we believe there is sufficient importance and new forms of results that are presented to continue the progress in understanding aerosol particle behavior in Metro Manila. As you will be able to see throughout the manuscript (a paragraph was added to the introduction as noted in the response to Specific Comment #2 below), we have made more revisions to hopefully drill home the point that the work is important to archive for the research community.

2. Significant part of case studies is based on NAAPS model outcome which is only used for regulatory forecast purposes and has uncertainty in model forecast over the Philippines.

Response: We used NAAPS maps to support the case studies which were based on the clustering results of AERONET VSD data. MERRA-2 was also used along with HYSPLIT back trajectories. The text was edited to show that the primary dataset used was AERONET (specifically VSD clustering results), with the other independent sources providing support. Reanalysis products such as MERRA-2 and NAAPS are quite helpful for conditions in which clouds affect remote sensing of aerosol particles such as in southeast Asia. NAAPS has been used in the way we did for a number of other studies aiming to have a supplementary source of support for air pollutant sources.

2.3 Extreme Event Analysis "Aerosol particle events based on the three clusters with the highest VSD concentrations were identified to characterize different types of sources and processes impacting aerosol particle columnar properties above Metro Manila. The three events are described below."

2.3.1. Smoke Long Range Transport "Events related to transported biomass burning/smoke were chosen from the AERONET VSD data that were clustered as urban/industrial (with a dominant submicrometer peak) (Eck et al., 1999) over Metro Manila. Cases with the highest black carbon contribution to total AOD from the MERRA-2 dataset were considered. Maps from NAAPS of high smoke contributions to AOD and surface smoke contributions in the direction of back-trajectories from the National Oceanic and Atmospheric Administration's (NOAA) Hybrid Single-Particle Lagrangian Integrated Trajectory (HYSPLIT) model (Stein et al., 2015; Rolph et al., 2017) were used to provide support for the likely source and transport pathway for the smoke cases."

2.3.2 Dust Long Range Transport "A dust transport case over Metro Manila was identified from the AERONET VSD dust cluster (with an enhanced coarse peak in the AERONET VSD compared to the submicrometer fraction) (Eck et al., 1999), the highest dust contribution to AOD from the MERRA-2 dataset, and high dust contributions to AOD from NAAPS. Surface dust concentrations from NAAPS along the HYSPLIT back-trajectories improved the plausibility of dust for this case."

3. Besides, there are some claims that need to be reverified by authors. For instance, availability of AOD dataset and related research over Southeast Asia (SEA) are plenty. SEA is one of the extensively explored regions of the world for aerosols because of its climate significance. However, in the Line 46, authors claim non availability of research on aerosols over Southeast Asia. This is certainly not true.

    Response: We have revised the text in question to better articulate what the pressing needs are and to of course give credit to the significant volume of work done already: Introduction. "Although Southeast Asia is one of the most rapidly developing regions in the world with a growing number of extensive research conducted (Reid et al., 2023), there remain knowledge gaps related to aerosol particles in the area (Tsay et al., 2013; Lee et al., 2018; Chen et al., 2020; Amnuaylojaroen, 2023)."

4. Again, August is pointed to be the highest biomass burning month for Insular SEA. However, in fact, Sept.-Oct. is primarily reported to have widespread forest and peatland

fires, burned over large parts of maritime southeast Asia, most notably in Indonesia, southern Sumatra and southern Kalimantan. In many reports, the increase in AOD in the Philippines during Oct. is a direct consequence of fire in neighboring Indonesia and corresponding wind movement in Sept. to Oct.

Response: The months of August to October were the months with the highest AERONET AOD median values. The text in the abstract noting only August as the month with highest biomass burning emissions was edited as follows. The text in 3.2.1 was edited to include "Indonesia" and references were added to the sentence. Other references were added to include studies showing AOD increase in the Philippines due to the Indonesia fires.

Abstract (L28): "Aerosol optical depth (AOD) values were highest from August to October, partly from fine urban aerosol particles, including soot, coinciding with the burning season in maritime Southeast Asia when smoke is often transported to Metro Manila during the southwest monsoon."

3.2.1: "This is the same time of year when biomass burning activities occur in the Indonesian region southwest of Metro Manila (Glover and Jessup, 1998; Kiely et al., 2019; Cahyono et al., 2022). Studies have shown that AOD in the Philippines increases during the biomass burning season in Indonesia (Nguyen et al., 2019; Caido et al., 2022)."

Specific comment:

1. There are many contradictory sentences explaining the results. Like in L28, highest AOD in August is contradictory to L325 and L329 with AOD 0.23 in October.

   Response: The highest AERONET AOD in Manila Observatory was from August (0.21) to September (0.23). The sentence (L28) was edited accordingly. MISR and MERRA-2 data represent regional AOD and show a peak at the same time beginning in September to October. The sentence (L325 and L329) was edited as well.

   Abstract (L28): "Aerosol optical depth (AOD) values were highest from August to October, partly from fine urban aerosol particles, including soot, coinciding with the burning season in Insular Southeast Asia when smoke is often transported to Metro Manila during the southwest monsoon."

   3.2.1: "Regional AOD (550 nm) over the larger Southeast Asia domain from MISR and MERRA-2 (Fig. 4) had a similarly large peak around the same time beginning in September until October which, however, was second only in magnitude to a March peak, which is influenced by biomass burning in Peninsular Southeast Asia (PSEA) (Gautam et al., 2013; Hyer et al., 2013)."

2. Introduction needs to be re-drafted. First paragraph does not conclude anything specific besides mentioning some previous research on the Philippines. Please include the findings on aerosols/aod/fire/trend from previous experiments. Content in the second paragraph is more relevant in the study area, section 2. Even the context of conducting this research is very briefly mentioned. Please emphasize on what new science questions can be answered by innovative analyses using combinations of data sets. Just because aerosol climatology has not been reported from a region using a new data product does not hold the novelty of the research.

Response: We have revised the introduction to emphasize more findings (in the text below) from past experiments and to move some content (previously paragraph 2) to Section 2. With regard to the concern over a lack of new science questions, we list four science questions at the end of the Introduction Section.

"Most of the past studies involving long-term remotely sensed aerosol particle data in Southeast Asia (Cohen, 2014; Nakata et al., 2018; Nguyen et al., 2019) had no specific focus on the Philippines. The Philippines is considered as part of the Maritime Continent (MC), the island nations sub-region of Southeast Asia. The other Southeast Asia sub-region, Peninsular Southeast Asia (PSEA), comprises those nations within the continental Asia land mass. These two regions have separate aerosol sources and climate, where MC is dependent on the intertropical convergent zone (ITCZ) and PSEA is dependent on both the ITCZ and monsoon systems (Dong and Fu, 2015). Only the southern part of the Philippines is climatologically part of MC (Ramage, 1971), however, and northwest Philippines, where Metro Manila is located, is affected by the monsoons and tropical cyclones aside from the ITCZ (Chang et al., 2005; Yumul Jr et al., 2010; Bagtasa, 2017). These unique meteorological influences and extensive local aerosol particle sources warrant a unique aerosol climatology over Metro Manila, one of a polluted source in a tropical marine environment, and its effects on cloud formation in the area. Aerosol effects on clouds in the marine environment are associated with the largest uncertainties in climate change research (Hendrickson et al., 2021; Wall et al., 2022) and the Philippines was ranked as the 5th country globally as most at risk to climate change and extreme weather from 1997 to 2018 (Eckstein et al., 2018). There have been several surface measurements of aerosol particles made in Metro Manila for the past 20 years (Oanh et al., 2006; Bautista VII et al., 2014; Cruz et al., 2019) but column-based ground-based measurements there are just beginning to be established (Dorado et al., 2001; Cruz et al., 2023; Ong et al., 2016). The AERONET sun photometer is one of the first long-term column-based aerosol instruments in Metro Manila and the Philippines (Ong et al., 2016)."

3. Drafting the manuscript in many cases is not appropriate. In L 88, authors emphasized that only AERONET data has been used to study whereas in table 1, it says for AERONET, MERRA-2 and PERSIANN. No discussion on MISR monthly AOD is included.

Response: The other complementary datasets used were also enumerated in the text (including MISR, HYSPLIT, NAAPS, and MODIS). Table 1 was updated to include the datasets specifically over Metro Manila, the other datasets over Southeast Asia like MISR, HYSPLIT, and NAAPS were discussed in sections 2.1.3, 2.1.4, and 2.1.5.

L88: "The goal of this study is to use multi-year AERONET data in Manila Observatory along with other complementary datasets (MERRA-2, PERSIANN, MISR, HYSPLIT, NAAPS, and MODIS) to address the following questions:"

2. Methods: "This work relies on analysis of several datasets over Metro Manila and regional Southeast Asia summarized in Table 1 and in the following subsections. The common time range used for all datasets is between January 2009 and October 2018."

Table 1: Summary of datasets over Metro Manila used in this work covering the period from January 2009 to October 2018.

Parameter	Data Source	Spatial Coverage	Time Coverage
Aerosol Optical Depth (500 nm)	AERONET	14.635°N, 121.078°E	Jan 2009 - Oct 2018
Asymmetry Factor (440 nm - 1020 nm)	AERONET	14.635°N, 121.078°E	Jan 2009 - Oct 2018
Extinction Angstrom Exponent (440 nm -870 nm)	AERONET	14.635°N, 121.078°E	Jan 2009 - Oct 2018
Fine Mode Fraction	AERONET	14.635°N, 121.078°E	Jan 2009 - Oct 2018
Precipitable Water	AERONET	14.635°N, 121.078°E	Jan 2009 - Oct 2018
Single Scattering Albedo (440 nm - 1020 nm)	AERONET	14.635°N, 121.078°E	Jan 2009 - Oct 2018
Refractive Index (Real and Imaginary; 440 nm - 1020 nm)	AERONET	14.635°N, 121.078°E	Jan 2009 - Oct 2018
Volume Size Distribution	AERONET	14.635°N, 121.078°E	Jan 2009 - Oct 2018
Low Cloud Fraction (MODIS)	MERRA-2	14.3°N - 14.8°N, 120.75°E - 121.25°E	Jan 2009 - Dec 2018
Planetary Boundary Layer Height	MERRA-2	14.3°N - 14.8°N, 120.75°E - 121.25°E	Jan 2009 - Dec 2018
Relative Humidity (975 mb)	MERRA-2	14.3°N - 14.8°N, 120.75°E - 121.25°E	Jan 2009 - Dec 2018
Sea Level Pressure	MERRA-2	14.3°N - 14.8°N, 120.75°E - 121.25°E	Jan 2009 - Dec 2018
Temperature (975 mb)	MERRA-2	14.3°N - 14.8°N, 120.75°E - 121.25°E	Jan 2009 - Dec 2018
Wind (975 mb)	MERRA-2	14.3°N - 14.8°N, 120.75°E - 121.25°E	Jan 2009 - Dec 2018
Total Extinction Aerosol Optical Depth (550 nm)	MERRA-2	14.3°N - 14.8°N, 120.75°E - 121.25°E	Jan 2009 - Dec 2018
Sulfate, Black Carbon, Organic Carbon, Dust, and Sea Salt Extinction Aerosol Optical Depth (550 nm)	MERRA-2	14.3°N - 14.8°N, 120.75°E - 121.25°E	Jan 2009 - Dec 2018
Precipitation	PERSIANN	14.3°N - 14.8°N, 120.75°E - 121.25°E	Jan 2009 - Dec 2018

4. 2.1.3 What was the purpose of comparing monthly MISR 0.5x0.5 data against AERONET and MERRA- AOD? This does not conclude anything scientific on aerosol climatology.

Response: The AERONET data over Metro Manila is influenced by both local and long-range aerosol particle sources, and the only way to assess the influence of these long-range sources is to look at a large (i.e. 30° × 30°) region around Manila, which is why we looked at both the MISR and MERRA-2 regional data. Regional AOD values from MISR (remote sensing) and MERRA-2 (reanalysis) were used as independent sources of

support for the long-range aerosol particles seen over Metro Manila AOD from AERONET. Supporting monthly regional AOD from independent instruments (AERONET and MISR remote sensors) and methods (MERRA-2 reanalysis which includes data assimilation from AOD from MODIS and MISR) helped to reinforce regional sources of aerosol particles that influence the Metro Manila air column. MISR also has aerosol particle shape and size speciated AOD, which provide further support for the other AERONET aerosol parameters. A figure was added to show the shape and size speciated AOD (Fig. S1). The size speciated data helps reinforce the regional influence on the aerosol particles over Metro Manila especially during high AOD times from July to September (when high AERONET EAE associated with fine, spherical, and absorptive particles based on MISR data) and times with the low AOD in December (large particles based on MISR size speciated AOD). Edits in the manuscript to reflect these responses are found below.
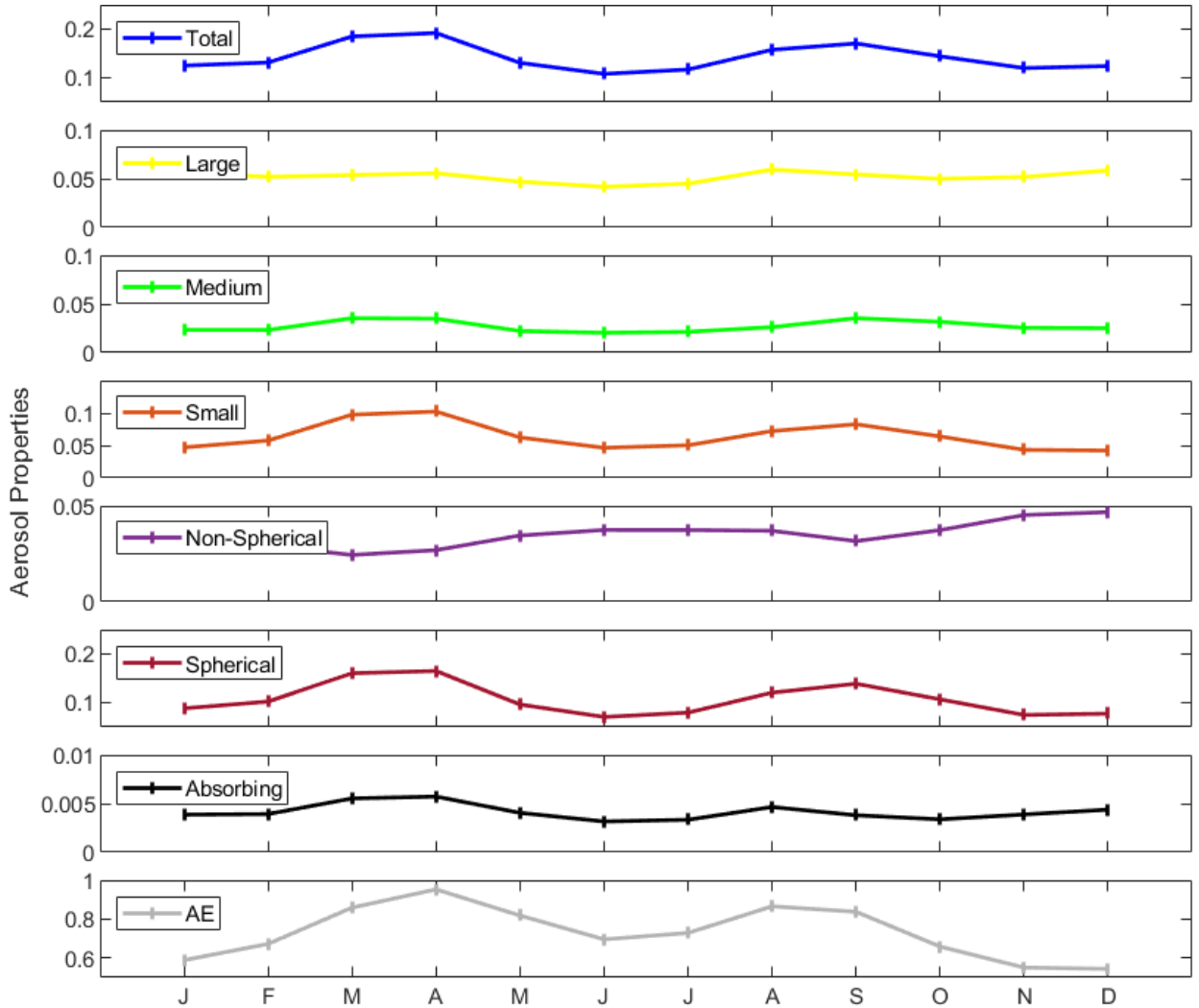
Figure S1: MISR monthly mean time series of 550 nm AOD (total, large (particle radii > 0.7 µm), medium (particle radii from 0.35 to 0.7 µm), small (particle radii < 0.35 µm),

non-spherical spherical, and absorption optical depth) and angstrom exponent (AE) for March 2000 to December 2020 for 116.5°E to 128.5°E; 6.5°N to 22.5°N.

2.1.2 "The total MERRA-2 AOD for the region was used along with MISR AOD data to assess the influence of long-range sources to the aerosol column over Manila Observatory."

2.1.4 "Monthly 500 nm AOD data (Level 3 Global Aerosol: 0.5° × 0.5° spatial resolution) from 2009 to 2018 are used from the Multi-angle Imaging SpectroRadiometer (MISR), (Diner et al., 2007; Garay et al., 2018) as regional (Southeast Asia) baseline remote sensing data to support the Manila Observatory AERONET data. The regional MISR data was used to confirm regional sources of aerosols that may be influencing the AOD over Metro Manila."

2.1.4 "MISR is ideal for remote sensing in the CAMP2Ex region because it has an overpass at 10:30 AM ECT (descending mode) (when cirrus is minimal) and its retrievals have been shown to be unimpacted by small cumulus (Zhao et al., 2009), which are typical in the region. MISR has relatively more accurate AOD and agrees better with AERONET data compared to other satellite products due to its multi-angle measurements (Choi et al., 2019; Kuttippurath and Raj, 2021). The MISR sampling noise is relatively small due to the large domain and seasonal averages that are considered in this study. MISR is also the only passive sensor that speciates aerosol particle size and shape. All these factors led to the choice of using regional MISR data to associate long-range sources influencing AERONET data in Manila Observatory."

3.2.1 "Regional AOD (550 nm) over the larger Southeast Asia domain from MISR and MERRA-2 (Fig. 4) had a similarly large peak from September to October which, however, was second only in magnitude to a March peak, which is influenced by biomass burning in Peninsular Southeast Asia (PSEA) (Gautam et al., 2013; Hyer et al., 2013). This is consistent with the peak in speciated AOD due to fine (radii <0.7 µm), spherical, and absorbing aerosols that were observed by MISR from March to April (Fig. S1).: 3.2.1 "This dip was also observed in the regional AOD data (MISR and MERRA-2, Fig. 4). This is most probably due to the decrease in the AOD contribution from fine (radii <0.7 µm) and spherical particles based on size speciated MISR AOD (Fig. S1). Larger and non-spherical particle contributions to AOD increase in November in the Southeast Asia region. The MERRA-2 AOD is relatively higher than the MISR AOD probably due to assimilation of MODIS data into MERRA-2. Studies in Asia (Xiao et al., 2009; Qi et al., 2013; Choi et al., 2019) have observed relatively higher MODIS AOD compared to MISR AOD."

3.2.2 "The high EAE over Manila Observatory from July to September is probably regional in nature based on the MISR data showing increased EAE with increased AOD from fine, spherical, and absorptive particles (Fig. S1) in Southeast Asia during the same months."

3.2.2 "The lowest EAE values (0.08) and thus the largest particles were observed in December, which again may be regional in nature with MISR EAE also lowest during this time with increased AOD from larger and non-spherical particles (Fig. S1)."

5. The criteria for considering Table 2 has some ambiguity. Please explain what was the basis of considering FMF to sort fine and coarse aerosols? Again for a country like the Philippines with a very low annual AOD (~0.2), how accurate is it to separate marine and industrial aerosols based on FMF?

Response: The table's criteria has been used in other regions with even lower AOD. The references are indicated in the table. An updated table, including more angstrom exponent threshold values, is shown in response #12. The table's criteria represents one possible way to do size classification (i.e. FMF has been used in other studies (Kleidman et al., 2005)) as a proxy for remotely sensed observations. We have also added a sentence at the end of the paragraph preceding the table to contextualize our use of the thresholds.

"While these classifications are not rigid definitions of air masses, they help in understanding the sources that contribute to aerosols in Metro Manila and in identifying cases where certain sources are more influential than others."

6. Table 2: Its also strange that no biomass burning aerosols were considered as air mass type when biomass burning is an important contributor. Beside authors are working on smoke aerosol transport in section 2.3.1 while no such classification was made in Table 2. Please justify.

Response: The long-range transport of biomass burning aerosol particles was considered as part of the urban/industrial air mass type which includes both local combustion and long-range transported biomass burning. The text in section 2.2 has been updated to include this information. Table 2 has also been updated to include a threshold for biomass burning based on literature. The changes to the texts are indicated below. The changes to the table are in response #12.

2.2 "The urban/industrial air mass type here refers to local combustion along with long-range transported biomass burning (Kaskaoutis et al., 2009)."

3.3.2 "Combining this and results from the previous sections confirms that cluster 4 can be an urban/industrial source given that it had the highest median accumulated mode peak and organic carbon contribution to total AOD among the clusters. The cluster 4 air mass is probably from local sources and transported biomass burning emissions. The high median EAE (1.40, Fig. 7c) may be associated with aerosol particles due to biomass burning (Deep et al., 2021).

7. The NAAPS model outputs are not always convincing enough to detect regional emission sources. NAAPS model aerosol forecasts are available on a 1°× 1° grid. However, use of NAAPS model forecast over Philippines is questionable as 'number of AOT assimilations available in and around the Philippines is limited because of the pervasive

cloud cover, making model outputs of AOT subject to uncertainty for this region (https://acp.copernicus.org/articles/22/12961/2022/)'.

Response: We use NAAPS to provide support for the AERONET data. We are not using it to detect the regional sources but just associate possible regional sources during extreme aerosol loading events based on AERONET data in Manila Observatory. We edited the text to note these points (including the resolution of NAAPS AOT reanalysis product).

2.1.5 NAAPS: "Archived maps of total and speciated optical depths and surface concentrations of sulfate, dust, and smoke for Southeast Asia are used from the Navy Aerosol Analysis and Prediction System (NAAPS: $1° \times 1°$ spatial resolution) (Lynch et al., 2016), and which are publicly available at https://www.nrlmry.navy.mil/aerosol/." "These maps help associate possible regional emission sources to extreme aerosol loading events in Manila Observatory."

2.3.1 Smoke Long Range Transport: "Maps of surface smoke contributions from NAAPS as well as back-trajectories from the National Oceanic and Atmospheric Administration's (NOAA) Hybrid Single-Particle Lagrangian Integrated Trajectory (HYSPLIT) model (Stein et al., 2015; Rolph et al., 2017) were used to provide support for the likely source and transport pathway for the smoke cases."

8. Section 2.4: Why not EOF was performed on monthly mean MISR AOD instead of a reanalysis product?

Response: EOF needs a data set with no data gaps, and the 10-year monthly MISR AOD for Southeast Asia had geographical data gaps at certain times. The sentence in section 2.4 was edited as follows.

"EOF analysis needs a complete dataset with no data gaps, which is not available with pure satellite retrievals like MISR; MERRA-2 reanalysis data alleviate this issue."

9. Fig. 1 & 2 is not required in the main text, move it to the supplementary file. Reduce the related discussion on meteorology as this paper is not focused on aerosol -meteorology interaction but the aerosol climatology. Entire section 3.1 should be removed/deleted keeping Fig. 1 and Fig. 2 in supplementary.

Response: We appreciate this comment in that it provides a perspective other than ours to let us think more deeply about the way we originally presented our results. After much more thought, we still feel Figures 1-2 and associated Section 3.1 are important to retain to provide context for the study and to allow it to be intercompared with related studies from other regions.

10. Fig. 3a: trend in AOD is not clear, make adjustments in y axis.

Response: The y-axis has been adjusted. The following text has been edited in the caption.
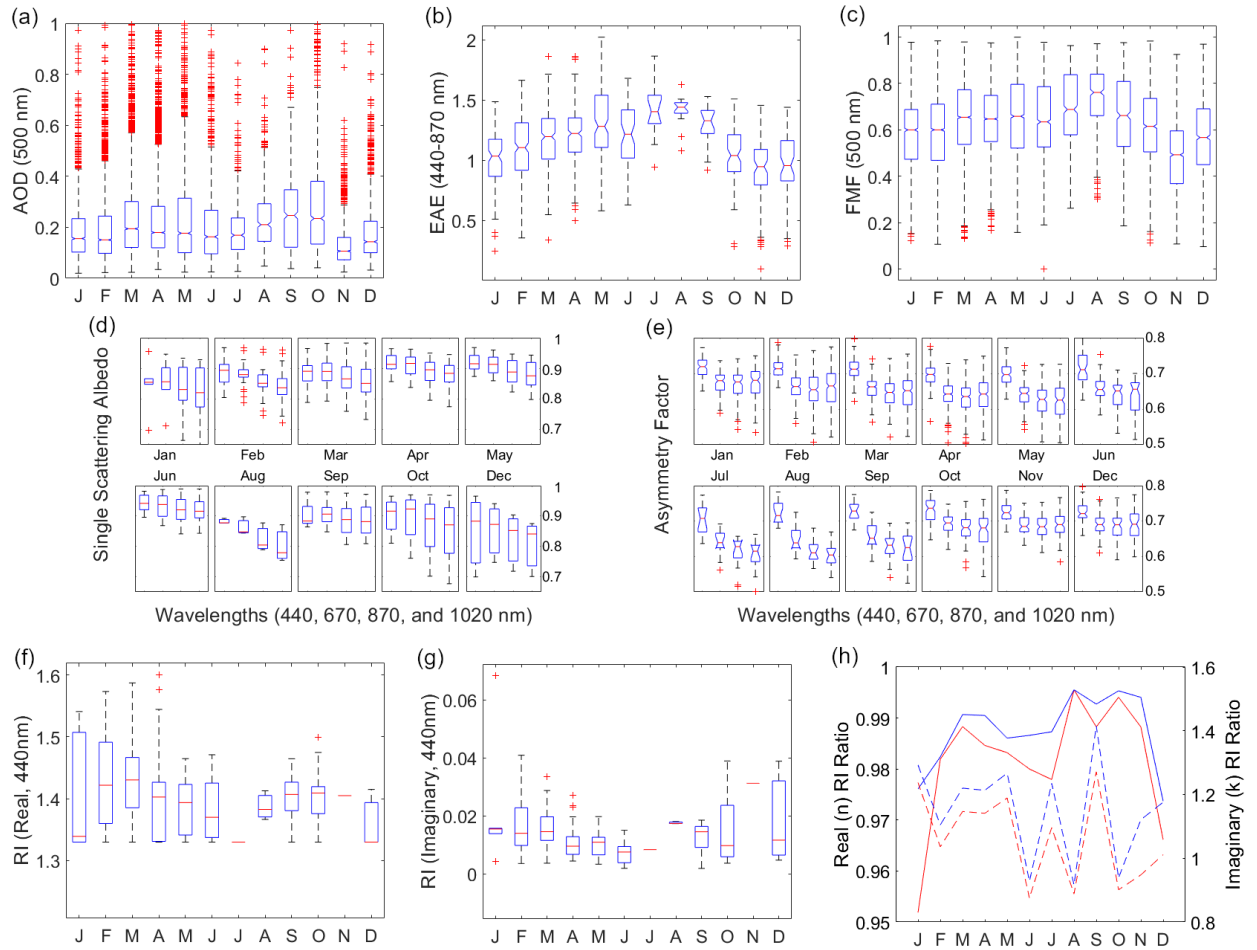
"Figure 3: Monthly characteristics of AERONET aerosol particle parameters: (a) aerosol optical depth (AOD, 500nm with y-axis until 1.0 only for larger boxplot resolution) with counts (Jan: 2107, Feb: 3931, Mar: 4923, Apr: 5755, May: 3389, Jun: 1653, Jul: 637, Aug: 483, Sep: 718, Oct: 1555, Nov: 2001, Dec: 1386)."

11. L 330: The major contributor of biomass burning emission in peninsular Southeast Asia is emission from Indonesia with much higher fire spots in October compared to that of Philippines in March. It's highly unusual to have a greater AOD peak in March compared to October. Justify.

Response: Biomass burning in Peninsular Southeast Asia (what is also referred to as Indochina Peninsula, (Dong and Fu, 2015)) peaks in March. Previous studies based on AERONET and MODIS data show peak AOD over Peninsular Southeast Asia in March (Gautam et al., 2013; Wang et al., 2015), MERRA-2 biomass burning emissions over Peninsular Southeast Asia peak in March as well (Yang et al., 2022). The text has been edited to include Dong and Fu, Wang et al., and Yang et al. as references. The

approximate distance from Peninsular Southeast Asia to the Philippines is also included in the text.

"Regional AOD (550 nm) over the larger Southeast Asia domain from MISR and MERRA-2 (Fig. 4) had a similarly large peak around the same time beginning in September until October which, however, was second only in magnitude to a March peak, which is influenced by biomass burning in Peninsular Southeast Asia (PSEA) (Gautam et al., 2013; Hyer et al., 2013; Dong and Fu, 2015; Wang et al., 2015; Yang et al., 2022). This is consistent with the peak in speciated AOD due to fine (radii <0.7 µm), spherical, and absorbing aerosols that were observed by MISR from March to April (Fig. S1). This larger peak in March, attributed to PSEA (which is ~2000 km west of the Philippines), was not as prevalent in the AERONET AOD data over Manila Observatory in Metro Manila due to the dominant easterly winds in the Philippines in March (Fig. 2c) and more localized sources."

12. 3.2.3: Author should add SSA to identify aerosol mass type as in Table 2. Besides avoid explaining individual aerosol optical properties in the result discussion part, instead focus on results. This is true for all sub sections in 3.2.

Response: SSA has been added as criteria in Table 2 as shown below. The text under SSA has been edited to include the comparison to biomass burning SSA observed values as indicated in Table 2. We maintained the flow of discussion for ease of reading and discussion.

Table 2: Summary of threshold values of aerosol optical depth (AOD), angstrom exponent (AE), fine mode fraction (FMF), and single scattering albedo (SSA) used to identify air mass types.

Air Mass Type	AOD	AE	FMF	SSA	Source
Clean Fine	< 0.1[a]	> 1[a]	> 0.7[a]	-	Sorooshian et al., 2013
Polluted Fine	> 0.1[a]	> 1[a]	> 0.7[a]	-	Sorooshian et al., 2013
Clean Coarse	< 0.1[a]	< 1[a]	< 0.3[a]	-	Sorooshian et al., 2013
Polluted Coarse	> 0.1[a]	< 1[a]	< 0.3[a]	-	Sorooshian et al., 2013
Clean Marine	< 0.2[b]	< 0.9[d]	-	0.98[e]	Kaskaoutis et al., 2009 Dubovik et al., 2002
Urban/Industrial	> 0.2[b]	> 1[d]	-	0.9-0.98[e]	Kaskaoutis et al., 2009 Dubovik et al., 2002
Biomass Burning	-	> 1.4[a]	-	0.89-0.95[e]	Deep et al., 2021 Dubovik et al., 2002
Desert Dust	> 0.3[c]	< 1[d]	-	0.92-0.93[e]	Kaskaoutis et al., 2009 Deep et al., 2021 Dubovik et al., 2002

[a] from MODIS   [c] AOD at 400 nm   [e] SSA at 440 nm

[b] AOD at 500 nm   [d] AE at 380 nm to 870 nm

"Monthly median SSA values were largest in June (0.94 at 440 nm), suggesting the presence of more reflective aerosol particles, and smallest in August (0.88 at 440 nm and 0.78 at 1020 nm) suggesting more absorptive particles that are similar in range to the SSA of biomass burning particles (Table 2)."

13. Section 3.3.2: Include SSA as an additional parameter to characterize aerosol mass and re discuss the result.

Response: SSA has been added to the figure referenced in section 3.3.2. The updated figure is shown below. The discussions in the text have also been updated to include SSA and are noted below as well.
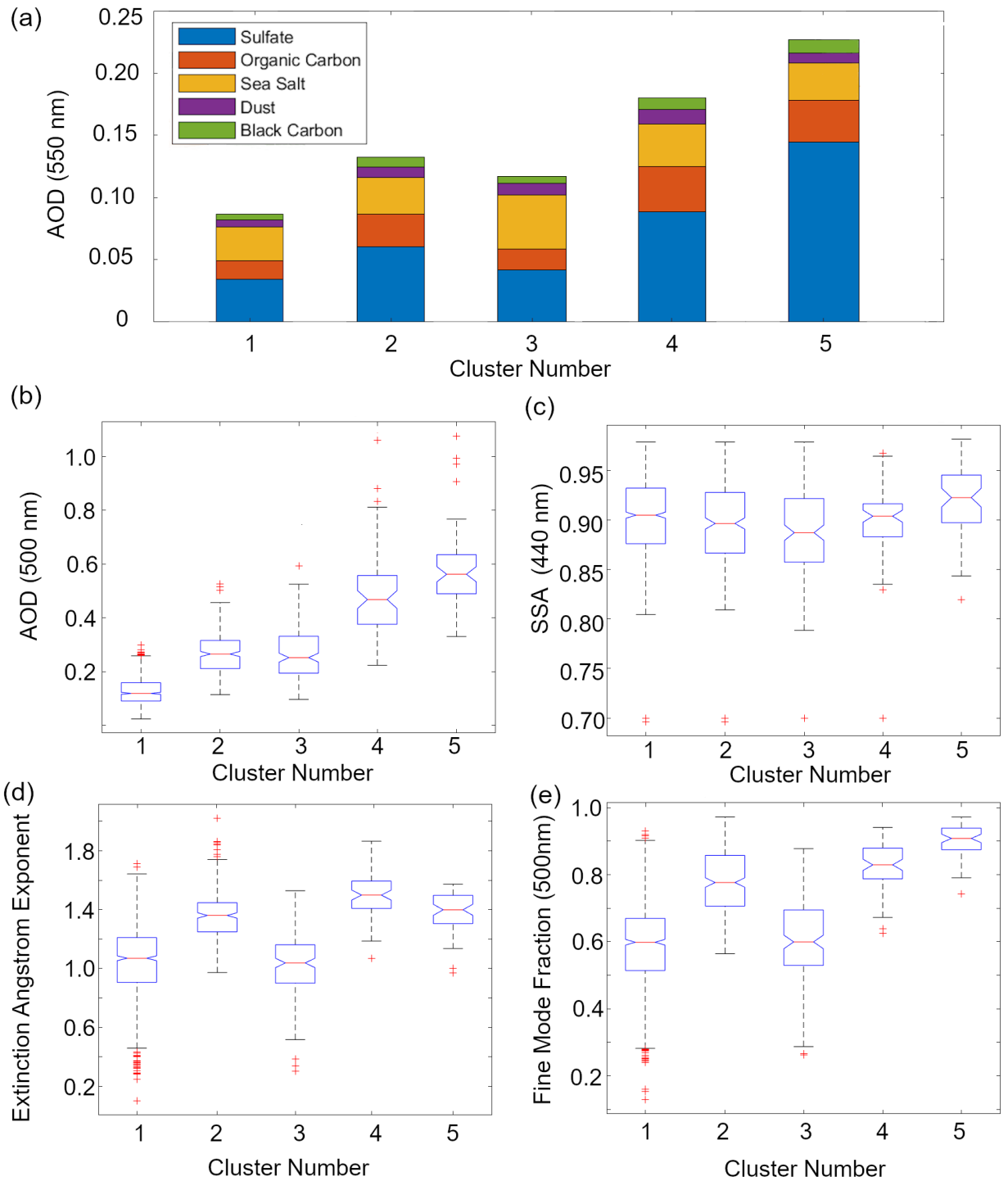
Figure 7: (a) Average compositional contributions to aerosol optical depth (AOD, 550 nm) from MERRA-2 per identified cluster (counts per cluster from 1 to 5: 830, 284, 166, 74, 65). Boxplots of AERONET (b) total AOD (500 nm), (c) single scattering albedo (SSA, 440 nm), (d) extinction angstrom exponent (EAE, 440 nm – 870 nm total), and (e) fine mode fraction (FMF, 500 nm) per cluster.

3.3.2 "The median SSA (0.90 at 440 nm) for cluster 1 (Fig. 7c), however, suggests the presence of absorbing particles most probably due to high black carbon in the local source (Cruz et al., 2019) that is mixed in with this generally clean marine source."

"The median SSA for cluster 2 (0.90 at 440 nm) is also similar to cluster 1 (Fig. 7c) where the local and background particles are mixed. Cluster 2 could be a fine polluted background source superimposed on the dominant marine source."

"Median SSA (0.89 at 440 nm) was lowest for cluster 3 (Fig. 7c), this and the relatively high coarse particle contribution suggests cluster 3 as a possible dust source based on past studies (Lee et al., 2010). This air mass can be a mixture of local and transported dust air masses, the large sea salt contribution (~37%) to total AOD (Sect. 3.3.1) can be related to long-range transport."

"The median SSA for cluster 4 (0.90 at 440 nm) was similar to clusters 1 and 2 (Fig. 7c), but the maximum SSA value for this cluster was lowest in general among all the clusters suggesting cluster 4 has the net most absorptive effect. The cluster 4 air mass is probably from local sources and transported biomass burning emissions."

"Cluster 5 had the highest median total AOD (0.56) and FMF (0.91) values (Fig. 7b and 7e). It also had the highest sulfate contribution (~64%) to total AOD (Fig. 7a), the highest median SSA (0.92 at 440 nm) (Fig. 7c), and a shifted accumulation mode peak (Fig. 6a). These characteristics suggest that cluster 5 is a possible cloud processing air mass (Eck et al., 2012)."

References:

Amnuaylojaroen, T.: Air Pollution Modeling in Southeast Asia—An Overview, Vegetation Fires and Pollution in Asia, 531-544, https://doi.org/10.1007/978-3-031-29916-2_31, 2023.
Bagtasa, G.: Contribution of tropical cyclones to rainfall in the Philippines, Journal of Climate, 30, 3621-3633, 2017.
Bautista VII, A. T., Pabroa, P. C. B., Santos, F. L., Racho, J. M. D., and Quirit, L. L.: Carbonaceous particulate matter characterization in an urban and a rural site in the Philippines, Atmospheric Pollution Research, 5, 245-252, https://doi.org/10.5094/APR.2014.030, 2014.
Cahyono, W. E., Setyawati, W., Hamdi, S., Cholianawati, N., Kombara, P. Y., and Sari, W. J.: Observations of aerosol optical properties during tropical forest fires in Indonesia, Materials Today: Proceedings, 63, S445-S450, https://doi.org/10.1016/j.matpr.2022.04.113, 2022.
Caido, N. G., Ong, P. M., Rempillo, O., Galvez, M. C., and Vallar, E.: Spatiotemporal analysis of MODIS aerosol optical depth data in the Philippines from 2010 to 2020, Atmosphere, 13, 939, https://doi.org/10.3390/atmos13060939, 2022.
Chang, C.-P., Wang, Z., McBride, J., and Liu, C.-H.: Annual cycle of Southeast Asia—Maritime Continent rainfall and the asymmetric monsoon transition, Journal of climate, 18, 287-301, https://doi.org/10.1175/JCLI-3257.1, 2005.
Chen, Q., McGowan, S., Gouramanis, C., Fong, L., Balasubramanian, R., and Taylor, D.: Rapidly rising transboundary atmospheric pollution from industrial and urban sources in

Southeast Asia and its implications for regional sustainable development, Environ. Res. Lett., 15, 1040a1045, https://doi.org/10.1088/1748-9326/abb5ce, 2020.

Cohen, J. B.: Quantifying the occurrence and magnitude of the Southeast Asian fire climatology, Environmental Research Letters, 9, 114018, https://dx.doi.org/10.1088/1748-9326/9/11/114018, 2014.

Cruz, M. T., Bañaga, P. A., Betito, G., Braun, R. A., Stahl, C., Aghdam, M. A., Cambaliza, M. O., Dadashazar, H., Hilario, M. R., Lorenzo, G. R., Ma, L., MacDonald, A. B., Pabroa, C., Yee, J. R., Simpas, J. B., and Sorooshian, A.: Size-resolved composition and morphology of particulate matter during the southwest monsoon in Metro Manila, Philippines, Atmos. Chem. Phys., 19, 10675–10696, https://doi.org/10.5194/acp-19-10675-2019, 2019.

Cruz, M. T., Simpas, J. B., Sorooshian, A., Betito, G., Cambaliza, M. O. L., Collado, J. T., Eloranta, E. W., Holz, R., Topacio, X. G. V., and Del Socorro, J.: Impacts of regional wind circulations on aerosol pollution and planetary boundary layer structure in Metro Manila, Philippines, Atmos. Environ., 293, 119455, https://doi.org/10.1016/j.atmosenv.2022.119455, 2023.

Dong, X., and Fu, J. S.: Understanding interannual variations of biomass burning from Peninsular Southeast Asia, part II: Variability and different influences in lower and higher atmosphere levels, Atmospheric Environment, 115, 9-18, https://doi.org/10.1016/j.atmosenv.2015.05.052, 2015.

Dorado, S. V., Holdsworth, J. L., Lagrosas, N. C., Villarin, J. R., Narisma, G., Ellis, J., and Perez, R.: Characterization of urban atmosphere of Manila with lidar, filter sampling, and radiosonde, Lidar Remote Sensing for Industry and Environment Monitoring, 2001, 591-598.

Eck, T. F., Holben, B., Reid, J., Dubovik, O., Smirnov, A., O'neill, N., Slutsker, I., and Kinne, S.: Wavelength dependence of the optical depth of biomass burning, urban, and desert dust aerosols, J. Geophys. Res.- Atmos., 104, 31333-31349, https://doi.org/10.1029/1999JD900923, 1999.

Eck, T. F., Holben, B. N., Reid, J., Giles, D., Rivas, M., Singh, R. P., Tripathi, S., Bruegge, C., Platnick, S., and Arnold, G.: Fog-and cloud-induced aerosol modification observed by the Aerosol Robotic Network (AERONET), J. Geophys. Res.- Atmos., 117, https://doi.org/10.1029/2011JD016839, 2012.

Eckstein, D., Hutfils, M.-L., and Winges, M.: Global climate risk index 2019, in: Who suffers most from extreme weather events, www.resourcewatch.org, Resource Watch, 36, 2018.

Gautam, R., Hsu, N. C., Eck, T. F., Holben, B. N., Janjai, S., Jantarach, T., Tsay, S.-C., and Lau, W. K.: Characterization of aerosols over the Indochina peninsula from satellite-surface observations during biomass burning pre-monsoon season, Atmos. Environ., 78, 51-59, https://doi.org/10.1016/j.atmosenv.2012.05.038, 2013.

Glover, D., and Jessup, T.: The Indonesian fires and haze of 1997: the economic toll, Economy and Environment Program for SE Asia (EEPSEA) Singapore and the World Wildlife Fund (WWF) Indonesia, Jakarta, 1998.

Hendrickson, B. N., Brooks, S. D., Thornton, D. C., Moore, R. H., Crosbie, E., Ziemba, L. D., Carlson, C. A., Baetge, N., Mirrielees, J. A., and Alsante, A. N.: Role of sea surface microlayer properties in cloud formation, Frontiers in Marine Science, 7, 596225, https://doi.org/10.3389/fmars.2020.596225, 2021.

Hyer, E. J., Reid, J. S., Prins, E. M., Hoffman, J. P., Schmidt, C. C., Miettinen, J. I., and Giglio, L.: Patterns of fire activity over Indonesia and Malaysia from polar and geostationary satellite observations, Atmos. Res., 122, 504-519, https://doi.org/10.1016/j.atmosres.2012.06.011, 2013.

Kiely, L., Spracklen, D. V., Wiedinmyer, C., Conibear, L., Reddington, C. L., Archer-Nicholls, S., Lowe, D., Arnold, S. R., Knote, C., and Khan, M. F.: New estimate of particulate emissions from Indonesian peat fires in 2015, Atmospheric Chemistry and Physics, 19, 11105-11121, https://doi.org/10.5194/acp-19-11105-2019, 2019.

Kleidman, R., O'Neill, N., Remer, L., Kaufman, Y., Eck, T., Tanré, D., Dubovik, O., and Holben, B.: Comparison of Moderate Resolution Imaging Spectroradiometer (MODIS) and Aerosol Robotic Network (AERONET) remote-sensing retrievals of aerosol fine mode fraction over ocean, Journal of Geophysical Research: Atmospheres, 110, 2005.

Lee, H.-H., Iraqui, O., Gu, Y., Yim, S. H.-L., Chulakadabba, A., Tonks, A. Y.-M., Yang, Z., and Wang, C.: Impacts of air pollutants from fire and non-fire emissions on the regional air quality in Southeast Asia, Atmos. Chem. Phys., 18, 6141-6156, https://doi.org/10.5194/acp-18-6141-2018, 2018.

Lee, J., Kim, J., Song, C., Kim, S., Chun, Y., Sohn, B., and Holben, B.: Characteristics of aerosol types from AERONET sunphotometer measurements, Atmospheric Environment, 44, 3110-3117, https://doi.org/10.1016/j.atmosenv.2010.05.035, 2010.

Lynch, P., Reid, J. S., Westphal, D. L., Zhang, J., Hogan, T. F., Hyer, E. J., Curtis, C. A., Hegg, D. A., Shi, Y., and Campbell, J. R.: An 11-year global gridded aerosol optical thickness reanalysis (v1. 0) for atmospheric and climate sciences, Geosci. Model Dev., 9, https://doi.org/10.5194/gmd-9-1489-2016, 2016.

Nakata, M., Mukai, S., and Yasumoto, M.: Seasonal and regional characteristics of aerosol pollution in east and southeast Asia, Frontiers in Environmental Science, 6, 29, https://doi.org/10.3389/fenvs.2018.00029, 2018.

Nguyen, T. T., Pham, H. V., Lasko, K., Bui, M. T., Laffly, D., Jourdan, A., and Bui, H. Q.: Spatiotemporal analysis of ground and satellite-based aerosol for air quality assessment in the Southeast Asia region, Environmental Pollution, 255, 113106, https://doi.org/10.1016/j.envpol.2019.113106, 2019.

Oanh, N. K., Upadhyay, N., Zhuang, Y.-H., Hao, Z.-P., Murthy, D., Lestari, P., Villarin, J., Chengchua, K., Co, H., and Dung, N.: Particulate air pollution in six Asian cities: Spatial and temporal distributions, and associated sources, Atmospheric environment, 40, 3367-3380, https://doi.org/10.1016/j.atmosenv.2006.01.050, 2006.

Ong, H. J. J., Lagrosas, N., Uy, S. N., Gacal, G. F. B., Dorado, S., Tobias Jr, V., and Holben, B.: Determination of Monthly Aerosol Types in Manila Observatory and Notre Dame of Marbel University from Aerosol Robotic Network (AERONET) measurements, AGU Fall Meeting Abstracts, 2016, A54E-03.

Ramage, C. S.: Monsoon meteorology, Academic Press, New York, 1971.

Reid, J., Maring, H., Narisma, G., van den Heever, S., Di Girolamo, L., Ferrare, R., Holz, R., Lawson, P., Mace, G., and Simpas, J.: The coupling between tropical meteorology, aerosol lifecycle, convection, and radiation, during the Cloud, Aerosol and Monsoon Processes Philippines Experiment (CAMP 2 Ex), B. Am. Meteorol. Soc., https://doi.org/10.1175/BAMS-D-21-0285.1, 2023.

Rolph, G., Stein, A., and Stunder, B.: Real-time environmental applications and display system: READY, Environ. Modell. Softw., 95, 210-228, https://doi.org/10.1016/j.envsoft.2017.06.025, 2017.

Stein, A., Draxler, R. R., Rolph, G. D., Stunder, B. J., Cohen, M., and Ngan, F.: NOAA's HYSPLIT atmospheric transport and dispersion modeling system, B. Am. Meteorol. Soc., 96, 2059-2077, https://doi.org/10.1175/BAMS-D-14-00110.1, 2015.

Tsay, S.-C., Hsu, N. C., Lau, W. K.-M., Li, C., Gabriel, P. M., Ji, Q., Holben, B. N., Welton, E. J., Nguyen, A. X., and Janjai, S.: From BASE-ASIA toward 7-SEAS: A satellite-surface perspective of boreal spring biomass-burning aerosols and clouds in Southeast Asia, Atmospheric environment, 78, 20-34, https://doi.org/10.1016/j.atmosenv.2012.12.013, 2013.

Wall, C. J., Norris, J. R., Possner, A., McCoy, D. T., McCoy, I. L., and Lutsko, N. J.: Assessing effective radiative forcing from aerosol–cloud interactions over the global ocean, Proceedings of the National Academy of Sciences, 119, e2210481119, https://doi.org/10.1073/pnas.2210481119, 2022.

Wang, S.-H., Welton, E. J., Holben, B. N., Tsay, S.-C., Lin, N.-H., Giles, D., Stewart, S. A., Janjai, S., Nguyen, X. A., and Hsiao, T.-C.: Vertical distribution and columnar optical properties of springtime biomass-burning aerosols over Northern Indochina during 2014 7-SEAS campaign, Aerosol and Air Quality Research, 15, 2037-2050, https://doi.org/10.4209/aaqr.2015.05.0310, 2015.

Yang, S., Lau, W. K., Ji, Z., Dong, W., and Yang, S.: Impacts of radiative effect of pre-monsoon biomass burning aerosols on atmospheric circulation and rainfall over Southeast Asia and southern China, Climate Dynamics, 59, 417-432, https://doi.org/10.1007/s00382-021-06135-7, 2022.

Yumul Jr, G. P., Cruz, N. A., Dimalanta, C. B., Servando, N. T., and Hilario, F. D.: The 2007 dry spell in Luzon (Philippines): its cause, impact and corresponding response measures, Climatic change, 100, 633-644, https://doi.org/10.1007/s10584-009-9677-0, 2010.

1   An Emerging Aerosol Climatology via Remote Sensing over Metro Manila, Philippines

3   Genevieve Rose Lorenzo[1,2], Avelino F. Arellano[1], Maria Obiminda Cambaliza[2,3], Christopher
4   Castro[1], Melliza Templonuevo Cruz[2,4], Larry Di Girolamo[5], Glenn Franco Gacal[2], Miguel
5   Ricardo A. Hilario[1], Nofel Lagrosas[6], Hans Jarett Ong[2], James Bernard Simpas[2,3], Sherdon Niño
6   Uy[2], and Armin Sorooshian[1,7]

8   [1]Department of Hydrology and Atmospheric Sciences, University of Arizona, Tucson, Arizona,
9   85721, USA
10   [2]Air Quality Dynamics-Instrumentation & Technology Development Laboratory, Manila
11   Observatory, Quezon City, 1108, Philippines
12   [3]Department of Physics, School of Science and Engineering, Ateneo de Manila University,
13   Quezon City, 1108, Philippines
14   [4]Institute of Environmental Science and Meteorology, University of the Philippines, Diliman,
15   Quezon City, 1101, Philippines
16   [5]Department of Atmospheric Science, University of Illinois, Urbana-Champlain, Illinois, 61801,
17   USA
18   [6]Center for Environmental Remote Sensing, Chiba University, Chiba, 263-8522, Japan
19   [7]Department of Chemical and Environmental Engineering, University of Arizona, Tucson,
20   Arizona, 85721, USA

22   *Correspondence to:* armin@arizona.edu

Abstract

Aerosol particles in Southeast Asia ~~have a complex life cycle and consequently~~ are challenging to characterize. ~~The~~ due to their complex life cycle within the diverse topography and weather in the region ~~complicate the situation.~~. An emerging aerosol climatology was established based on AERONET data (December 2009 to October 2018) for clear sky days in Metro Manila, Philippines. Aerosol optical depth (AOD) values were highest ~~in~~from August~~, coinciding with the summer southwest monsoon, due~~ to October, partly ~~to~~from fine ~~particles from~~ urban aerosol particles, including soot~~. Also, August corresponds to~~, coinciding with the burning season in Insular Southeast Asia when smoke is often transported to Metro Manila during the southwest monsoon. Clustering of AERONET volume size distributions (VSD) resulted in five aerosol particle sources based on the position and magnitude of their peaks in the VSD and the contributions of specific particle species to AOD per cluster based on MERRA-2. The clustering showed that the majority of aerosol particles above Metro Manila were from a clean marine source (58%), which could be related to AOD values there being relatively smaller than in other cities in the region. The following are the other particle sources over Metro Manila: fine polluted (20%), mixed ~~polluted~~dust (12%), urban/industrial (5%), and cloud processing (5%). Furthermore, MERRA-2 AOD data over Southeast Asia were analyzed using empirical orthogonal functions. Along with AOD fractional compositional contributions and wind regimes, four dominant aerosol particle air masses emerged: two sulfate air masses from East Asia, an organic carbon source from Indonesia, and a sulfate source from the Philippines. Knowing the local and regional aerosol particle air masses that impact Metro Manila is useful in identifying the sources while gaining insight on how aerosol particles are affected by long-range transport and their impact on regional weather.

1. Introduction

Although Southeast Asia is one of the most rapidly developing regions in the world, ~~there have been limited studies characterizing~~ with a growing number of extensive research conducted (Reid et al., 2023), there remain knowledge gaps related to aerosol particles in the area (Tsay et al., 2013; Lee et al., 2018; Chen et al., 2020; Amnuaylojaroen, 2023). The region represents a complex geographic, meteorological, and hydrological environment making it challenging to understand aerosol particle characteristics, especially interactions between aerosol particles with their environment (Reid et al., 2013). The island of Luzon in the Philippines in particular is very populated and is characterized by high levels of anthropogenic emissions superimposed on natural emissions from the surrounding waters (AzadiAghdam et al., 2019) and long-range transport of emissions from areas such as Indonesia and East Asia (Braun et al., 2020; Hilario et al., 2020a; Hilario et al., 2020b; Hilario et al., 2021a). Aerosol particle lifecycle in the region is impacted by Philippine weather that is marked by two distinct monsoons, typhoons, the intertropical convergent zone, and impacts from El Niño-Southern Oscillation and Madden-Julian Oscillation (Cruz et al., 2013; Xian et al., 2013; Reid et al., 2012; Reid et al., 2015; Hilario et al., 2021b). Studying this area is informative owing to the wide dynamic range in aerosol particle and weather conditions, which are interconnected. ~~The presence of~~The overlapping of large fraction of cirrus clouds with lower clouds in the area (Hong and Di Girolamo, 2020) makes space-borne remote sensing of aerosol particles very challenging (Reid et al., 2013; Lin et al., 2014). These reasons motivated the NASA Cloud, Aerosol, and Monsoon Processes Philippines Experiment (CAMP^{2}Ex) airborne measurement campaign in 2019 to understand the interaction between tropical meteorology and aerosol particles (Di Girolamo et al., 2015; Reid et al., 2023). ~~Prior to the airborne measurements, intensive surface-based measurements were conducted as part of the CAMP^{2}Ex weatHEr and CompoSition Monitoring (CHECSM) study between July 2018 and October 2019~~However, those short terms measurements cannot provide an adequate assessment of aerosol behavior across all seasons and over many years.

~~Aerosol climatology studies in different regions have proved beneficial to understand temporal characteristics of aerosol particle concentrations and properties, in addition to identifying potential source regions along with interactions with clouds and rainfall (Stevens and Feingold, 2009; Li et al., 2011; Tao et al., 2012; Crosbie et al., 2014; Kumar et al., 2015; Alizadeh-Choobari and Gharaylou, 2017; Mora et al., 2017; Aldhaif et al., 2021).~~The NASA AErosol RObotic NETwork (AERONET) (Holben et al., 1998) is pivotal in providing broad temporal coverage of aerosol characteristics in specific locations with a column-based perspective from the ground up. Aerosol climatology studies in different regions have proved beneficial to understand temporal characteristics of aerosol particle concentrations and properties, in addition to identifying potential source regions along with interactions with clouds and rainfall (Stevens and Feingold, 2009; Li et al., 2011; Tao et al., 2012; Crosbie et al., 2014; Kumar et al., 2015; Alizadeh-Choobari and Gharaylou, 2017; Mora et al., 2017; Aldhaif et al., 2021). ~~in specific locations with a column-based perspective from the ground up.~~To our knowledge, there has not been a remote sensing-based aerosol climatology study for the Metro Manila region of Luzon, which has approximately 16 cities, a population of 12.88 million, and a high population density of 20,800 km^{-2} (PSA, 2016; Alas et al., 2018). ~~Studying this area is informative owing to the wide dynamic range in aerosol particle and weather conditions, which are interconnected. Aerosol particle lifecycle in the region is impacted by Philippine weather that is marked by two distinct monsoons, typhoons, and impacts from El Niño-Southern Oscillation and Madden-Julian~~

91 ~~Oscillation (Cruz et al., 2013; Xian et al., 2013; Reid et al., 2012; Reid et al., 2015; Hilario et al.,~~
92 ~~2021b).~~

93 ~~Regional analysis of aerosol particles in Southeast Asia and Asia in general show the prevalence~~
94 ~~of biomass burning in the region, as well as the larger influence of anthropogenic emissions in~~
95 ~~East Asia (Nakata et al., 2018). These large prevalent sources may overshadow other relevant but~~
96 ~~weaker sources in the region, such as local sources. Due to the complex nature of aerosol~~
97 ~~particles, analysis techniques such as principal component analysis and clustering along with~~
98 ~~recent improvements in gridded datasets help detect spatial and temporal patterns that would~~
99 ~~otherwise be difficult to make with noise interference and even weak signals (Li et al., 2013;~~
100 ~~Sullivan et al., 2017; Plymale et al., 2021). Understanding the dominant air masses around~~
101 ~~Southeast Asia will help in distinguishing local and transported particles that influence the~~
102 ~~aerosol climatology in Metro Manila.~~ Most of the past studies involving long-term remotely
103 sensed aerosol particle data in Southeast Asia (Cohen, 2014; Nakata et al., 2018; Nguyen et al.,
104 2019b) had no specific focus on the Philippines. The Philippines is considered as part of the
105 Maritime Continent (MC), the island nations sub-region of Southeast Asia. The other Southeast
106 Asia sub-region, Peninsular Southeast Asia (PSEA), comprises those nations within the
107 continental Asia land mass. These two regions have separate aerosol sources and climate, where
108 MC is dependent on the intertropical convergent zone (ITCZ) and PSEA is dependent on both
109 the ITCZ and monsoon systems (Dong and Fu, 2015). Only the southern part of the Philippines
110 is climatologically part of MC (Ramage, 1971), however, and northwest Philippines, where
111 Metro Manila is located, is affected by the monsoons and tropical cyclones aside from the ITCZ
112 (Chang et al., 2005; Yumul Jr et al., 2010; Bagtasa, 2017). These unique meteorological
113 influences and extensive local aerosol particle sources warrant a unique aerosol climatology over
114 Metro Manila, one of a polluted source in a tropical marine environment, and its effects on cloud
115 formation in the area. Aerosol effects on clouds in the marine environment are associated with
116 the largest uncertainties in climate change research (Hendrickson et al., 2021; Wall et al., 2022)
117 and the Philippines was ranked as the 5th country globally as most at risk to climate change and
118 extreme weather from 1997 to 2018 (Eckstein et al., 2018). There have been several surface
119 measurements of aerosol particles made in Metro Manila for the past 20 years (Oanh et al., 2006;
120 Bautista VII et al., 2014; Cruz et al., 2019) but columnar ground-based measurements there are
121 just beginning to be established (Dorado et al., 2001; Ong et al., 2016; Cruz et al., 2023). The
122 AERONET sun photometer is one of the first long-term column-based aerosol instruments in
123 Metro Manila and the Philippines (Ong et al., 2016).

124 The goal of this study is to use multi-year AERONET data in Manila Observatory along with
125 other complementary datasets (MERRA-2, PERSIANN, MISR, HYSPLIT, and NAAPS) to
126 address the following questions: (1) what are the monthly characteristics of aerosol particles over
127 Metro Manila, Philippines?; (2) what are the possible sources and factors influencing the
128 observed characteristics?; (3) what relationships are evident between aerosol particles and cloud
129 characteristics?; and (4) what are the regional and local aerosol particle air masses that influence
130 Metro Manila?
131

2. Methods

This work relies on analysis of several datasets summarized in Table 1 and the following subsections. The common time range used for all datasets is between January 2009 and October 2018.

Table 1: Summary of datasets over Metro Manila used in this work covering the period from January 2009 to October 2018.

Parameter	Data Source	Spatial Coverage	~~Data Repository~~ Time Coverage
			~~(AERONET)~~
Aerosol Optical Depth (500 nm)	AERONET	14.635°N, 121.078°E	~~https://aeronet.gsfc.nasa.gov~~ Jan 2009 - Oct 2018
Asymmetry Factor (440 nm - 1020 nm)	AERONET	14.635°N, 121.078°E	Jan 2009 - Oct 2018
Extinction Angstrom Exponent (440 nm -870 nm)	AERONET	14.635°N, 121.078°E	Jan 2009 - Oct 2018
Fine Mode Fraction	AERONET	14.635°N, 121.078°E	Jan 2009 - Oct 2018
Precipitable Water	AERONET	14.635°N, 121.078°E	Jan 2009 - Oct 2018
Single Scattering Albedo (440 nm - 1020 nm)	AERONET	14.635°N, 121.078°E	Jan 2009 - Oct 2018
Refractive Index (Real and Imaginary; 440 nm - 1020 nm)	AERONET	14.635°N, 121.078°E	Jan 2009 - Oct 2018
Volume Size Distribution	AERONET	14.635°N, 121.078°E	Jan 2009 - Oct 2018
Low Cloud Fraction (MODIS)	MERRA-2	14.~~25~~3°N - 14.~~75~~8°N, 120.~~9375~~75°E - 121.~~5625~~25°E	~~(MERRA-2)~~ ~~https://disc.gsfc.nasa.gov/~~ Jan 2009 - Dec 2018
Planetary Boundary Layer Height	MERRA-2	14.~~25~~3°N - 14.~~75~~8°N, 120.~~9375~~75°E - 121.~~5625~~25°E	Jan 2009 - Dec 2018
Relative Humidity (975 mb)	MERRA-2	14.~~25~~3°N - 14.~~75~~8°N, 120.~~9375~~75°E - 121.~~5625~~25°E	Jan 2009 - Dec 2018
Sea Level Pressure	MERRA-2	14.~~25~~3°N - 14.~~75~~8°N, 120.~~9375~~75°E - 121.~~5625~~25°E	Jan 2009 - Dec 2018
Temperature (975 mb)	MERRA-2	14.~~25~~3°N - 14.~~75~~8°N, 120.~~9375~~75°E - 121.~~5625~~25°E	Jan 2009 - Dec 2018
Wind (975 mb)	MERRA-2	14.~~25~~3°N - 14.~~75~~8°N, 120.~~9375~~75°E - 121.~~5625~~25°E	Jan 2009 - Dec 2018
Total Extinction Aerosol Optical Depth (550 nm)	MERRA-2	14.3°N - 14.8°N, 120.75°E - 121.25°E	Jan 2009 - Dec 2018
Sulfate, Black Carbon, Organic Carbon, Dust, and Sea Salt Extinction Aerosol Optical Depth (550 nm)	MERRA-2	14.3°N - 14.8°N, 120.75°E - 121.25°E	Jan 2009 - Dec 2018
Precipitation	PERSIANN	14.~~5~~3°N - ~~15.0~~14.8°N, 120.75°E - 121.25°E	~~(PERSIANN)~~ ~~https://chrsdata.eng.uci.edu/~~ Jan 2009 - Dec 2018

2.1 Datasets

2.1.1 AERONET

The central dataset used is that of sun photometer measurements and derived (inversion) parameters from the AERONET (Holben et al., 1998) site at the Manila Observatory in Quezon City, Philippines (14.64°-N, 121.08°-E, ~70 m. a. s. l.). Direct sunlight extinction measurements were made at nominal wavelengths of 340, 380, 440, 500, 675, 870, 940, and 1020 nm, from

145 which aerosol optical depth (AOD) was calculated (except for 940 nm, which is for water vapor)
146 (Eck et al., 2013). AOD is a commonly used proxy for aerosol particle loading in the air column
147 from the ground up (Holben et al., 2001); higher AOD translates to more aerosol particle
148 extinction in the column above a location. The extinction angstrom exponent (EAE) and the fine
149 mode fraction (FMF) are also AERONET direct sun products that are retrieved after the
150 application of a spectral de-convolution algorithm (O'Neill et al., 2003). For the inversion
151 products, it is through radiative retrievals that the volume size distribution (VSD) and complex
152 refractive index (RI) are gathered (Schuster et al., 2005) and from which single scattering albedo
153 (SSA) and asymmetry factor (AF) are calculated. and from which single scattering albedo (SSA)
154 and asymmetry factor (AF) are calculated. The AERONET observations were made during clear
155 sky conditions, which has been shown (Hong and Di Girolamo, 2022) to be able to represent all
156 sky conditions.

157 For the inversions, four wavelengths (440, 670, 870, and 1020 nm) of the radiometer spectral
158 channels were chosen for diffuse radiance measurements and to avoid gas absorption (Dubovik
159 et al., 1998). Version 3 Direct Sun and Inversion algorithms (AERONET, 2019; Giles et al.,
160 2019) were used with the Almucantar Sky Scan Scenario to derive the following parameters with
161 level 2.0 (automatically cloud-cleared and quality controlled datasets with pre- and post-field
162 calibrations) data quality: column AOD (500 nm), fine mode fraction (500 nm), extinction
163 angstrom exponent (440 – 870 nm), precipitable water (940 nm), SSAsingle scattering albedo
164 (440, 670, 870, and 1020 nm), asymmetry factor (440, 670, 870, and 1020 nm), refractive index
165 (440, 670, 870, and 1020 nm), and VSD. The version 3 products are able to keep fine mode
166 aerosol particle data (haze and smoke) as well as remove optically thin cirrus clouds in order to
167 retain more aerosol particle measurements in the database (Giles et al., 2019). Cloud screening in
168 the version 3 product improves remote sensing measurements in Southeast Asia in general,
169 where cirrus clouds are pervasive (Reid et al., 2013). At most, a total of 29,037 direct sun and
170 1419 inversion AERONET daytime data points were available between January 2009 and
171 October 2018.

172 2.1.2 MERRA-2
173 Modern Era-Retrospective Analysis for Research and Applications, Version 2 (MERRA-2: 0.5°
174 × 0.625° approximate resolution) meteorological and aerosol particle composition reanalysis data
175 (Bosilovich, 2016; Gelaro et al., 2017; Randles et al., 2017) were acquired for the area around
176 Manila Observatory (14.25°N – 14.75°N, 120.9375°E – 121.5625°E). The aerosol reanalysis
177 data includes data assimilation of AOD from the Moderate Resolution Imaging
178 Spectroradiometer (MODIS: Terra, 2000 to present and Aqua, 2002 to present), Advanced Very
179 High Resolution Radiometer (AVHRR, 1979-2002), and Multiangle Imaging SpectroRadiometer
180 (MISR, 2000-2014) (Buchard et al., 2017; Rizza et al., 2019). The following products were used:
181 M2I3NPASM Assimilated Meteorological Fields (3-hourly) for 975 mb level winds,
182 temperature, relative humidity, and sea level pressure; M2T1NXFLX Surface Flux Diagnostics
183 (1-hourly from 00:30 UTC time-averaged) 2D for planetary boundary layer height; and
184 M2T1NXCSP COSP Satellite Simulator (1-hourly from 00:30 UTC time-averaged) for MODIS
185 mean low cloud fraction (cloud top pressure > 680 hPa); and M2T1NXAER Aerosol Diagnostics
186 (1-hourly from 00:30 UTC time-averaged) for Total AOD and speciated AOD (Sulfate, Black
187 Carbon (BC), Organic Carbon (OC), Dust, and Sea Salt).

188 MERRA-2 meteorological and aerosol particle composition monthly mean reanalysis data
189 (Bosilovich, 2016; Gelaro et al., 2017; Randles et al., 2017) were also acquired for a larger
190 region, (30° × 30°), the Southeast Asia region (0°–N – 30°N, 105°E – 135°E) for the period from
191 2009 to 2018. This is within the spatial domain of the CAMP^{2}Ex airborne measurement
192 campaign which, as mentioned earlier, targets the interaction between tropical meteorology and
193 aerosol particles. The following datasets (0.5° latitude and 0.625° longitude resolution) were
194 used: MERRA-2 tavgM_2d_aer_Nx: Aerosol Assimilation (M2TMNXAER) for Total 500 nm
195 AOD and speciated 500 nm AOD (Sulfate, Black Carbon (BC), Organic Carbon (, OC),, Dust,
196 and Sea Salt) and MERRA-2 instM_3d_ana_Np: Analyzed Meteorological Fields
197 (M2IMNPANA) for 1000 hPa and 725 hPa level U and V winds. The total MERRA-2 AOD for
198 the region was used along with MISR AOD data to assess the influence of long-range sources to
199 the aerosol column over Manila Observatory. The monthly meteorological and aerosol particle
200 composition data for the region will be used for empirical orthogonal functions, which will be
201 described later.

202 2.1.3 MISR
203 Monthly AOD data (Level 3 Global Aerosol: 0.5° × 0.5° spatial resolution) from 2009 to 2018
204 are used from the Multi-angle Imaging SpectroRadiometer (MISR), (Diner et al., 2007; Garay et
205 al., 2018). Level 3 products are global maps of parameters available in Level 2 (measurements
206 derived from the instrument data) products. MISR has relatively more accurate AOD and agrees
207 better with AERONET data compared to other satellite products due to its multi-angle
208 measurements (Choi et al., 2019; Kuttippurath and Raj, 2021). Monthly median AOD (bin 0)
209 were extracted for Southeast Asia (0.25° – 30.25°N, 104.75°E – 134.75°E) within the CAMP^{2}Ex
210 region. They are used for comparison to the AERONET (over Metro Manila) and MERRA-2
211 (Southeast Asia) monthly AOD values.

212 2.1.4 PERSIANN
213 Hourly precipitation data were obtained from the Precipitation Estimation from the Remotely
214 Sensed Information using Artificial Neural Networks (PERSIANN) (Nguyen et al.,
215 2019)(Nguyen et al., 2019a) database of the Center for Hydrometeorology and Remote Sensing
216 (CHRS) at the University of California, Irvine (UCI). Hourly data were accumulated for running
217 three-day totals, which were compared to AERONET data. The data were averaged between the
218 four grids that included the area of interest as well as ensuring a similar spatial domain (14.5°N –
219 – 15.0°N, 120.75°E –– 121.25°E) to the MERRA-2 dataset.

220 2.1.4 MISR
221 Monthly 500 nm AOD data (Level 3 Global Aerosol: 0.5° × 0.5° spatial resolution) from 2009 to
222 2018 are used from the Multi-angle Imaging SpectroRadiometer (MISR), (Diner et al., 2007;
223 Garay et al., 2018) as regional (Southeast Asia) baseline remote sensing data to support the
224 Manila Observatory AERONET data. The regional (30° × 30°) MISR data was used to confirm
225 regional sources of aerosols that may be influencing the AOD over Metro Manila. Level 3 MISR
226 products are global maps of parameters available in Level 2 (measurements derived from the
227 instrument data) products. MISR is ideal for remote sensing in the CAMP^{2}Ex region because it
228 has an overpass at 10:30 AM ECT (descending mode) (when cirrus is minimal) and its retrievals
229 have been shown to be unimpacted by small cumulus (Zhao et al., 2009), which are typical in the
230 region. MISR has relatively more accurate AOD and agrees better with AERONET data
231 compared to other satellite products due to its multi-angle measurements (Choi et al., 2019;

7

232 Kuttippurath and Raj, 2021). The MISR sampling noise is relatively small due to the large
233 domain and seasonal averages that are considered in this study. MISR is also the only passive
234 sensor that speciates aerosol particle size and shape. All these factors led to the choice of using
235 regional MISR data to associate long-range sources influencing AERONET data in Manila
236 Observatory. Monthly mean AOD (bin 0) were extracted for Southeast Asia (0.25°N – 30.25°N,
237 104.75°E – 134.75°E) within the CAMP^{2}Ex region. Monthly mean AOD values were then
238 calculated for each 0.5° grid point and then for the 30° × 30° region, where the standard error in
239 the monthly mean for the region is less than 0.002. MISR monthly mean time series of size,
240 shape, and absorption speciated 550 nm AOD and angstrom exponent in the CAMP^{2}Ex domain
241 (6.5°N – 22.5°N, 116.5°E – 128.5°E; March 2000 to December 2020) are also used to support
242 the findings from the AERONET data.

243 2.1.5 NAAPS
244 Archived maps of total and speciated optical depths along withand surface concentrations of
245 sulfate, dust, and smoke for Southeast Asia are used from the Navy Aerosol Analysis and
246 Prediction System (NAAPS: 1⁄3° × 1⁄3° spatial resolution) (Lynch et al., 2016), and which isare
247 publicly available at https://www.nrlmry.navy.mil/aerosol/. This reanalysis product relies on the
248 Navy Global Environmental Model (NAVGEM) for meteorological fields (Hogan et al., 2014).
249 Hourly maps were downloaded for Southeast Asia for aerosol particle events of interest based on
250 AERONET data. These maps help in the identification ofassociate possible regional emission
251 sources. to extreme aerosol loading events in Manila Observatory.

252 2.1.6 NASA WorldviewHYSPLIT
253 Archived maps of cloud fraction (Aqua MODIS and Terra MODIS) were downloaded from
254 NASA Worldview (https://worldview.earthdata.nasa.gov) for events of interest based on
255 AERONET data.
256
257 **2.22.1 Clustering**
258 Available AERONET VSD data (0.050 μm to 15.000 μm particle radius in 22 logarithmically
259 equidistant bins, 1419 data points) were clustered via k-means clustering (Lloyd, 1982). The
260 algorithm used was k-means++ (Arthur and Vassilvitskii, 2006). The ideal number of clusters
261 was chosen based on relatively highest (>0.5) average silhouette value and the presence of a
262 cluster with a second peak in the larger accumulation mode of the VSD. The clusters were
263 analyzed based on their associated meteorological conditions and aerosol particle characteristics
264 and were classified into air mass types (Table 2) based on previous studies (Pace et al., 2006;
265 Kaskaoutis et al., 2007; Sorooshian et al., 2013; Kumar et al., 2014; Sharma et al., 2014; Che et
266 al., 2015; Kumar et al., 2015).

267 **Table 2:** Summary of threshold values of aerosol optical depth (AOD), angstrom exponent (AE),
268 and fine mode fraction (FMF) used to identify air mass types.

Air Mass Type	AOD	AE	FMF	Source
Clean Fine	< 0.1	> 1	> 0.7	Sorooshian et al., 2013
Polluted Fine	> 0.1	> 1	> 0.7	Sorooshian et al., 2013
Clean Coarse	< 0.1	< 1	< 0.3	Sorooshian et al., 2013
Polluted Coarse	> 0.1	< 1	< 0.3	Sorooshian et al., 2013

Desert Dust	> 0.3	-	< 0.6	Kaskaoutis et al., 2007
Clean Marine	< 0.2	-	< 0.7	Kaskaoutis et al., 2007
Urban/Industrial	> 0.2	-	> 0.8	Kaskaoutis et al., 2007

269

270 **2.32.1 Extreme Event Analysis**

271 Selected types of aerosol particle events were identified to characterize different types of sources
272 and processes impacting aerosol particle columnar properties above Metro Manila. The three
273 events are described below.

274 2.3.12.1.1 Smoke Long Range Transport

275 Events related to transported biomass burning/smoke were chosen based on the highest black
276 carbon contribution to total AOD from the MERRA-2 dataset, high smoke contributions to AOD
277 from NAAPS, and a dominant submicrometer peak in the AERONET VSD (Eck et al., 1999)
278 over Metro Manila. Maps of surface smoke contributions from NAAPS as well as backBack-
279 trajectories from the National Oceanic and Atmospheric Administration's (NOAA) Hybrid
280 Single-Particle Lagrangian Integrated Trajectory (HYSPLIT) model (Stein et al., 2015; Rolph et
281 al., 2017) were used to identify the likely source and transport pathway for the smoke cases.
282 Threeprovide support for the AERONET monthly aerosol characteristics and the chosen case
283 studies. Three and seven-day back-trajectories with six-hour resolution were generated based on
284 the NCEP/NCAR reanalysis meteorological dataset and with a resolution of 1° and a vertical
285 wind setting of "model vertical velocity". The three-day data were used to map the density of
286 trajectories reaching Manila Observatory in each month from 2008 to 2019. The seven-day data
287 were used in the analysis of the case studies. Trajectories were computed for an end point with
288 an altitude of 500 m above ground level at the Manila Observatory. This altitude represents the
289 mixed layer based on related surface air quality studies (Crosbie et al., 2014; Mora et al., 2017;
290 Schlosser et al., 2017; Aldhaif et al., 2020), including a previous study for the same area (Stahl et
291 al., 2020).

292 2.1.7 NASA Worldview
293 Archived maps of cloud fraction (Aqua MODIS and Terra MODIS) over Metro Manila and
294 Southeast Asia were downloaded from NASA Worldview (https://worldview.earthdata.nasa.gov)
295 for events of interest based on AERONET data.

296

297 **2.2 Clustering**
298 Available AERONET VSD data (0.050 μm to 15.000 μm particle radius in 22 logarithmically
299 equidistant discrete points, 1419 data points) were clustered via k-means clustering (Lloyd,
300 1982). The algorithm used was k-means++ (Arthur and Vassilvitskii, 2006). The ideal number
301 of clusters was chosen based on relatively highest (>0.5) average silhouette value and the
302 presence of a cluster with a second peak in the larger accumulation mode of the VSD. The
303 clusters were analyzed based on their associated meteorological conditions and aerosol particle
304 characteristics and were classified into air mass types (Table 2) based on estimates from previous
305 studies (Dubovik et al., 2002; Pace et al., 2006; Kaskaoutis et al., 2007; Kaskaoutis et al., 2009;
306 Sorooshian et al., 2013; Kumar et al., 2014; Sharma et al., 2014; Che et al., 2015; Kumar et al.,
307 2015; Deep et al., 2021). The first four mentioned air mass types in Table 2 are the most general,
308 and four more classifications based on aerosol particle sources are included. The urban/industrial
309 air mass type here refers to local combustion along with long-range transported biomass burning

310 (Kaskaoutis et al., 2009). While these classifications are not rigid definitions of air masses, they
311 help in understanding the sources that contribute to aerosols in Metro Manila and in identifying
312 cases where certain sources are more influential than others.

313 **Table 2:** Summary of threshold values of aerosol optical depth (AOD), angstrom exponent (AE),
314 fine mode fraction (FMF), and single scattering albedo (SSA) used to identify air mass types.

Air Mass Type	AOD	AE	FMF	SSA	Source
Clean Fine	$< 0.1^a$	$> 1^a$	$> 0.7^a$	-	Sorooshian et al., 2013
Polluted Fine	$> 0.1^a$	$> 1^a$	$> 0.7^a$	-	Sorooshian et al., 2013
Clean Coarse	$< 0.1^a$	$< 1^a$	$< 0.3^a$	-	Sorooshian et al., 2013
Polluted Coarse	$> 0.1^a$	$< 1^a$	$< 0.3^a$	-	Sorooshian et al., 2013
Clean Marine	$< 0.2^b$	$< 0.9^d$	-	0.98^e	Kaskaoutis et al., 2009 Dubovik et al., 2002
Urban/Industrial	$> 0.2^b$	$> 1^d$	-	0.9-0.98^e	Kaskaoutis et al., 2009 Dubovik et al., 2002
Biomass Burning	-	$> 1.4^a$	-	0.89-0.95^e	Deep et al., 2021 Dubovik et al., 2002
Desert Dust	$> 0.3^c$	$< 1^d$	-	0.92-0.93^e	Kaskaoutis et al., 2009 Deep et al., 2021 Dubovik et al., 2002

[a] from MODIS [c] AOD at 400 nm [e] SSA at 440 nm
[b] AOD at 500 nm [d] AE at 380 nm to 870 nm

315

316 **2.3 Extreme Event Analysis**
317 Aerosol particle events based on the three clusters with the highest VSD concentrations were
318 identified to characterize different types of sources and processes impacting aerosol particle
319 columnar properties above Metro Manila. The three events are described below.

320 2.3.1   Smoke Long Range Transport
321 Events related to transported biomass burning/smoke were chosen from the AERONET VSD
322 data that were clustered as urban/industrial (with a dominant submicrometer peak) (Eck et al.,
323 1999) over Metro Manila. Cases with the highest black carbon contribution to total AOD from
324 the MERRA-2 dataset were considered. Maps from NAAPS of high smoke contributions to
325 AOD and surface smoke contributions in the direction of back-trajectories HYSPLIT were used
326 to provide support for the likely source and transport pathway for the smoke cases.

327 2.3.2   Dust Long Range Transport
328 A dust transport case over Metro Manila was identified based on the highest dust contribution to
329 AOD from the MERRA-2 dataset, high dust contributions to AOD from NAAPS, andAERONET
330 VSD dust cluster (with an enhanced coarse peak in the AERONET VSD (compared to the
331 submicrometer fraction) (Eck et al., 1999) over Metro Manila., the highest dust contribution to
332 AOD from the MERRA-2 dataset, and high dust contributions to AOD from NAAPS. Surface

333 dust concentrations from NAAPS along ~~with~~the HYSPLIT back-trajectories ~~confirmed~~improved
334 the plausibility of dust for this case.

2.3.3 Cloud Processing

336 Cloud processing events were identified based on bimodal submicrometer VSDs (Eck et al.,
337 2012) and a relatively large sulfate contribution to AOD over Metro Manila from the MERRA-2
338 dataset, since this species is predominantly produced via cloud processing (Barth et al., 2000;
339 Faloona, 2009). The presence of clouds was verified qualitatively with MODIS (Aqua and Terra)
340 imagery from NASA Worldview in the path of air parcels reaching Metro Manila based on
341 HYSPLIT back-trajectories.

2.4 Empirical Orthogonal Functions

344 Regional analysis of aerosol particles in Southeast Asia and Asia in general show the prevalence
345 of biomass burning in the region, as well as the larger influence of anthropogenic emissions in
346 East Asia (Nakata et al., 2018). These large prevalent sources may overshadow other relevant but
347 weaker sources in the region, such as local sources. Due to the complex nature of aerosol
348 particles, analysis techniques such as principal component analysis and clustering along with
349 recent improvements in gridded datasets help detect spatial and temporal patterns that would
350 otherwise be difficult to make with noise interference and even weak signals (Li et al., 2013;
351 Sullivan et al., 2017; Plymale et al., 2021). Understanding the dominant air masses around
352 Southeast Asia will help in distinguishing local and transported particles that influence the
353 aerosol climatology in Metro Manila.~~Empirical orthogonal function (EOF) analysis was~~
354 ~~performed to be able to associate the air mass clusters identified earlier with regional scale~~
355 ~~aerosol particle sources.~~

356 To contextualize the analysis of aerosol particle masses in Metro Manila, major regional sources
357 of aerosol particles in Southeast Asia were identified based on the dominant principal
358 components from empirical orthogonal (EOF) analysis of AOD. EOF analysis was done on the
359 monthly AOD data (January 2009 to December 2018) from MERRA-2 for the Southeast Asia
360 region for the months similar in scope to the AERONET data. EOF analysis needs a complete
361 dataset with no data gaps, which is not available with pure satellite retrievals~~;~~ like MISR; the
362 MERRA-2 reanalysis ~~data alleviate~~dataset alleviates this issue.

363 The monthly MERRA-2 AOD maps (0° - 30°N, 105°E – 135°E with 0.5° latitude and 0.625°
364 longitude resolution) (Lat: 61 rows x Lon: 49 columns) for the Southeast Asia region (presented
365 subsequently) were first deseasonalized. Then, the AOD anomaly per grid per year (of the 120
366 months) was calculated by subtracting the monthly mean AOD from each value of a given month
367 (Li et al., 2013). The anomalies per grid were weighted depending on their latitude by
368 multiplying the anomalies by the square root of the cosine of their latitudes.

369 EOF, specifically singular value decomposition (SVD), analysis (Björnsson and Venegas, 1997)
370 was then performed. To prepare the data for the analysis, they were transformed such that the
371 final matrix was a 2D matrix (120 x 2989) with each row representing a year, and each column
372 representing a grid in the map. The matrix was analyzed for eigenvalues using SVD in Matlab,
373 which ~~outputted~~outputs the eigenvalue (S) and eigenvector (U: principal components and V:
374 empirical orthogonal functions) matrices. The eigenvalues were, by default, arranged in

375 descending order. Each PC time series was standardized by dividing each PC value by the
376 standard deviation per PC time series (120 months).

377 An eigenvalue spectrum was also plotted based on the variance explained by each eigenvalue
378 and error bars that were calculated using the North test (North et al., 1982). Then, the
379 unweighted AOD anomalies were regressed onto the first three standardized PCs. Each grid
380 therefore had a regression between 120 pairs (unweighted AOD anomalies vs standardized PCs).
381 From the linear regression equation, the regression coefficient per grid was calculated and
382 plotted. Each grid on the Southeast Asia map was colored based on the calculated regression
383 coefficient value.

2.5 Correlations
385
386 The first three standardized PCs of AOD anomalies were correlated to deseasonalized
387 compositional AOD fractions (Sulfate, BC, OC, Dust, and Sea Salt). For each correlation, the t-
388 test value was calculated, and the resulting t-score was compared to a t-critical value for ~n= 100
389 pairs (n is the number of pairs of data, in this case 120 months) for 0.90 confidence level, which
390 is 1.660. Correlations that have t-values exceeding +1.660 or less than -1.660 (two-tailed test) are
391 significant (90% confidence).

3 Results and Discussion
394 **3.1 Meteorology and Atmospheric Circulation**
395 Knowledge of monthly behavior of weather in the study region helps interpretation of aerosol
396 particle data. Philippine climate is influenced both by the winter northeast monsoon
397 (~November to April, Amihan) and the summer southwest monsoon (~May to October, Habagat)
398 (Coronas, 1920; Flores, 1969; Matsumoto et al., 2020). Median 3-hourly temperatures at 975 mb
399 per month (MERRA-2, 975 mb) (Fig. 1a) ranged from 23.2 °C in January during the winter
400 northeast monsoon, to 27.0 °C in May during the transition from the summer season, as defined
401 in (Bañares et al., 2021), to the southwest monsoon. May was also the month with the lowest
402 median 3-hourly relative humidity (76.6%) (MERRA-2, 975 mb) (Fig. 1b). The highest median
403 level of relative humidity at 975 mb for a month was in August (86.5 %) during the summer
404 southwest monsoon, which is also the time of the year (June to August) when rainfall peaks in
405 the region where the sampling station (Manila Observatory) is located (Coronas, 1920; Cruz et
406 al., 2013). The highest mean hourly precipitation (Fig. 1i) per month was from July (0.46 mm hr^{-1}
407 ^{1}) to September (0.42 mm hr^{-1}), while March exhibited the lowest mean hourly rainfall (0.02 mm
408 hr^{-1}). Like relative humidity and precipitation, median precipitable water (from available
409 AERONET data) (Fig. of 513 points in August, 4015 points in February, and 5049 points in
410 March) (Fig. 1h) was highest in August (4.9 cm) and lowest in February and March (3.1 cm and
411 3.2 cm, respectively).

413

414
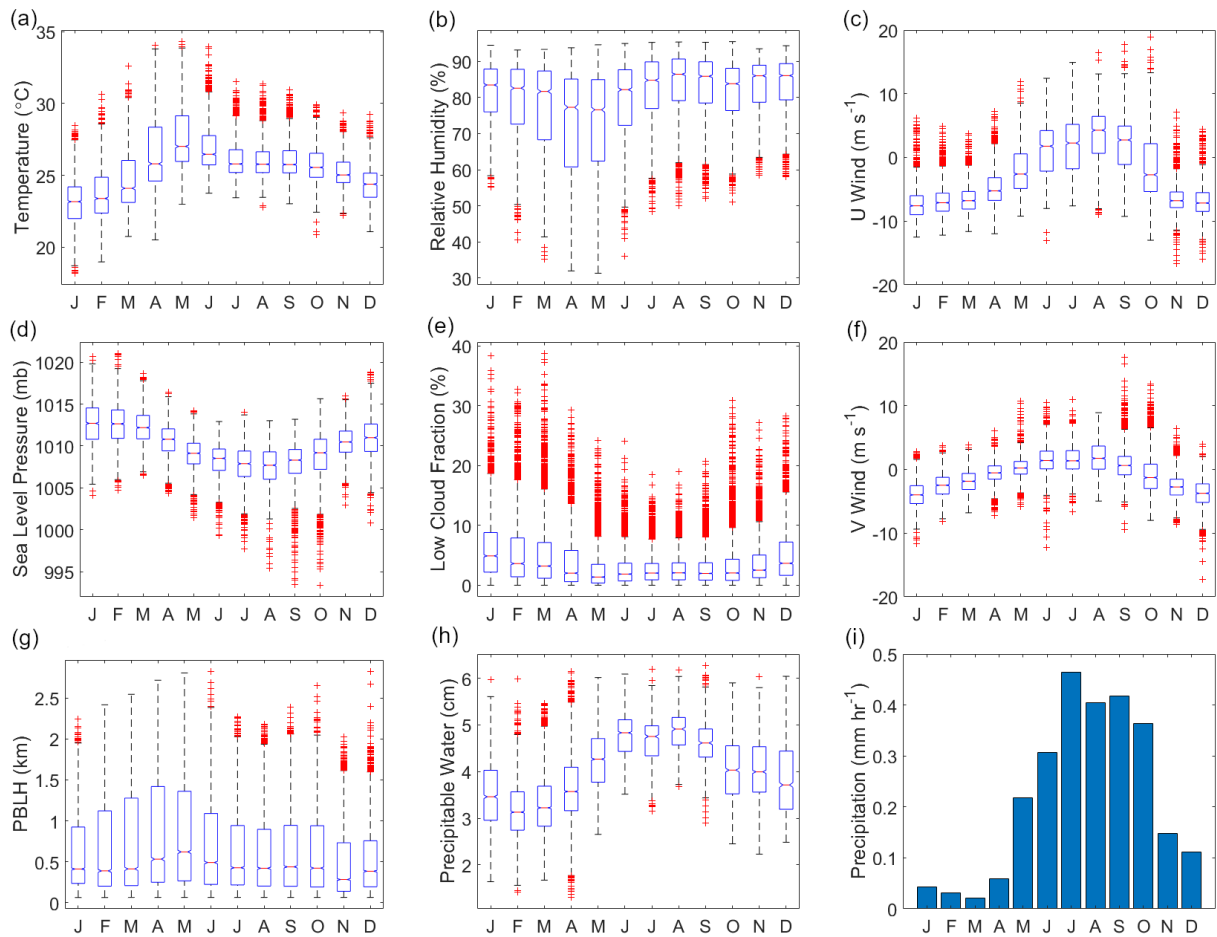
Figure 1: Monthly characteristics of meteorological parameters for Metro Manila, Philippines based on data between January 2009 and October 2018. MERRA-2 parameters: (a) temperature at 975 mb, (b) relative humidity at 975 mb, (c/f) u and v wind at 975 mb, (d) sea level pressure, (g) planetary boundary layer height (PBLH), (e) low cloud fraction; (cloud top pressure > 680 hPa); AERONET: (h) precipitable water; (data counts per month Jan: 2131, Feb: 4015, Mar: 5049, Apr: 5844, May: 3448, Jun: 1696, Jul: 652, Aug: 513, Sep: 753, Oct: 1700, Nov: 2084, Dec: 1449); PERSIANN: (i) mean hourly precipitation per month.

The lowest 3-hourly median pressures (MERRA-2) were observed (Fig. 1d) between July and September during the southwest monsoon season (~985.2 – 985.8 mb). This is also the time when the most number of tropical cyclones pass the island of Luzon (Wu and Choy, 2016). The highest 3-hourly median pressures (988.1 – 990.0 mb) were during the winter northeast monsoon.

Median winds (MERRA-2) were from the south/southwest direction from June to September (Fig. 1c and 1f), associated with the summer southwesterly monsoon. HYSPLIT back-trajectories show the same wind pattern (Fig. 2f to 2i). The highest median 3-hourly wind speeds (MERRA-2) (Fig. 1c and 1f) during the southwest monsoon were recorded for August (u: 4.2 m s^{-1} and v: 1.7 m s^{-1}). Median winds begin to transition in October and November (to the northeast

13

433   monsoon: Amihan) (Fig. 2j and 2k) coming from the east/northeast and maintained until
434   February (Fig. 2b), which is towards the end of the winter northeast monsoon. There were
435   generally higher wind speeds and the highest median 3-hourly wind speeds of the year
436   (MERRA-2) (Fig. 1c and 1d) in January (u: -7.6 m s^{-1} and v: -4.0 m s^{-1}). Median winds shifted
437   toward a more easterly source from March to May (transition time before the Habagat monsoon)
438   (Fig. 2c to 2e) accompanied by decreasing median 3-hourly wind speeds (u = -6.8 m s^{-1}, v = -1.9
439   m s^{-1} to u: -2.6 m s^{-1}, v = 0.2 m s^{-1}).

440
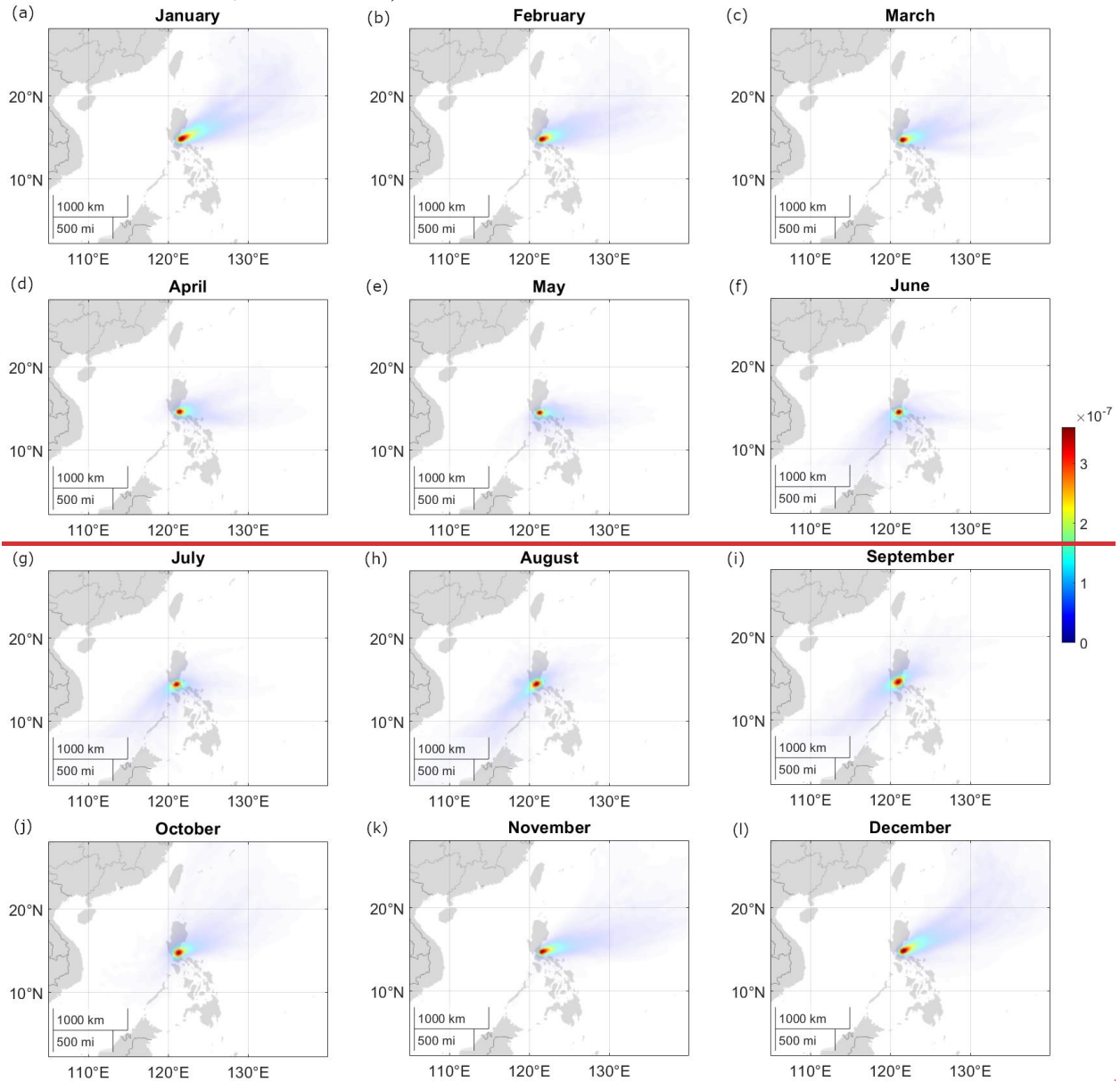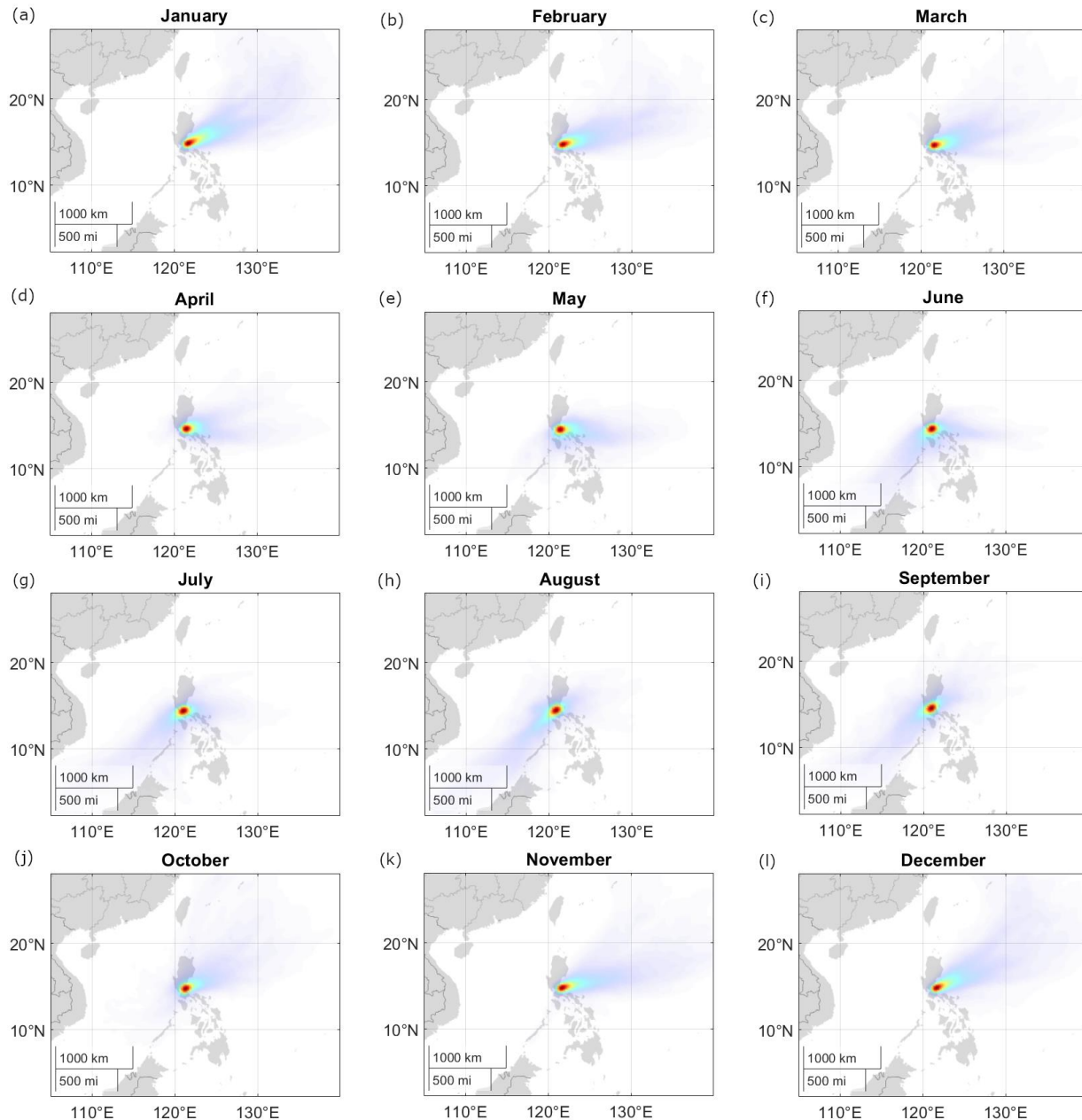
Figure 2: Density plots of <u>HYSPLIT</u> trajectories reaching Manila Observatory per month from 2009 to 2018. <u>Red denotes areas with the greatest number of back trajectories within a 100 km radius. The colors represent density value contributions to Matlab-calculated cumulative probability distribution surfaces (100 km radius) from coordinates of three-day back trajectories of the specific months.</u>

The transition times between the monsoons (when the wind directions shift and wind speeds change) are also the times of the highest (May, Fig. 1g, 621.2 m) and lowest (November, Fig. 1g, 279.6 m) median planetary boundary layer heights (MERRA-2). The median planetary boundary layer height was highest during the period (May) of highest temperatures, lowest relative humidity, reduced air pressure, and lowest monthly median low cloud fraction (MERRA-2) (Fig. 1e) (1.4 %). The lowest monthly median planetary boundary layer height was observed during

15

453 the period (November) when temperatures were beginning to cool and air pressure was rising.
454 The monthly maximum low cloud fraction was lowest in July (18.5 %) during the summer
455 southwest monsoon while the monthly median and monthly maximum low cloud fractions
456 (MERRA-2) (Fig. 1e) were highest (38.3 % max, 4.9 % median) in January during the winter
457 northeast monsoon.
458

459 **3.2 Aerosol Particle Characteristics**
460 3.2.1   Aerosol Optical Depth
461 Monthly median AOD (AERONET, 500 nm) (Fig. 3a) over the Manila Observatory was highest
462 from August (0.21) to October (0.23) around the time of the summer monsoon when winds were
463 coming from the southwest (Figs. 2h to 2i) (Holben et al., 2001). This is the same time of year
464 when biomass burning activities occur in the Indonesian region southwest of Metro Manila.
465 (Glover and Jessup, 1998; Kiely et al., 2019; Cahyono et al., 2022). Studies have shown that
466 AOD in the Philippines increases during the biomass burning season in Indonesia (Nguyen et al.,
467 2019b; Caido et al., 2022). Regional AOD (550 nm) over the larger Southeast Asia
468 regiondomain from MISR and MERRA-2 (Fig. 4) had a similarly large peak fromaround the
469 same time beginning in September tountil October which, however, was second only in
470 magnitude to a March peak, which is influenced by biomass burning in Peninsular Southeast
471 Asia (PSEA) (Gautam et al., 2013; Hyer et al., 2013; Dong and Fu, 2015; Wang et al., 2015;
472 Yang et al., 2022). This is consistent with the peak in speciated AOD due to fine (radii <0.7
473 µm), spherical, and absorbing aerosols that were observed by MISR from March to April (Fig.
474 S1). This larger peak in March, attributed to PSEA (which is ~2000 km west of the
475 Philippines,), was not as prevalent in the AERONET AOD data over Manila Observatory in
476 Metro Manila due to the dominant easterly winds in the Philippines in March (Fig. 2c) and more
477 localized sources.

478
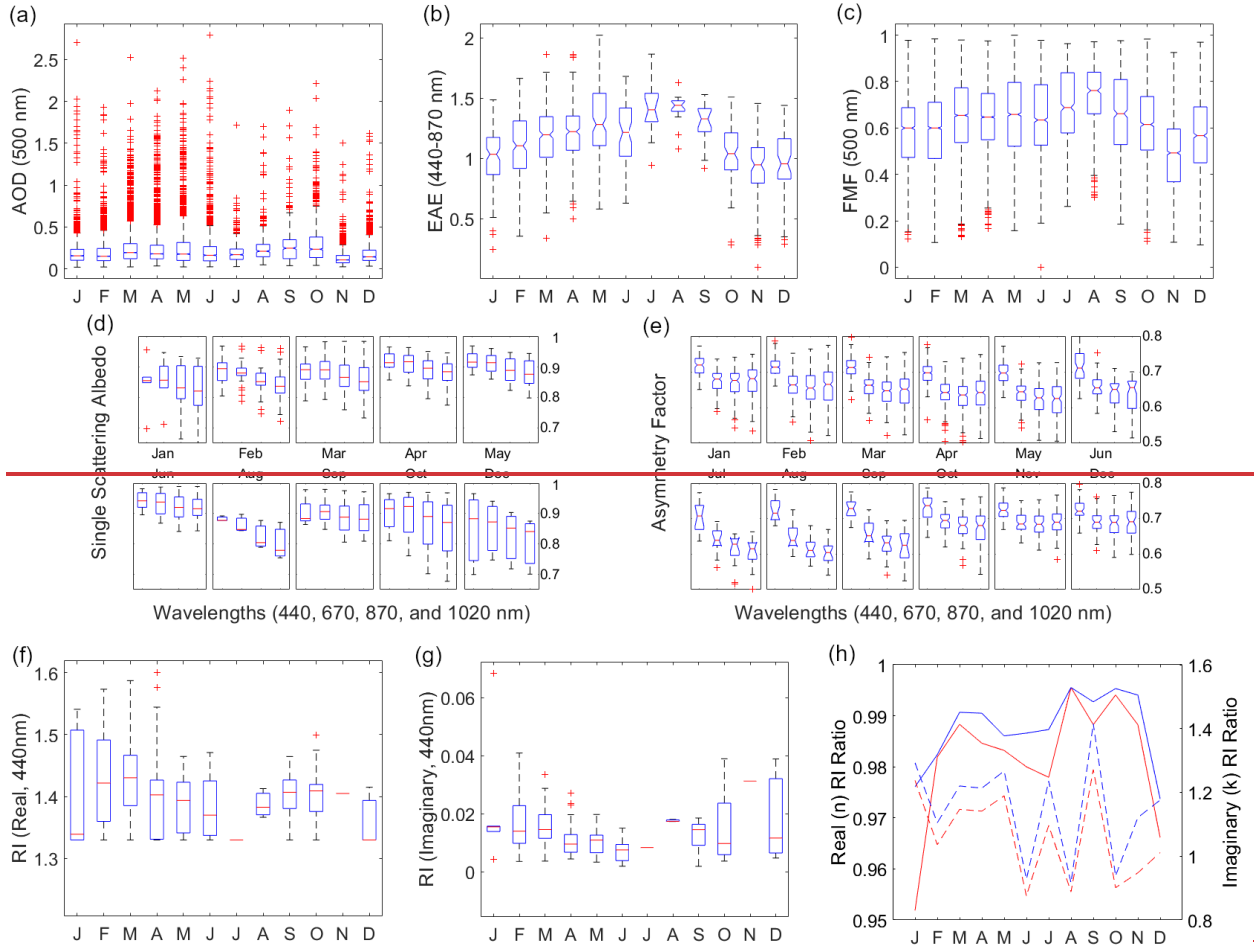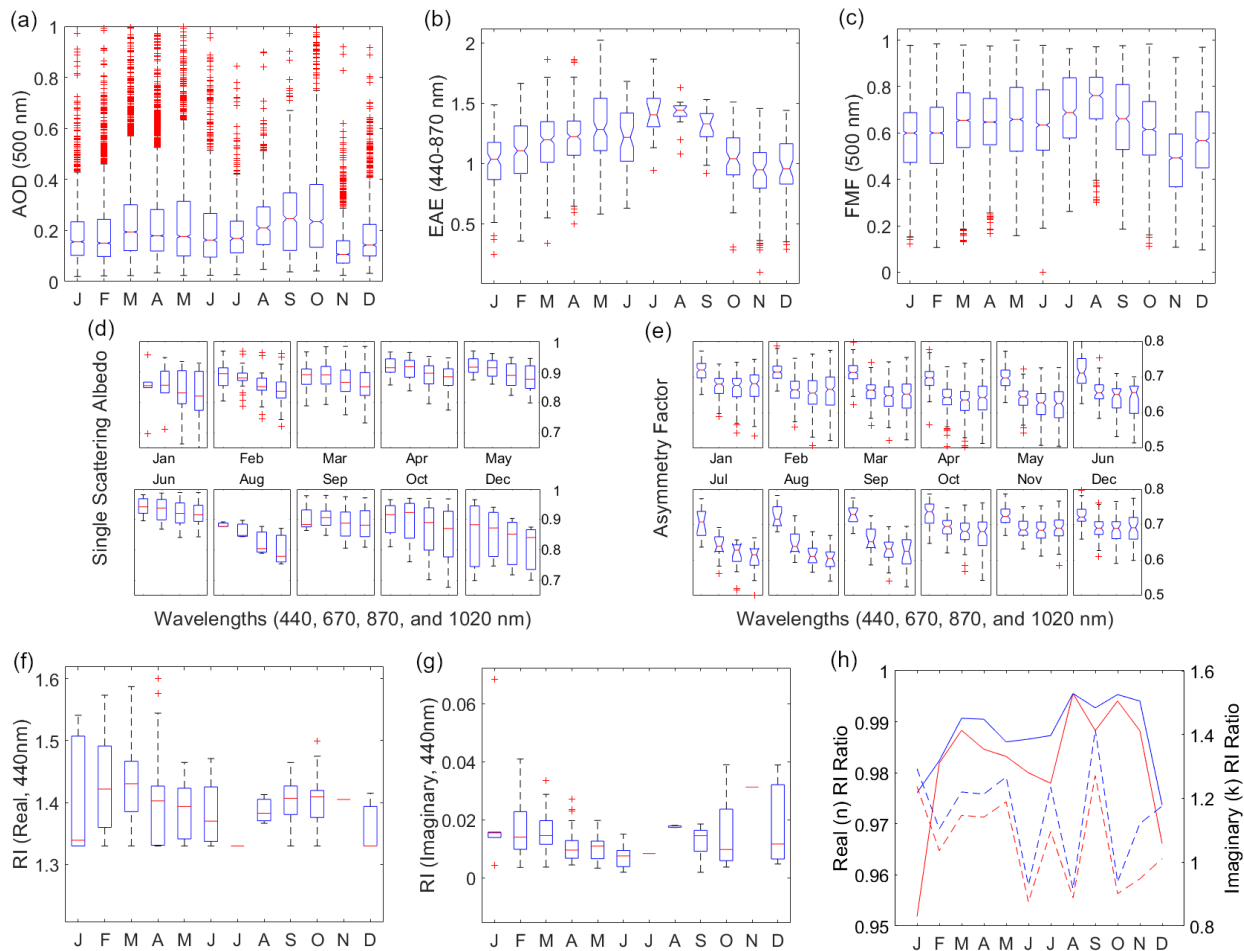
17

Figure 3: Monthly characteristics of AERONET aerosol particle parameters: (a) aerosol optical depth (AOD at 500 nm with y-axis until 1.0 only for larger boxplot resolution) with counts (Jan: 2107, Feb: 3931, Mar: 4923, Apr: 5755, May: 3389, Jun: 1653, Jul: 637, Aug: 483, Sep: 718, Oct: 1555, Nov: 2001, Dec: 1386), (b) extinction angstrom exponent (EAE at 440-870 nm) with counts (Jan: 102, Feb: 248, Mar: 312, Apr: 309, May: 137, Jun: 53, Jul: 14, Aug: 18, Sep: 18, Oct: 79, Nov: 77, Dec: 52), (c) spectral de-convolution algorithm (SDA) retrievals of fine mode fraction (FMF), at 500 nm) with the same counts as AOD, (d) single scattering albedo (SSA) from 440 nm (leftmost boxplot) to 1020 nm (rightmost boxplot) with counts (Jan: 6, Feb: 31, Mar: 62, Apr: 50, May: 29, Jun: 8, Aug: 3, Sep: 5, Oct: 17, Dec: 3), (e) asymmetry factor (AF),) from 440 nm (leftmost boxplot) to 1020 nm (rightmost boxplot) with the same counts as EAE, (f) real and (g) imaginary refractive index (RI) values (440 nm),) with the same counts as SSA, and (h) refractive index ratios (where the blue line is the ratio of RI at 440 nm and 675670 nm, the red line is the ratio of RI at 440 nm and the average RI for the 670675–1020 nm wavelengths, and the broken lines are the imaginary refractive index ratios) for Metro Manila, Philippines based on data between January 2009 and October 2018.

There is a notable dip in the monthly median AERONET AOD over Manila Observatory from the peak in October to the lowest monthly median AOD (0.11) in November, (Fig. 3a), just slightly above defined background levels (<0.1) (Holben et al., 2001), when the windspeeds were picking up and were coming from the east to northeast directions (Fig. 2k) in the direction of the Philippine Sea and the West Pacific Ocean. This dip was also observed in the regional

18

501 ~~AOD data (MISR and MERRA-2, Fig. 4).~~ This dip was also observed in the regional (30° × 30°)
502 AOD data (MISR and MERRA-2, Fig. 4). This is most probably due to the decrease in the AOD
503 contribution from fine (radii <0.7 µm) and spherical particles based on size speciated MISR
504 AOD (Fig. S1). Larger and non-spherical particle contributions to AOD increase in November in
505 the Southeast Asia region. The MERRA-2 AOD is relatively higher than the MISR AOD
506 probably due to assimilation of MODIS data into MERRA-2. Studies in Asia (Xiao et al., 2009;
507 Qi et al., 2013; Choi et al., 2019) have observed relatively higher MODIS AOD compared to
508 MISR AOD.

509

510
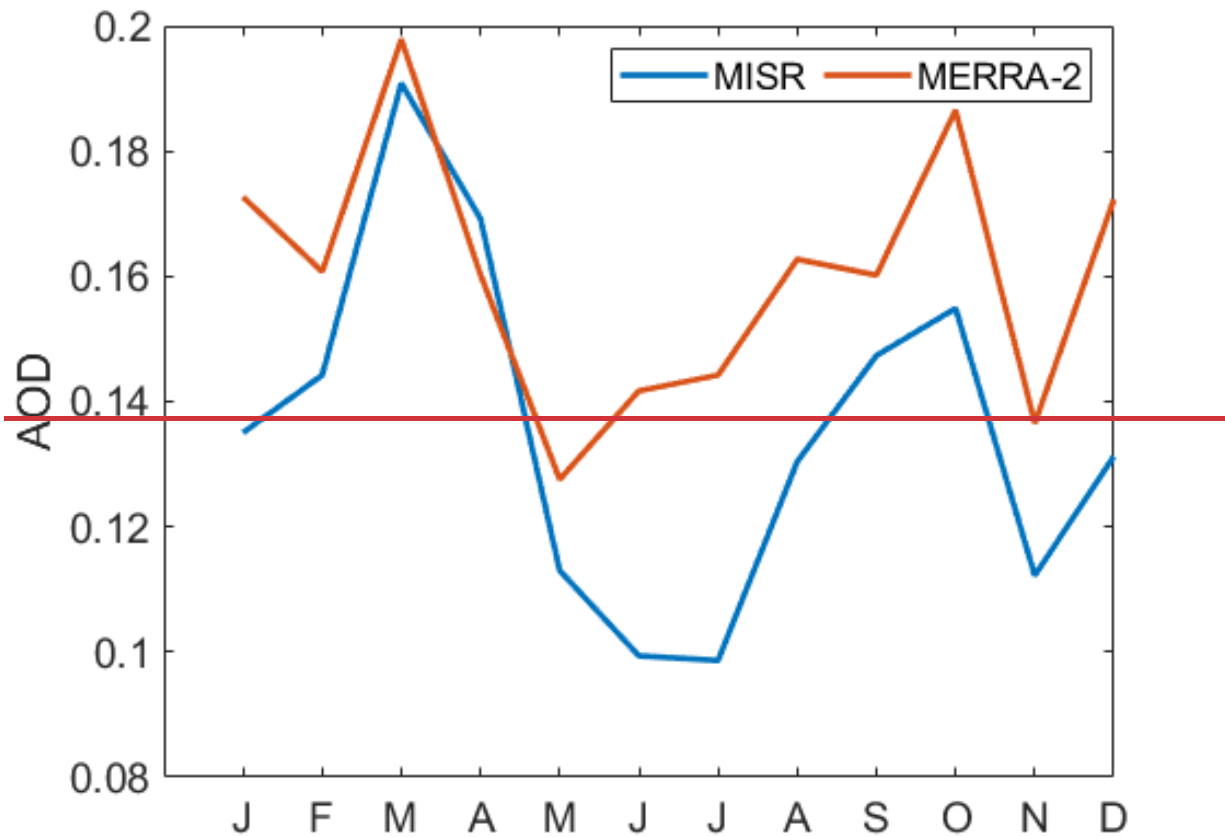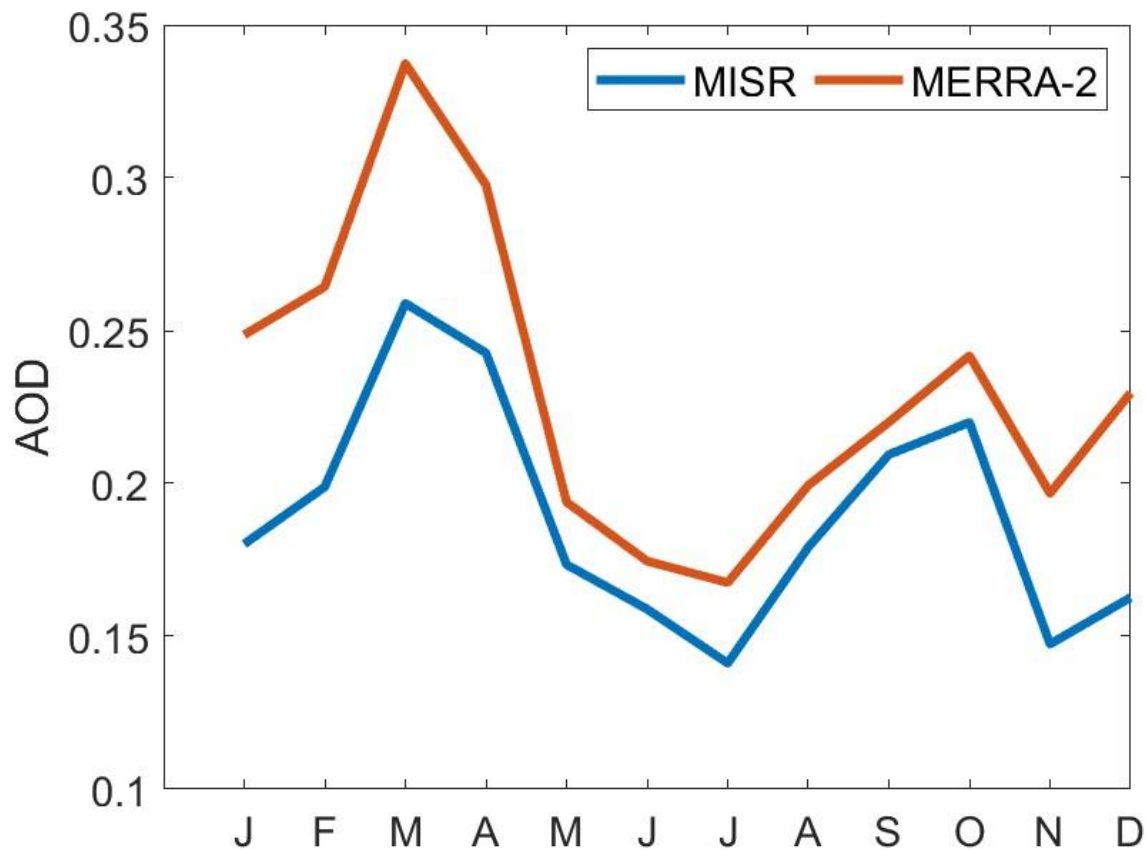
Figure 4: Monthly ~~median~~mean AOD (550 nm) in Southeast Asia (30° × 30°) from 2009 to 2018 from MISR (blue line) and MERRA-2 (red line).

There were 338 instances (~1.2 % of the time based on the total number of 28,538 valid AERONET AOD data points) of AOD values exceeding 1, indicative of heavy aerosol particle loading (Huang et al., 2021). Because AOD is extrinsic (it depends on mass), AOD describes total aerosol particle loading and we examine other aerosol particle parameters from AERONET to make more informed inferences about size and composition.

3.2.2   Extinction Angstrom Exponent and Fine Mode Fraction

The extinction angstrom exponent (EAE) relates the extinction of light at specific wavelengths and is indicative of aerosol particle size (Ångström, 1929). ~~The EAE is usually greater for smaller particles (~4 for very small particles that undergo Rayleigh scattering and 0 for particles as large as cloud drops) (Bergstrom et al., 2007), except for when the coarse mode has a large impact on the angstrom exponent (Schuster et al., 2006).~~The EAE is usually greater for smaller particles (~4 for very small particles that undergo Rayleigh scattering, > 2 for small particles, < 1 for large particles like sea salt and dust, and 0 for particles as large as cloud drops) (Schuster et al., 2006; Bergstrom et al., 2007). The highest monthly median EAE (Fig. 3b) from 2009 to 2018 over the Manila Observatory was observed from July (~1.4) to September (~1.3), during the southwest monsoon. This period is associated with the biomass burning southwest of the

20

530 Philippines (Oanh et al., 2018; Stahl et al., 2021; Crosbie et al., 2022). The median (per month)
531 EAE ranged from ~0.9 in November to ~1.4 in August, a range which is within the values from
532 previous studies collected from mixed sites and urban/industrial areas with both fine and coarse
533 particles (Eck et al., 2005; Giles et al., 2012). The high EAE over Manila Observatory from July
534 to September is probably regional in nature based on the MISR data showing increased EAE
535 with increased AOD from fine, spherical, and absorptive particles (Fig. S1) in Southeast Asia
536 during the same months.

537 EAE increases with AOD (Fig. S1S2), which means that the greater particle loading is
538 contributed by smaller particles (Smirnov et al., 2002). Of the high loading cases (AOD >1),)
539 over Manila Observatory, the EAE values ranged fromwere mostly greater than 0.6 to 1.6,8
540 indicating fine mode particles (Che et al., 2015). The EAE values in August were the highest
541 compared to other months including having the highest minimum value of any month (0.71)
542 (Fig. S1S2), due to smaller particles (~EAE >1 for fine particles, Table 2). The lowest EAE
543 values (0.08) and thus the largest particles were observed in December., which again may be
544 regional in nature with MISR EAE also lowest during this time with increased AOD from larger
545 and non-spherical particles (Fig. S1).

546 The fine mode fraction (FMF) describes the prevalence of fine mode particles in the column of
547 air above the surface. The fine mode fraction (Fig. 3c) from 2009 to 2018 was highest in August
548 (monthly median of 0.75) and lowest in November (monthly median of 0.45). This is consistent
549 with the EAE values discussed earlier with the prevalence of smaller particles in August and
550 larger particles in November. In August (Fig. 2h) the southwest monsoon is known to coincide
551 with transportedthe transporting of fine smoke particles to Luzon. In November (Fig. 2k), the
552 prevalent winds may have already shifted to easterly (Matsumoto et al., 2020) implying more
553 marine-related sources associated with coarser particles.

554 3.2.3   Single Scattering Albedo
555 The single scattering albedo (SSA) is the most important aerosol particle parameter determining
556 whether aerosol particles will have a warming or cooling effect (Reid et al., 1998). SSA is the
557 ratio of the scattering coefficient to the total extinction (scattering and absorption) coefficient
558 (Bohren and Clothiaux, 2006) of aerosol particles. Higher SSAs are related to more reflective
559 aerosol particles while more absorbing aerosol particles will have lower SSA values; values
560 range from 1 (reflective) to 0 (absorbing). Monthly median SSA values were largest in June
561 (0.94, at 440 nm), suggesting the presence of more reflective aerosol particles, and smallest in
562 August (0.78,88 at 440 nm and 0.78 at 1020 nm) suggesting more absorptive particles that are
563 similar in range to the SSA of biomass burning particles (Table 2). August is when biomass
564 burning is prevalent to the southwest of the Philippines and associated with soot particles that are
565 absorptive.

566 The sensitivity of SSA to different wavelengths depends on the type of aerosol particles present.
567 More specifically, aerosol particle size and refractive index (which is related to aerosol particle
568 composition) both affect the SSA (Dubovik and King, 2000; Bergstrom et al., 2007; Moosmüller
569 and Sorensen, 2018). For dust-type particles, SSA increases with wavelength because of lower
570 dust absorption in the higher visible to infrared wavelengths (Dubovik et al., 2002), while for
571 urban particles (including black carbon), which absorb light at longer wavelengths, SSA
572 decreases with wavelength (Reid et al., 1998; Bergstrom et al., 2002). The presence of organic

573   carbon may affect this spectral dependence; however, because organic particles absorb in the
574   UV, this lowers SSA at wavelengths shorter than 440 nm (Kirchstetter et al., 2004). Monthly
575   median SSA generally decreased with increasing wavelength for all months with available data
576   (Fig. 3d) presumably due to the influence of more urban particles in contrast to dust.
577   Noteworthy though are the monsoon transition months of April, September, and October (Fig.
578   3d), which had increased SSA from 440 nm to 670 nm, possibly from organics along with black
579   carbon due to transported smoke. The back-trajectories for these months (Figs. 2d, 2i, and 2j)
580   suggest sources from the northeast that are closer to Luzon during these months compared to
581   other months. This indicates the possibility of more local sources. Increasing the certainty of
582   sources associated with aerosol particles necessitates looking at other available aerosol particle
583   parameters, discussed subsequently.

584   3.2.4   Asymmetry Factor
585   The asymmetry factor quantifies the direction of scattering of light due to aerosol particles, with
586   values ranging from -1 (back scatter) to 0 (uniform scattering) to 1 (forward scatter). It is
587   important in modeling climate forcing because it affects the vertical distribution of the radiation
588   in the atmosphere (Kudo et al., 2016; Zhao et al., 2018). The asymmetry factor is dependent on
589   particle size, shape, and composition and the value of 0.7 is used in radiative models (Pandolfi et
590   al., 2018).

591   Lower asymmetry factors are related to smaller particles (at constant AOD) (Bi et al., 2014).
592   Measured values due to biomass burning, for example, are 0.54 (550 nm) in Brazil (Ross et al.,
593   1998) and 0.45 – 0.53 (550 nm and including dust) over central India (Jose et al., 2016). There
594   have been relatively higher values observed in western, central, and eastern Europe (0.57 – 0.61
595   at 520 – 550 nm) (Pandolfi et al., 2018) and the U.S. East Coast (0.7 at 550 nm) (Hartley and
596   Hobbs, 2001). In Norway, the asymmetry factor for background summer conditions was 0.62
597   and was higher in the springtime at 0.81 (862 nm) during Arctic haze events (Herber et al.,
598   2002). Highest values are associated with dust such as those measured in the Sahara being 0.72 –
599   0.73 (500 nm) (Formenti et al., 2000). Over Metro Manila, the asymmetry factors from the
600   AERONET data at the 675, 870, and 1020 nm were similar across months (Fig. 3e). The monthly
601   median asymmetry factors at 440 nm ranged from 0.70 (April and May) to 0.74 (October), while
602   for 670, 870, and 1020 nm the monthly median asymmetry factors were smaller and ranged from
603   0.62 – 0.69. These values were closely related to those observed over the U.S. East Coast as
604   mentioned earlier, perhaps due to the proximity of the location to the coast (10 km east of Manila
605   Bay and 100 km west of the Philippine Sea) as well as its location in Manila, which is a large
606   local source due mostly to vehicles (Cruz et al., 2019).

607   The monthly median asymmetry factor in Metro Manila was greatest towards the end of the year
608   (October to December) for all the wavelengths, suggesting larger particles when winds (Figs. 2j
609   to 2l) come from the Philippine Sea in the northeast. It was in March and April that the monthly
610   median asymmetry factor was minimal for 440 nm and in August for 670, 870, and 1020 nm.
611   These were the times when ~~the~~ aerosol particles were smallest. March to April represents the
612   driest time of the year in Manila (Fig. 1b and 1h) perhaps preventing particle growth and where
613   the local sources may be dominating, even as back-trajectories (Fig. 2c and 2d) extend all the
614   way from the Philippine Sea to the east. This is corroborated by results from other studies
615   showing that the asymmetry factor seems to be enhanced by relative humidity (Zhao et al.,
616   2018). The unexpected low asymmetry factor values in August, however, are probably because

617   of the source of the particles. August had the highest relative humidity and precipitable water
618   (Fig. 1b and 1h) but is also when the back-trajectories (Fig. 2h) were from the southwest,
619   possibly affected by the Indonesia fires, which could have transported more non-hygroscopic
620   fine particles.

621   Fine particles have been observed to exhibit decreasing asymmetry factors with increasing
622   wavelength (Bergstrom et al., 2003). This trend is observed in all the months for the monthly
623   median asymmetry factors (Fig. 3e) suggesting the predominance of smaller aerosol particles.
624   The greatest decrease in the asymmetry factor (all wavelengths) was in August, consistent with
625   the lowest observed values of the year (670, 870, and 1020 nm). Transported biomass burning
626   particles are the probable dominant particles during this time. They are usually composed of
627   hygroscopic inorganics, non-hygroscopic soot, and relative non-hygroscopic organic fractions
628   (Petters et al., 2009). Knowing the composition of biomass burning particles over the study
629   region will help in the understanding of hygroscopicity and its impacts on radiation.

630   3.2.5   Refractive Index
631   Refractive index is an intrinsic parameter as it does not depend on the mass or the size of
632   particles, and thus can be used to infer aerosol particle composition (Schuster et al., 2016). For
633   the case of the AERONET data, which include refractive index values that are insensitive to
634   coarse particles (Sinyuk et al., 2020), the focus of the discussion will be for fine mode particles
635   and may be limited when coarse particles are involved.   Refractive index measurements are
636   complex since they include real and imaginary parts related to light scattering and absorption,
637   respectively. All aerosol particles scatter light but only certain types absorb light significantly.
638   The most prominent particle absorbers in the atmosphere are soot carbon, brown carbon (organic
639   carbon that absorbs light), and free iron from dust (hematite and goethite in the ultraviolet to
640   mid-visible) (Schuster et al., 2016). For this study, we examine refractive index values at 440 nm
641   wavelength because this is the wavelength used to calculate SSA (Andrews et al., 2017).For this
642   study, we examine refractive index values at 440 nm wavelength. Pure sources of soot carbon
643   have the highest real refractive index values (~1.85) as well as the highest imaginary refractive
644   index (~0.71), both independent of wavelength (Koven and Fung, 2006; Van Beelen et al.,
645   2014). Brown carbon and dust have relatively lower real refractive index values at 440 nm
646   (~1.57 and ~1.54) and imaginary refractive index values (~0.063 and ~0.008) that decrease with
647   increasing wavelength (Xie et al., 2017).

648   In this study the range of the monthly median real refractive index values (440 nm) was from
649   1.33 (December and January) to 1.43 (March) (Fig. 3f). Water uptake by aerosol particles
650   decreases the real refractive index values (Xie et al., 2017) and thus the lowered real refractive
651   indices over the Manila Observatory can be due to the presence of more water in the atmosphere
652   in general and/or the increased presence of more hygroscopic particles. December and January
653   are not necessarily the months that have the highest moisture content, but they are months when
654   back-trajectories reaching the column over the Manila Observatory are from the Philippine Sea
655   to the northeast presumably transporting hygroscopic particles. As reported in previous sections,
656   relatively larger particles are observed around this time of the year and thus sea salt can be an
657   important contributor. The greatest change in the monthly median real refractive index with
658   increasing wavelength also was observed in December (Fig. 3h), possibly due the increased
659   fractional contribution of constituents other than soot carbon (because the real refractive index of
660   soot carbon is invariant with wavelength). Noteworthy as well is the month of August (Fig. 3f),

661   which has the smallest range of real refractive index values, possibly indicating a more
662   homogenous aerosol particle source compared to other months. August is the month with the
663   highest relative humidity (Fig. 1b) as well as highest precipitable water (Fig. 1h), while this is
664   also the month when long-range biomass burning emissions are observed to be highest, and
665   when the real refractive index values would otherwise be expected to be highest.

666   Water content seems to play a significant role in the real refractive index values in Manila.
667   March, when the monthly median real refractive index values are highest (Fig. 3f), is when
668   precipitable water vapor (Fig. 1h) is among the lowest in the year. The months around March are
669   also when maximum real refractive indices (1.57 in February, 1.59 in March, and 1.60 in April)
670   were observed (Fig. 3f). March was when there was a relatively small change in real refractive
671   index value with wavelength perhaps related to greater soot carbon fractions during this time,
672   due possibly to the contribution of biomass burning from Peninsular Southeast Asia (Shen et al.,
673   2014). Looking more closely at the imaginary refractive index values will help elucidate this
674   issue.

675   Monthly median imaginary refractive index values (440 nm) ranged from 0.007 in June to 0.015
676   in September and December (Fig. 3g). These are low compared to those of the pure soot carbon
677   mentioned earlier because of the mixed nature of the sampling site with contributions from
678   brown carbon and dust. The highest imaginary refractive index values in September and
679   December suggest the greatest fractional contribution of soot because the highest imaginary
680   refractive index values are associated with soot. These are also similar in magnitude to biomass
681   burning particles in the Amazon (0.013) (Guyon et al., 2003). The key distinction between soot
682   carbon and other major absorbers (brown carbon and dust) is that its imaginary refractive index
683   is invariant with wavelength. Both brown carbon and dust exhibit a decrease in the imaginary
684   refractive index with increasing wavelength (Xie et al., 2017). The ratios of imaginary refractive
685   index values (440 nm to average of 670–1020 nm) (Fig. 3h) show a relative invariance with
686   wavelength (ranging from 0.88 to 1.4), which indicates the dominance of soot as the major
687   absorber in the region (Eck et al., 2003). While observed wavelength invariance points to high
688   soot contributions, the size of the particles can help distinguish between brown carbon, which
689   reside mainly in the fine mode, and dust sources, which yield more coarse particles (Schuster et
690   al., 2016). September is during the southwest monsoon, which is when, as noted in the earlier
691   sections, fine particles were most prevalent. This is also the time when the imaginary refractive
692   index varied most with wavelength (1.4 ratio of the imaginary refractive index at 440 nm and the
693   imaginary refractive index average for 670 nm to 1020 nm in Fig. 3h) possibly with greater
694   absolute contributions from brown carbon, even with the highest soot carbon fractional
695   contributions. Brown carbon has been observed both from primary and aged aerosol particle
696   emissions from biomass burning (Saleh et al., 2013). As noted earlier, December also had the
697   highest imaginary refractive index values as well as relatively coarser particles, possibly due to
698   larger dust absolute contributions even with the highest soot carbon fraction contributions. The
699   lowest monthly median imaginary refractive index values in June, on the other hand, when fine
700   mode particles prevail suggest highest fractional contributions of brown carbon relative to other
701   months (Fig. 3h).

702   3.2.6   Volume Size Distributions
703   The volume size distribution (VSD) is another way to be able to more deeply characterize
704   aerosol particles, specifically related to their effect on climate, weather, and clouds (Haywood

705 and Boucher, 2000; Feingold, 2003). In the Manila Observatory dataset, there was a bi-modal
706 VSD for the entire dataset (Fig. 5a). The fine mode median values peaked in the accumulation
707 mode at 0.148 µm particle radius while the coarse mode median values peaked at 3.857 µm.
708 (Fig. 5a and Table S1). The median coarse mode amplitudes and volume concentrations were
709 higher than the fine mode amplitudes and volume concentrations for most of the year (DJF,
710 MAM, and SON, Fig. 5b and Table S1), except during the southwest monsoon (JJA) when the
711 fine mode amplitude and volume concentration was higher. This is consistent with observations
712 earlier of fine mode prevalence during the southwest monsoon. Median VSD amplitudes (Fig.
713 5c) were greater in the afternoon, with higher peaks and volume concentrations for both the fine
714 and coarse modes, compared to the morning. There was a slightly larger coarse median
715 amplitude and volume concentration, compared to the accumulation mode median amplitude and
716 volume concentration, for both the morning and afternoon size distributions. While the VSDs
717 confirm several observations based on the analysis of the aerosol particle parameters presented
718 earlier, not much further information is gained especially regarding chemical composition. Size
719 distributions are a result of contributions from multiple sources, and thus being able to
720 discriminate the sources based on their characteristic size distributions will help identify relevant
721 sources.
722
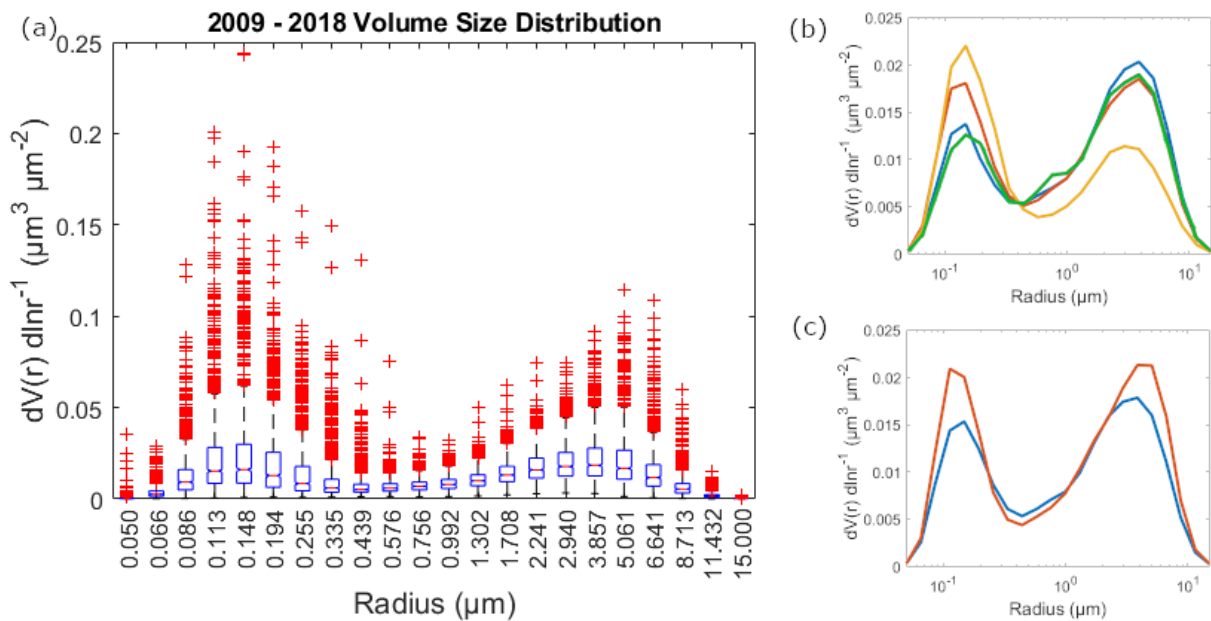
724 **Figure 5:** (a) VSD results derived from AERONET measurements at Metro Manila between
725 January 2009 and October 2018. Median VSDs over the study period based on (b) season (blue:
726 DJF, red: MAM, orange: JJA, green: SON) and (c) time of day (blue: AM, red: PM).

727

728 **3.3 Clusters**
729 3.3.1 VSD Cluster Profiles

730 Five clusters were identified to best represent the VSD (Fig. 6a). The average of the VSDs in
731 each cluster varied depending on the height of the peaks in the accumulation mode and the
732 coarse mode. In Metro Manila, the accumulation mode is associated with aged aerosol particles
733 and combustion (Cruz et al., 2019). The majority of the data (830 count out of 1419 total VSD

25

734 profiles) were clustered together in a profile (cluster 1) that had relatively low average
735 magnitudes of volume concentration for both the accumulation (0.01 μm^3 μm^{-2}) and coarse (0.02
736 μm^3 μm^{-2}) modes, with the volume concentration magnitude of the coarse mode peak slightly
737 higher than the volume concentration magnitude of the accumulation mode peak. The next
738 prevalent cluster profile (284 counts, cluster 2) had an average fine mode peak for the volume
739 concentration (0.04 μm^3 μm^{-2}) which was more than twice as much than the previous profile but
740 with a similar coarse mode peak for the volume concentration (0.02 μm^3 μm^{-2}). The average
741 coarse mode peak for the volume concentration (0.04 μm^3 μm^{-2}) was the highest (compared to
742 the four other cluster profiles) for the third prevalent cluster profile (166 counts, cluster 3);
743 cluster 3 ~~was~~ also had a slightly shifted volume concentration peak in the coarse mode to a
744 higher radius (5.06 μm) compared to other clusters. The coarse mode dominated this VSD
745 compared to other profiles (lower magnitude for the accumulation mode peak for the volume
746 concentration, 0.02 μm^3 μm^{-2}). The two remaining cluster profiles exhibited high average
747 magnitudes of volume concentration in both the accumulation and coarse modes. The fourth
748 prevalent cluster profile (74 counts, cluster 4) had the highest average absolute magnitude for the
749 volume concentration in the accumulation mode (0.11 μm^3 μm^{-2}), while the fifth prevalent
750 cluster profile (65 counts, cluster 5) had a slightly smaller accumulation mode peak for the
751 volume concentration (0.07 μm^3 μm^{-2}) that was shifted to a slightly higher radius (0.19 μm
752 compared to 0.15 μm). Both clusters 4 and 5 had similar average coarse mode peak volume
753 concentration magnitudes (0.04 μm^3 μm^{-2}).

754
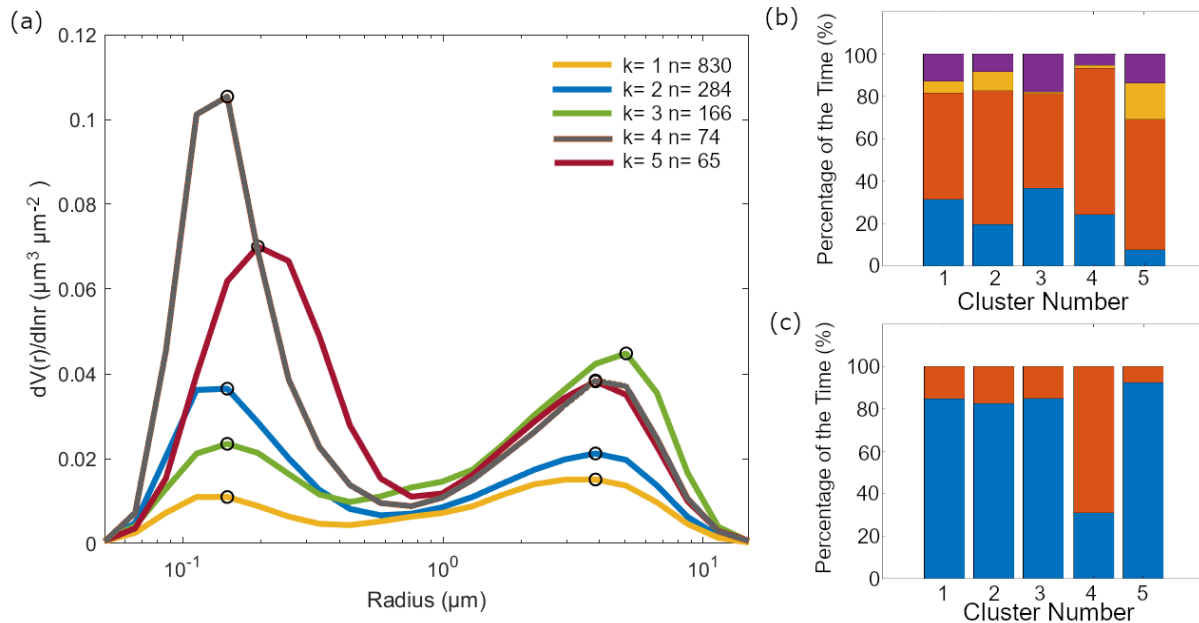
756 **Figure 6:** (a) Cluster analysis of VSD data yielding five characteristic and averaged VSDs with
757 the number of points per cluster shown in the legend. The black circles on the curves show the
758 peak locations in the submicrometer (<1 μm) and coarse ($\geq$1 μm) modes. The relative abundance
759 of each cluster is shown for different (b) seasons (blue: DJF, red: MAM, orange: JJA, violet:
760 SON) and (c) times of day (blue: AM, red: PM).

761 The clusters were distributed across seasons (Fig. 6b), with clusters 1 and 2 being the most
762 evenly distributed among the clusters. Cluster 3, which had the highest coarse mode peak, had
763 the greatest contribution from September to November compared to other clusters. Cluster 4,
764 which had the highest accumulated mode peak compared to other clusters, had the greatest
765 contribution from March to May as well as to afternoon VSDs compared to other clusters (Fig.
766 6b and 6c). Relative contributions of VSDs from June to August were highest for cluster 5,
767 which had the shifted accumulated mode peak.

768 Median total (AERONET) AOD values (Fig. 7b) were lowest (0.12) for cluster 1, though it had
769 the second highest sea salt fractional contributions (31%) (Fig. 7a) to total AOD (MERRA-2)
770 (31%) among all the clusters. Cluster 2 had relatively mid-range median total AOD values (0.27)
771 that, along with clusters 4 and 5, were dominated by sulfate and organic carbon (46% and 20%).
772 Cluster 3 had similar, but slightly lower median total AOD (0.25) compared to cluster 2. Cluster
773 3 was distinct because it had the largest total (0.04) and fractional contribution (37%) from sea
774 salt among all clusters. Clusters 4 and 5 had the highest median total AOD values (0.47 and
775 0.56), with cluster 5 having the highest absolute and fractional sulfate contributions (0.14 and
776 64%) among the clusters. Integrating the above results with their corresponding aerosol particle
777 properties can help associate the clusters to air masses.

778
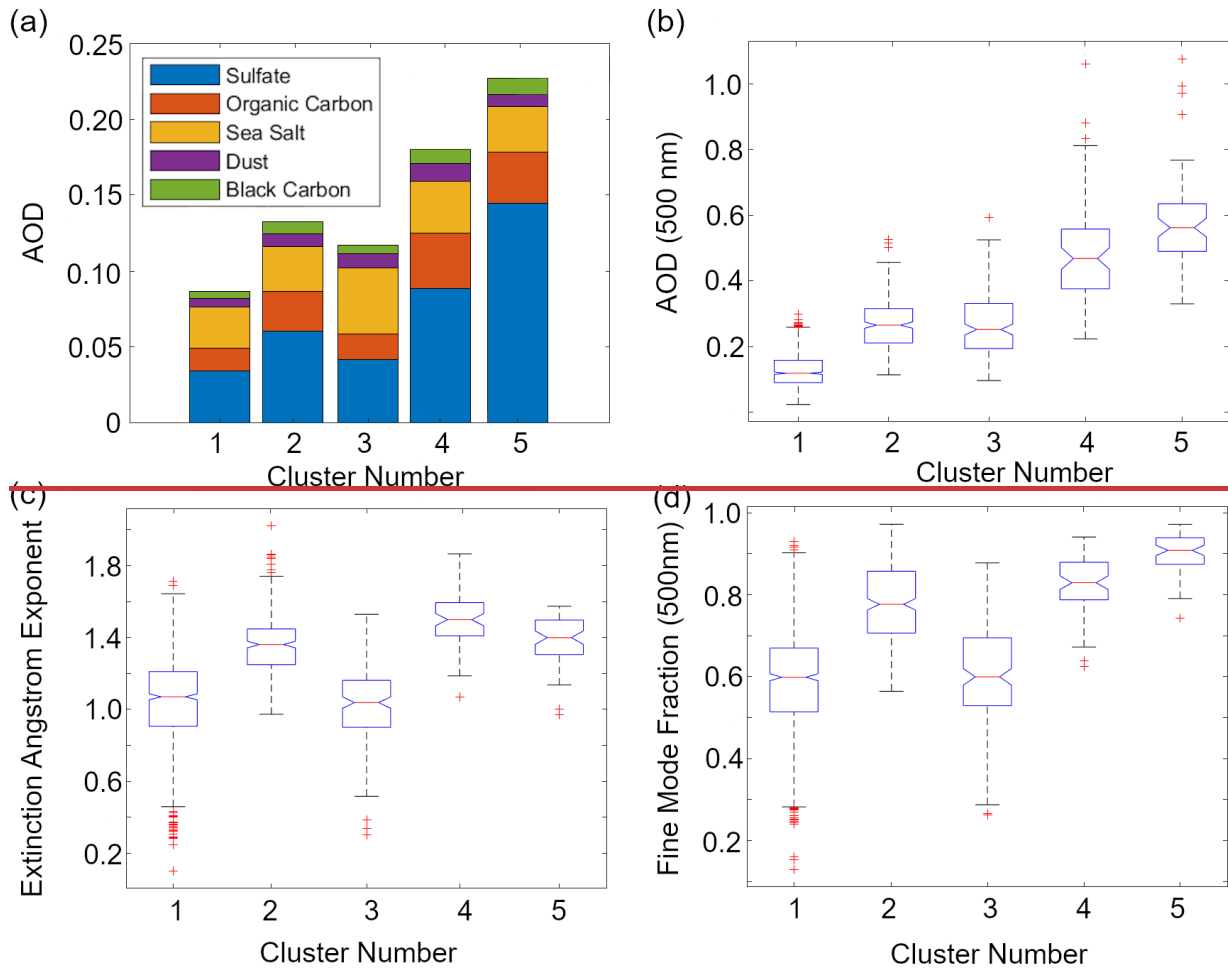
779
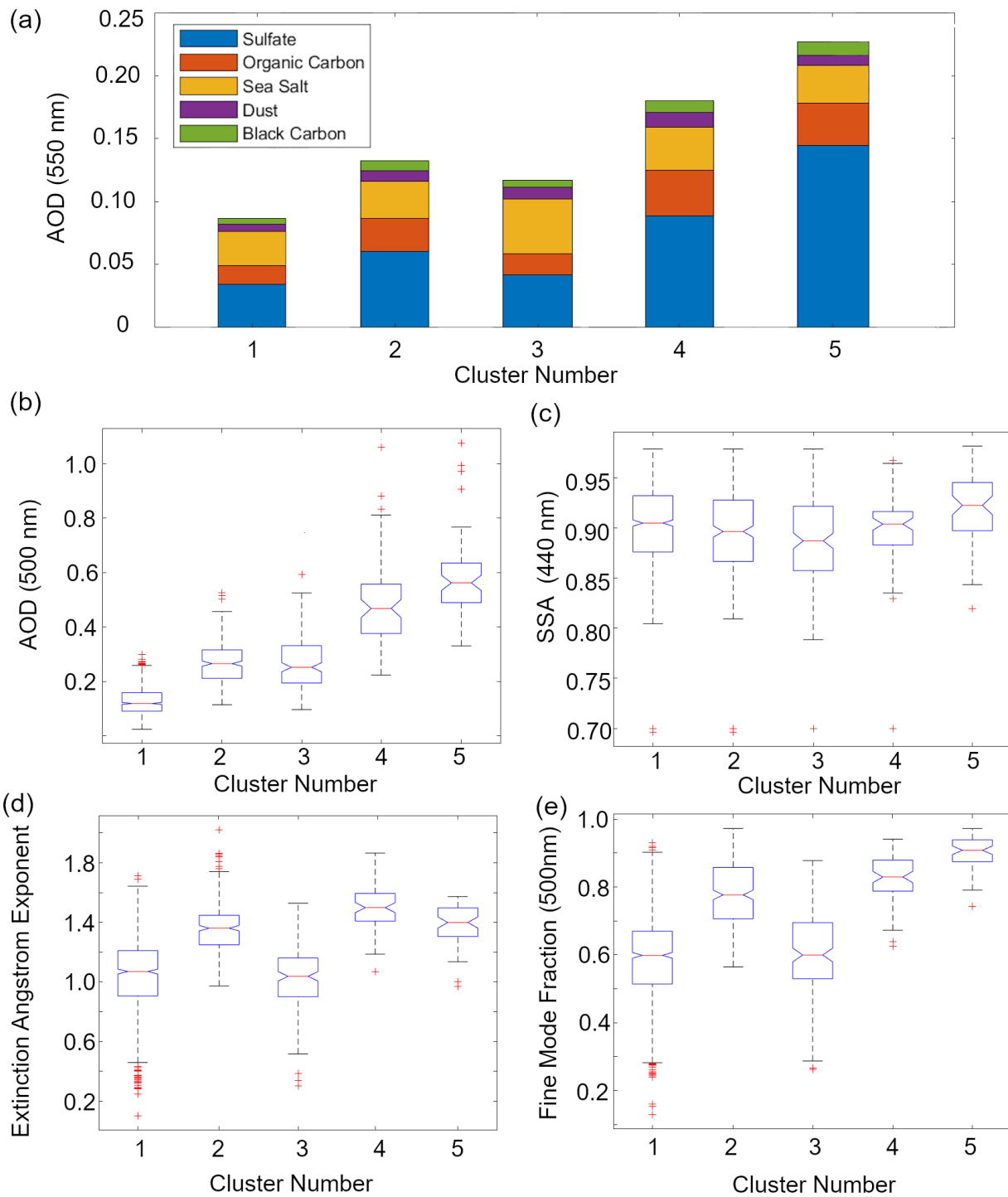
Figure 7: (a) Average compositional contributions to aerosol optical depth (AOD at 550 nm) from MERRA-2 per identified cluster. (counts per cluster from 1 to 5: 830, 284, 166, 74, 65). Boxplots of AERONET (b) total AOD (500 nm), (c) single scattering albedo (SSA at 440 nm), (d) extinction angstrom exponent (EAE, at 440 nm – 870 nm total), and (de) fine mode fraction (FMF, at 500 nm) per cluster.

3.3.2   Air Mass Types

28

788   Air masses have been classified in previous studies based on their AOD, EAE, FMF, and
789   FMFSSA values (e.g., Lee et al., 2010 and Aldhaif et al., 2021). The criteria from different
790   studies (Table 2) were applied per cluster. Median total AOD of cluster 1 (0.12) was less than 0.2
791   (Fig. 7b), which is the threshold for sea salt sources (Kaskaoutis et al., 2007)(Kaskaoutis et al.,
792   2009; Kaskaoutis et al., 2007). Half of the data points in cluster 1 also fall below the threshold
793   for clean environments (AOD < 0.1) (Sorooshian et al., 2013). Based on its median FMF (0.60)
794   and EAE (1.07, where EAE < 1 is coarse and EAE >1 is fine) and FMF (0.60) values (Fig. 7c7d
795   and 7d7e), cluster 1 is a mixture of fine and coarse particles. The fine Cluster 1 is the only cluster
796   with a median that meets that threshold value for clean marine sources (AOD < 0.2), and we
797   know from Sect. 3.3.1 that its average VSD magnitude was greater for the coarse fraction and
798   that its sea salt contribution to total AOD was second greatest among the clusters. Thus, we can
799   say that most probably, cluster 1 is a background clean marine source, since it also is
800   predominant throughout the seasons (Fig. 6b). This makes sense given the proximity of the ocean
801   to Metro Manila from both the east and the west. The median SSA (0.90 at 440 nm) for cluster 1
802   (Fig. 7c), however, suggests the presence of absorbing particles most probably due to high black
803   carbon in the local source (Cruz et al., 2019) that is mixed in with this generally clean marine
804   source.

805   Most of the data from the other clusters all fall in the polluted category (Table 2), based on their
806   median total AODs (>0.1) (Fig. 7b). Cluster 2 has a median FMF value of 0.78 (Fig. 7c7e),
807   which suggests that most of the particles in this air mass are in the fine fraction. They are,
808   however, not sufficiently dominant in the aerosol for them to be typical of urban/industrial
809   sources. The average VSDs (Fig. 6a) of cluster 2 similarly suggest that their relative
810   accumulation mode magnitude is higher than the coarse magnitude, but not much higher. Like
811   cluster 1, cluster 2 is also more evenly distributed across the seasons (Fig. 6b)). The median SSA
812   for cluster 2 (0.90 at 440 nm) is also similar to the SSA of cluster 1 (Fig. 7c) where the local and
813   background particles are mixed. Cluster 2 could be a fine polluted background source
814   superimposed on the dominant marine source. Metro Manila is a megacity with continuous and
815   large amounts of sources that could be, due to its proximity to the ocean, interacting with the
816   background.

817   Based on its median EAE value (1.04) (Fig. 7d), cluster 3 is mixed but mostly in the coarse
818   fraction, consistent with its VSD profile (Fig. 6a) which has the highest coarse magnitude (FMF
819   = 0.60) compared to the other clusters. The contribution of data from September to February is
820   greatest in cluster 3, consistent with expected coarser particles during this period when the winds
821   are initially shifting from the southwest before becoming more northeasterly, as previously
822   noted. This air mass can be a mixed polluted air mass, which is possibly transported due to the
823   large sea salt contribution to total AOD (Sect. 3.3.1).Median SSA (0.89 at 440 nm) was lowest
824   for cluster 3 (Fig. 7c), this and the relatively high coarse particle contribution suggests cluster 3
825   as a possible dust source based on past studies (Lee et al., 2010). This air mass can be a mixture
826   of local sources and transported dust air masses, the large sea salt contribution (~37%) to total
827   AOD (Sect. 3.3.1) can be related to long-range transport.

828   Both clusters 4 and 5 have median total FMF (0.83 and 0.91) (Fig. 7c7e) values exceeding the
829   mark (> 0.8, Table 2) for urban/industrial air masses. Combining this and results from the
830   previous sections confirms that cluster 4 can be an urban/industrial source given that it had the
831   highest median accumulated mode peak and organic carbon contribution (~20%) to total AOD

832 among the clusters. The median SSA for cluster 4 (0.90 at 440 nm) was similar to the median
833 SSA of clusters 1 and 2 (Fig. 7c), but the maximum SSA value for this cluster was lowest in
834 general among all the clusters suggesting cluster 4 has the net most absorptive effect. The cluster
835 4 air mass is probably from local sources and transported biomass burning emissions. The high
836 median EAE (1.40, Fig. 7d) may be associated with aerosol particles due to biomass burning
837 (Deep et al., 2021).

838 Cluster 5 had the highest median total AOD (0.56) and FMF (0.91) values (Fig. 7c7b and 7e). It
839 also had the highest (Fig. 7a) sulfate contribution (~64%) to total AOD as well as(Fig. 7a), the
840 highest median SSA (0.92 at 440 nm, thus most reflective particles among the clusters) (Fig. 7c),
841 and a shifted accumulation mode peak (Fig. 6a). These characteristics suggest that cluster 5 is a
842 possible cloud processing air mass (Eck et al., 2012). The larger peak in the accumulation mode
843 is possibly the cloud signature. Previous studies have attributed this larger mode to cloud
844 processing due to the conversion of SO_2 to sulfate (Hoppel et al., 1994). Cloud processing is a
845 major source of sulfate (Barth et al., 2000).

846 The distribution of the air masses based on the abundance of the VSD profiles per cluster suggest
847 prevalent clean marine (58% of the total VSD counts) and background fine polluted (20%) air
848 masses over Metro Manila. The mixed polluteddust (12%), urban/industrial (5%), and cloud
849 processing (5%) air masses contribute 22% all togetheraltogether. We can investigate more
850 deeply and look at specific case studies that can better describe the air masses identified here.
851
852 **3.4   Case Studies**
853 Selected case studies are used to highlight periods with the highest AOD values and strongest
854 clear sky (no rain and heavy clouds) daytime aerosol particle sources within the sampling period.
855 As such, the clusters that are associated with the selected case studies are the clusters (3-5) with
856 higher VSD concentration magnitudes.
857
858 3.4.1   Long Range Transport of Smoke
859 Both cases of long-range transport of smoke discussed below have similar VSDs (Fig. 8a and 9a)
860 to the urban/industrial cluster VSD (cluster 4, Fig. 6a). Organic carbon was the dominant
861 contributor to AOD (Fig. 8b and 9b) for both long-range transport cases. The first of two events
862 occurred around 1 April 2020 with smoke presumed to come from East Asia. The VSD of this
863 specific case (Fig. 8a) is most like the urban/industrial cluster (cluster 4 in 3.3.2, Fig. 6a) because
864 of the high magnitude of its accumulated mode peak, its timing (April), and the enhanced
865 organic carbon contribution to AOD in the area (Fig. 8b). Though the absolute black carbon
866 contribution to AOD was highest here compared to the other case studies, and in general for the
867 AERONET data, it was organic carbon that was more prevalent in terms of contribution to total
868 AOD. Smoke is comprised of both soot carbon and organic carbon, amongst other constituents
869 (Reid et al., 2005).
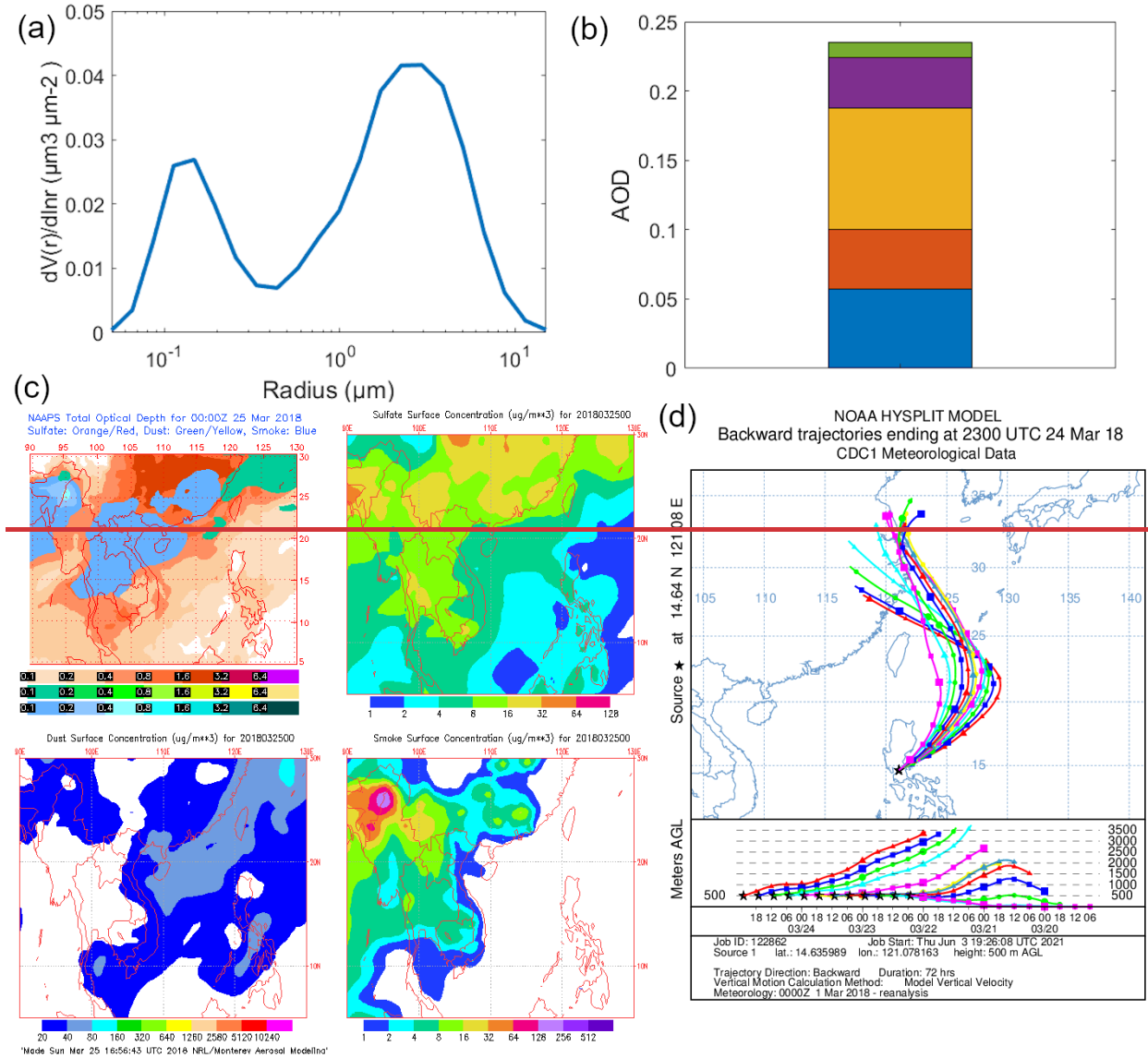
Figure 8: Case study of long-range transport (smoke – East Asia) around 1 April 2010. (a)
AERONET VSDs at (blue) 00:01 and (red) 00:26 UTC, (b) AOD from AERONET (gray:
median AOD at 500 nm) and MERRA-2 hourly (green: black carbon, violet: dust, yellow: sea
salt, orange: organic carbon, blue: sulfate) compositional contributions to AOD (550 nm) closest
in time to 00:01 UTC, (c) NAAPS maps of total and compositional hourly AOD (orange/red:
sulfate, green/yellow: dust, blue: smoke) and sulfate, dust, and smoke surface concentrations at
00:00 UTC, and (d) HYSPLIT threeseven-day back-trajectories arriving at Manila Observatory
at 00:00 UTC.

The smoke contribution to AOD from NAAPS (Fig. 8c) for the first smoke case was visible in
the Philippines (0.2) and seemed to come from East Asia were the smoke contribution to AOD
was greater (reaching 0.8) especially in Peninsular Southeast Asia. Smoke surface concentrations
were also widespread (Fig. 8c) with greatest concentrations in East Asia that reached the
Western Philippines, though seemingly disconnected over the sea. There were observed biomass

32

885   burning emissions in the Peninsular Southeast Asia (southern China, Burma, and Thailand) at
886   this time (Shen et al., 2014). The direction of the air mass coming into Metro Manila was from
887   the northeast, which curved from the west in the direction of East Asia based on HYSPLIT back-
888   trajectories (Fig. 8d).

889   The second smoke case was on 15 September 2009 with the source being Southeast Asia. The
890   back-trajectories of this case study (Fig. 9d) are from the southwest of the Philippines, and in the
891   direction of the Malaysia and Indonesia. NAAPS maps likewise show elevated AOD,
892   specifically smoke contribution to AOD (Fig. 9c), as well as enhanced smoke surface
893   contributions in the area around Metro Manila for this second smoke case study. The observed
894   AOD and smoke surface concentration increased specifically from the southwest of the
895   Philippines in the same direction of the back-trajectories. There were fires in the lowland (peat)
896   forests of Borneo around this time (NASA, 2009). MERRA-2 AOD contributions for this case
897   were greatest due to organic carbon as well as sulfate (Fig. 9b), and the absolute black carbon
898   contributions were greatest compared to other cases. The VSD of this smoke case from Southeast
899   Asia (Fig. 9a) resembled that from long-range transported smoke from East Asia (Fig. 8a) and
900   the urban/industrial air mass (cluster 4, Fig. 6a). This case occurred in the afternoon, which was
901   the prevalent time that the urban/industrial air mass was observed (Fig. 6c).
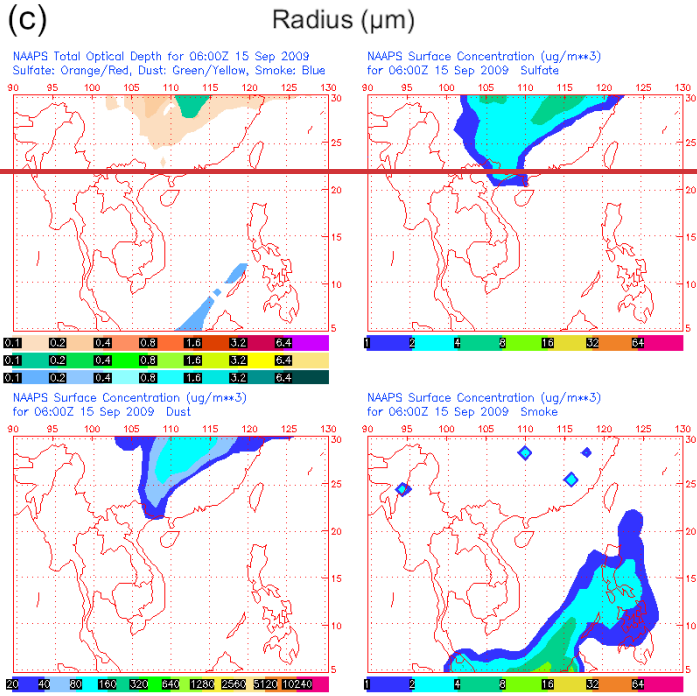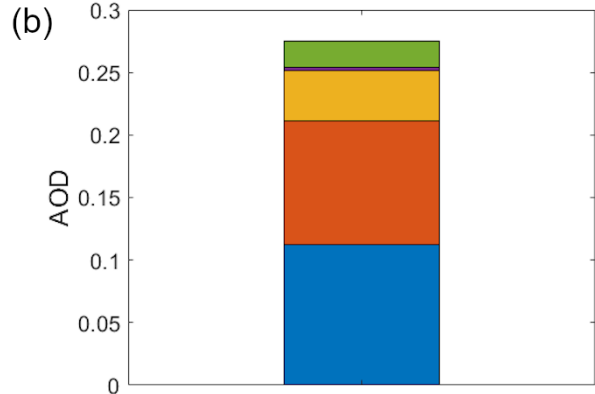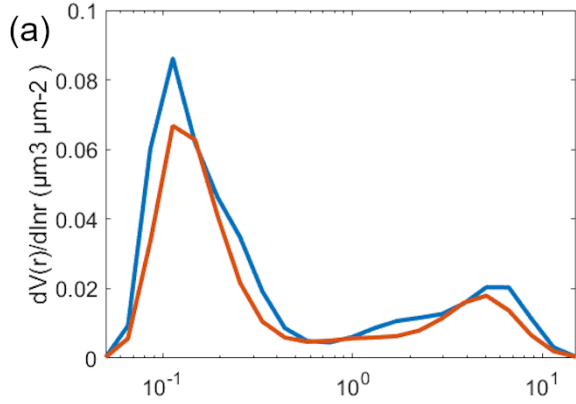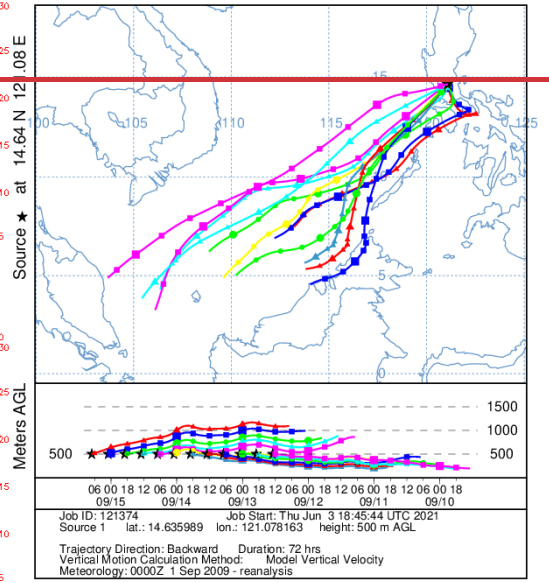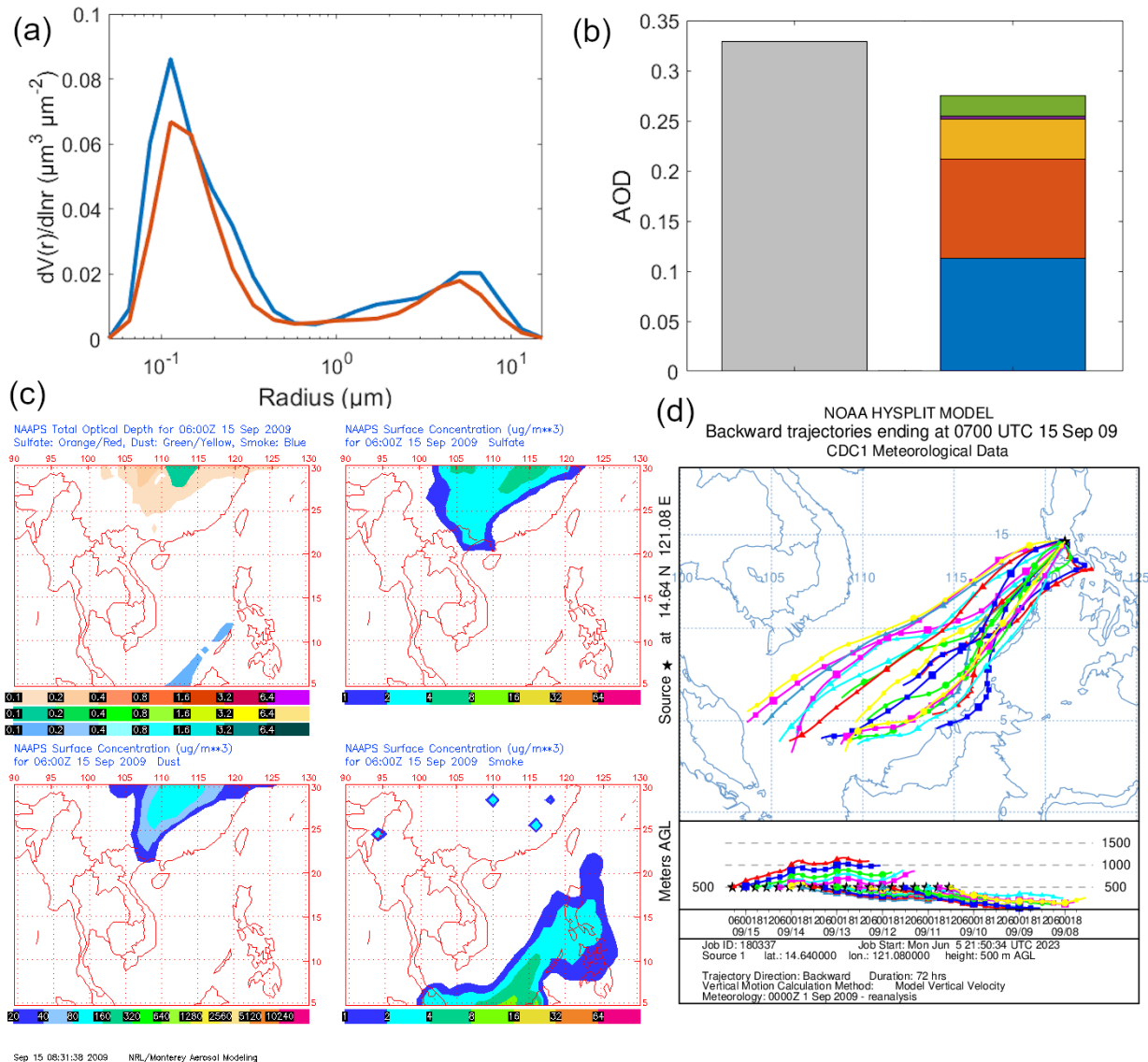
34

Figure 9: Case study of long-range transport (smoke – Southeast Asia) around 15 September 2009. (a) AERONET VSDs at (blue) 07:27 and (red) 07:52 UTC, (b) AOD from AERONET (gray: median AOD at 500 nm) and MERRA-2 hourly (green: black carbon, violet: dust, yellow: sea salt, orange: organic carbon, blue: sulfate) compositional contributions to AOD (550 nm) closest in time to 07:27 UTC, (c) NAAPS maps of total and compositional hourly AOD (orange/red: sulfate, green/yellow: dust, blue: smoke) and sulfate, dust, and smoke surface concentrations at 06:00 UTC, and (d) HYSPLIT threeseven-day back-trajectories arriving at Manila Observatory at 07:00 UTC.

3.4.2 Long Range Transport of Dust

The VSD of this specific case on 24 March 2018 (Fig. 10a) was most similar to the mixed polluteddust cluster (cluster 3), which had a mixed size distribution but a more dominant coarse contribution. This is consistent with the most dominant contribution to AOD in the area, which was sea salt and dust (Fig. 10b). The back-trajectories were from East Asia around the same latitude as Taiwan (Fig. 10d). That area, at that time, had increased AOD in general from sulfate

919 and dust (Fig. 10c). The AOD from both AERONET and MERRA-2 (Fig. 10b) are lower than
920 0.3 (the AOD threshold for dust in other studies, Table 2) because of the long distance from the
921 source (thousands of kilometers). The dust and sulfate seemed to have been transported to Metro
922 Manila from East Asia based on the NAAPS sulfate and dust surface concentrations (Fig. 10c).
923

924

925
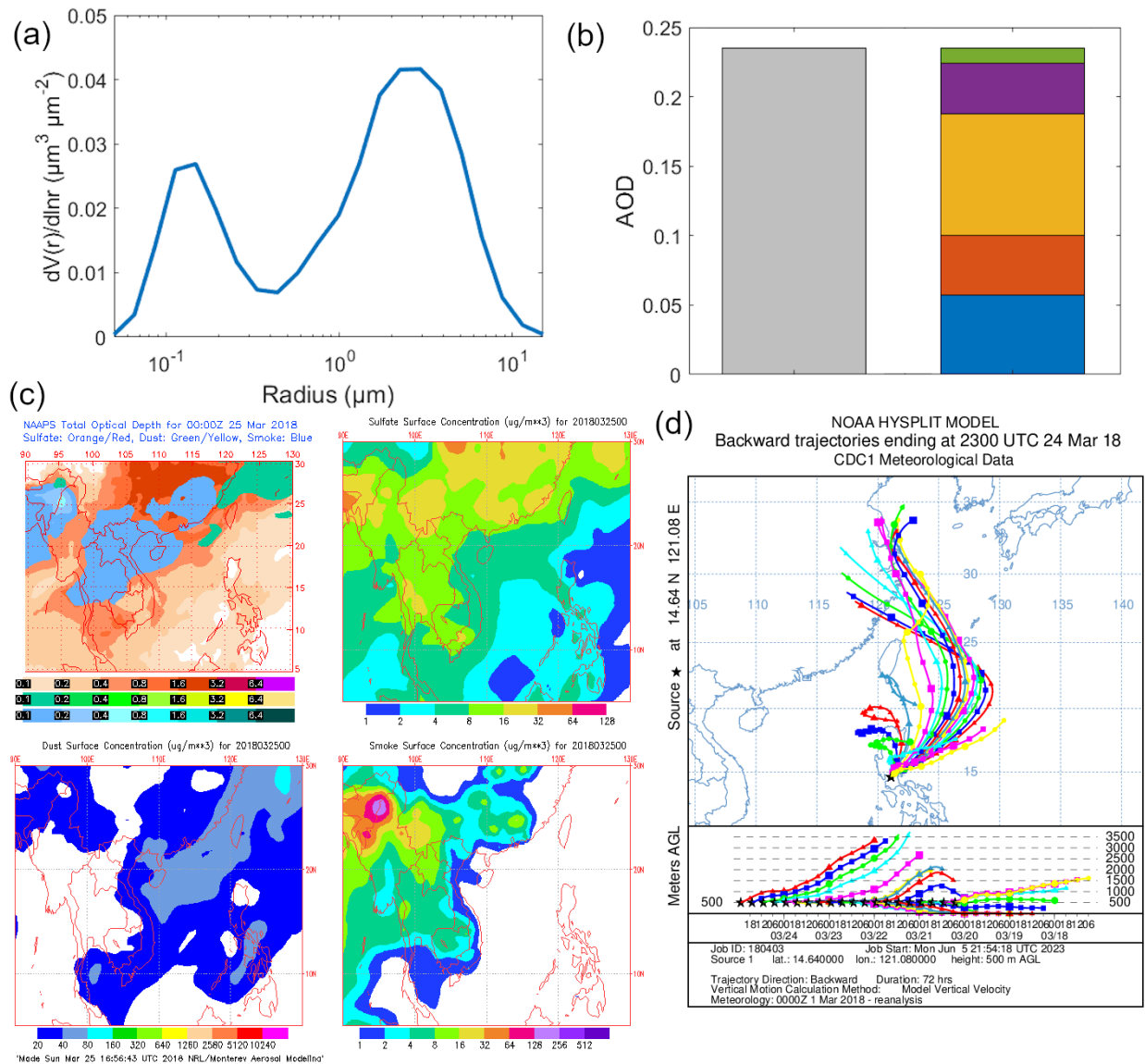
Figure 10: Case study of long-range transport (dust) around 24-25 March ~~2009~~2018. (a)
AERONET VSD at (blue) 23:23 UTC, (b) AOD from AERONET (gray: AOD at 500 nm) and
MERRA-2 hourly (green: black carbon, violet: dust, yellow: sea salt, orange: organic carbon,
blue: sulfate) compositional contributions to AOD (550 nm) closest in time to 23:23 UTC, (c)
NAAPS maps of total and compositional hourly AOD (orange/red: sulfate, green/yellow: dust,
blue: smoke) and sulfate, dust, and smoke surface concentrations at 00:00 UTC on March 25,
and (d) HYSPLIT ~~three~~seven-day back-trajectories arriving at Manila Observatory at 23:00
UTC.

~~3.5~~3.4.3   Cloud Processing

Sulfate dominated the AOD (Fig. 11b) for this case on 26 August 2009 in the area around Metro
Manila. This along with its VSD exhibiting a second peak (Fig. 11a) in the accumulation mode
make it very similar to the cloud processing cluster (cluster 5). Sulfate has been known to be
enhanced through chemical productions in clouds and is used as a signature for cloud processing
(Barth et al., 2000; Ervens et al., 2018). Aqueous production of sulfate is significant in areas with

37

941 sources and clouds (Barth et al., 2000), and this case study has both. Aside from the high sulfate
942 contribution to AOD, the cloud fraction (Aqua/MODIS, Terra/MODIS, Fig. S3) is very high
943 (~100%) in the area of the back-trajectories (Aqua/MODIS, Terra/MODIS, Fig. S211d).
944 Interestingly, there is no regional AOD elevation observed in the NAAPS maps (Fig. 11c) for
945 this time. There are increased surface smoke and sulfate levels in East Asia as well as southwest
946 of the Philippines, and though the back-trajectories (Fig. 11d) do show a northeastward direction,
947 they do not reach far enough into mainland East Asia. It is possible that even while there are
948 known regional sources of sulfate in Southeast Asia (Smith et al., 2011; Li et al., 2017), this case
949 could be local to the Philippines. There is in fact a large power plant northwest of Metro Manila
950 (Jamora et al., 2020).
951
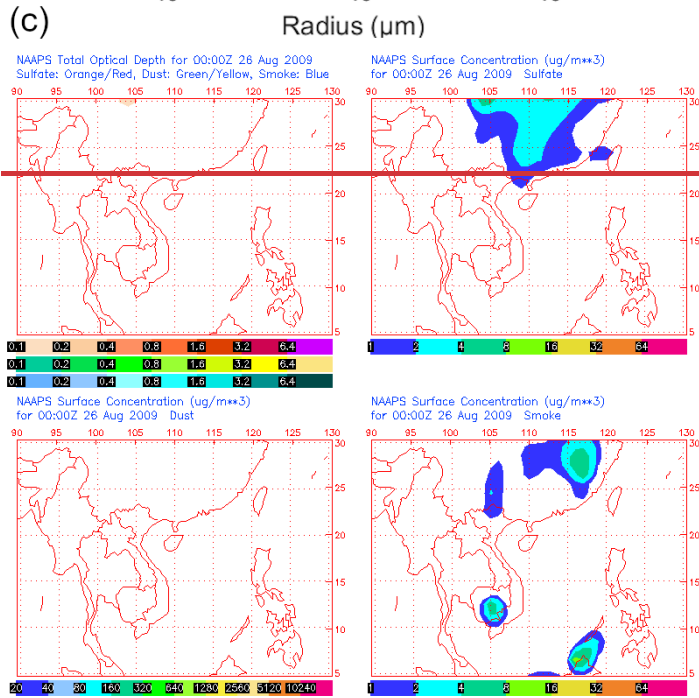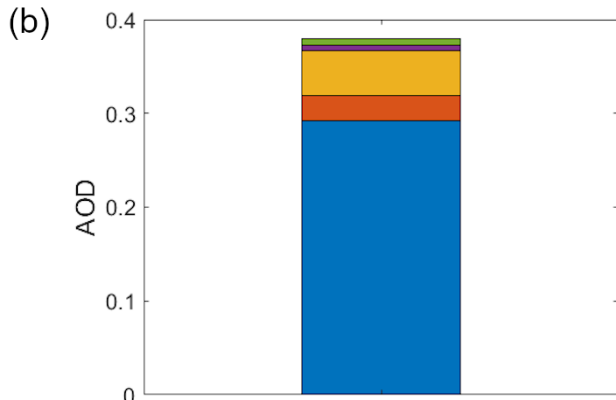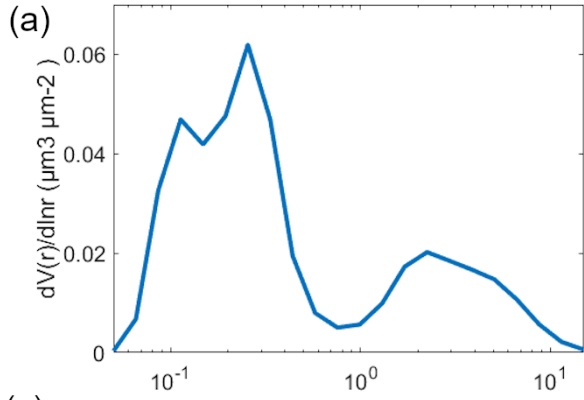
953
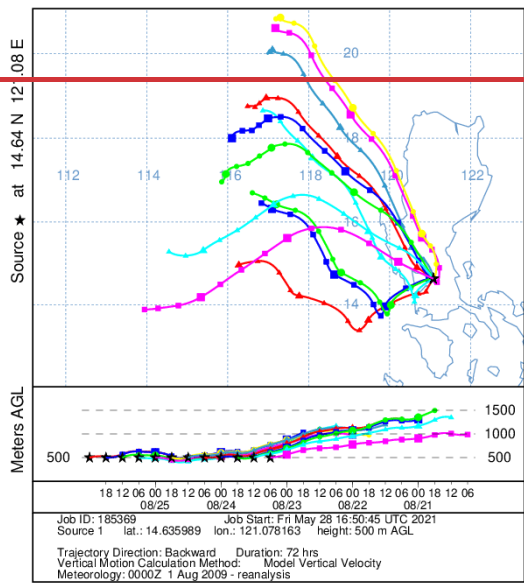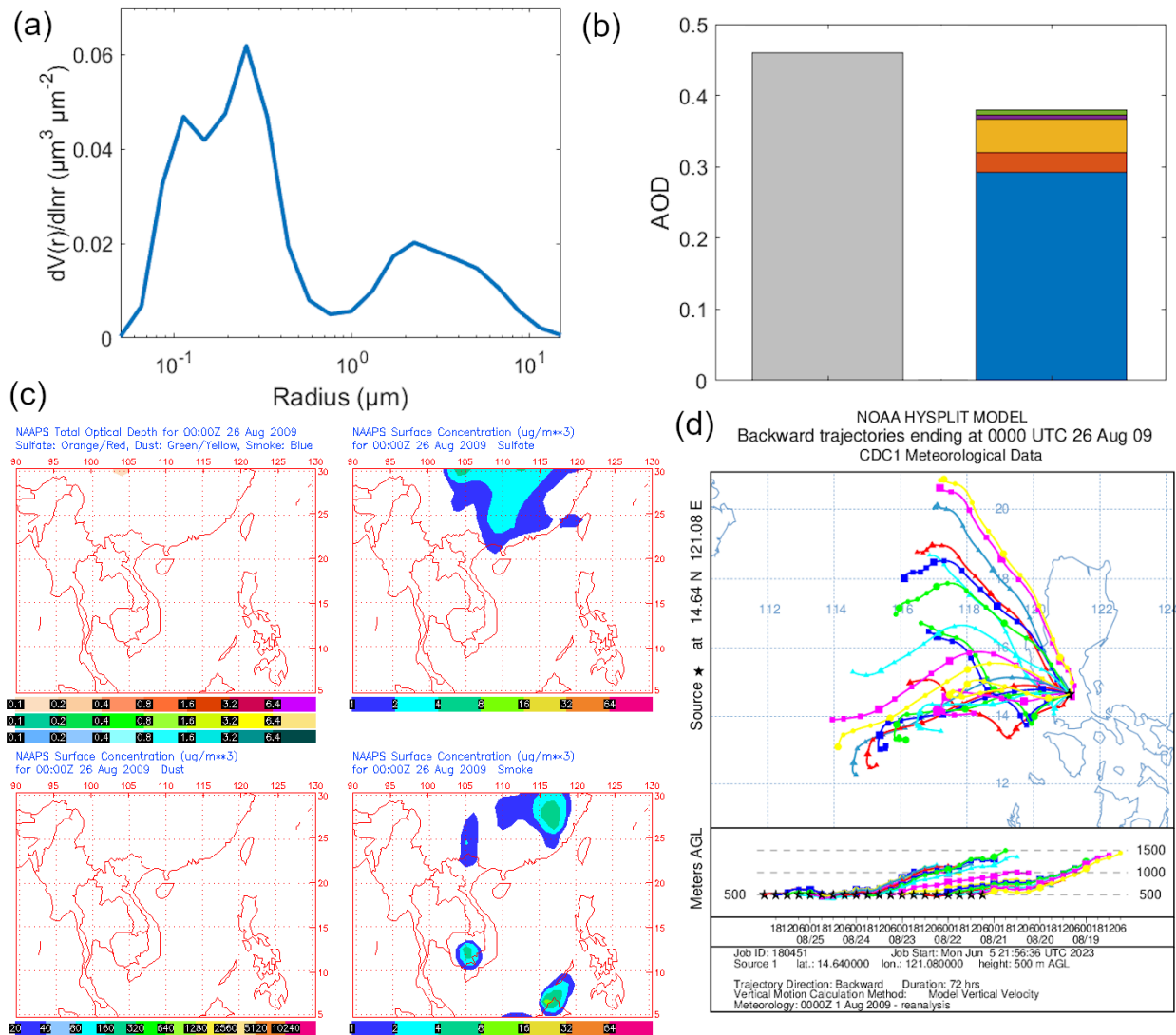
Figure 11: Case study of cloud processing on 26 August 2009. (a) AERONET VSDs at 00:18
UTC, (b) AOD from AERONET (gray: median AOD at 500 nm) and MERRA-2 hourly (green:
black carbon, violet: dust, yellow: sea salt, orange: organic carbon, blue: sulfate) compositional
contributions to AOD (550 nm) closest in time to 00:18 UTC, (c) NAAPS maps of total and
compositional hourly AOD and contributions and smoke surface concentrations at 00:00 UTC,
and (d) HYSPLIT threeseven-day back-trajectories arriving at Manila Observatory at 00:00
UTC.

3.63.5 EOF Analysis of AOD in Southeast Asia

To contextualize the analysis of aerosol particle

The air masses in Metro Manila, major are influenced by regional sources of aerosol particles in
Southeast Asiawhich were identified based on the dominant principal components fromthrough
EOF analysis of AOD. Three principal components (PC, Fig. 12) explained most of the data
variance (73.77%) (Fig. 12a) and were all well-separated from each other and are therefore most

40

968 probably the major distinct aerosol particle sources in the region. They will be the focus of the
969 subsequent discussion.
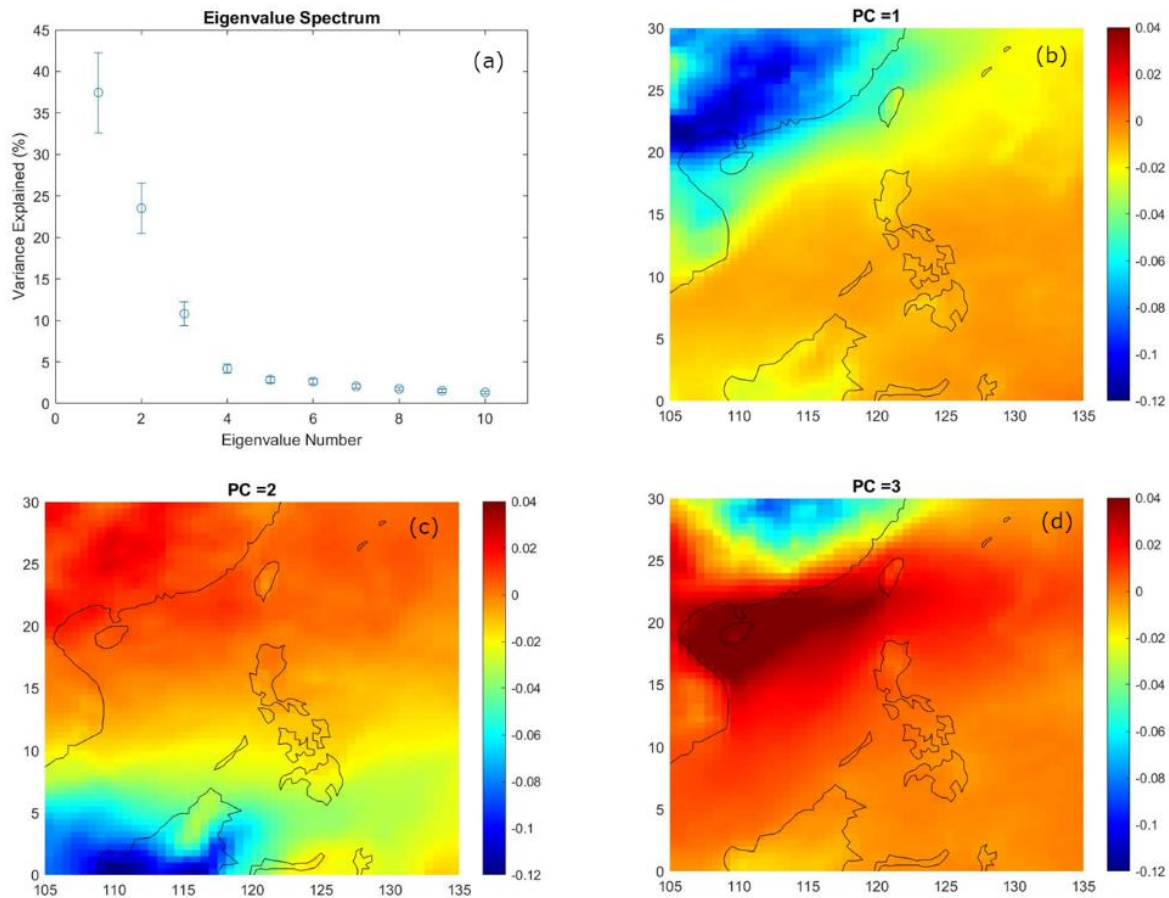
970
971 **Figure 12:** Results of the singular value decomposition. (a) Eigenvalue spectrum of the first ten
972 eigenvalues, (b-d) maps of the coefficients of regression AOD anomalies onto the first three
973 principal components.

974 The first PC explains 37.46% of the data variance (Fig. 12a) and, based on the map of the
975 regression coefficients (Fig. 12b), separates mainland East Asia from the Philippines and
976 Indonesia. East Asia is a globally recognized source for high AOD (Li et al., 2013), and its
977 contribution to particles in Southeast Asia possibly corresponds to the first PC. The second PC
978 explains 25.51% of the data variance (Fig. 12a) and separates ~~the~~ southern Southeast Asia from
979 northern Southeast Asia at around 15°N (Fig. 12c). Southern Southeast Asia is a known regional
980 source of aerosol particles due to biomass burning (Cohen et al., 2017) and could be associated
981 with the second PC. The third PC explains 10.80% of the data variance (Fig. 12a) and separates
982 northern East Asia from southern East Asia mainland and the rest of Southeast Asia (Fig. 12d).

983 To gain confidence in the association of the PCs with their sources, we present correlation maps
984 between the first three PCs to the fractional contributions of sulfate and organic carbon to AOD
985 for the entire dataset.

986　The correlation maps of the first PC and the sulfate contribution to AOD (Fig. 13a and 13d)
987　show high and statistically significant correlations (gray areas) in mainland East Asia and
988　Taiwan, parts of western Philippines and Borneo, which are the probable sulfate sources. Clues
989　from the mean monthly wind vector maps in April (Fig. 14a and 14d) and mean monthly AOD in
990　either March or April (Fig. S3c or S3e) most resembling the features of regression map of the
991　first PC (Fig. 12b) and the PC time series peaking in March (Fig. S4) together suggest that the
992　first PC may be associated with air masses that are present around March or April. Emissions
993　sources and meteorology that are dominant during the peak dates in the PC time series offer
994　clues to the attribution of each PC. The Southeast Asia region and the Philippines is influenced
995　by the monsoon systems (Coronas, 1920; Matsumoto et al., 2020) and February to March is the
996　time when the winds are transitioning from the northeasterly to easterly. The first PC could be
997　affected by the easterly winds, which are dominant around March when its PC values peaked.
998　The higher-level winds (free troposphere) (Fig. 14a) in April are from the west in mainland East
999　Asia and are from the east in the Philippines and it is possible that the different wind regimes are
1000　distinguishing the sulfate sources in East Asia and the Philippines and beyond. Sulfate is a
1001　known product of industry in East Asia (Smith et al., 2011; Li et al., 2017) while the West Luzon
1002　and West Visayas islands have large power plants (Jamora et al., 2020).
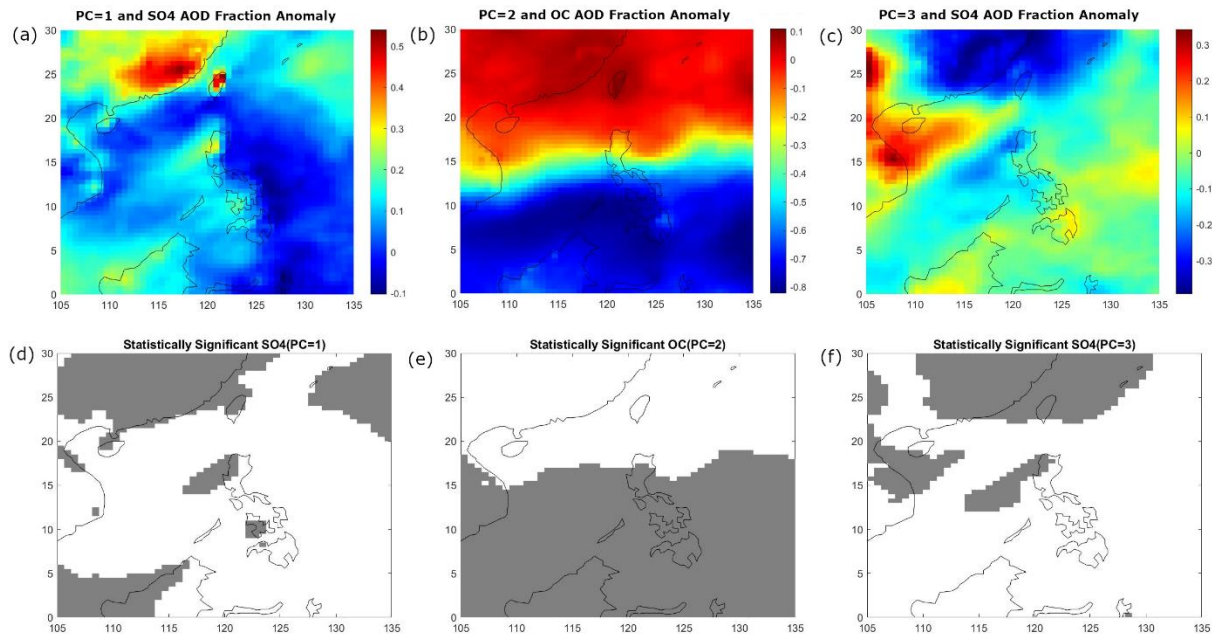
1003
1004　**Figure 13:** Correlation coefficients of principal components with (a/c) sulfate AOD fraction and
1005　(b) organic carbon AOD fraction. Statistically significant (90%, d-f) areas are shaded gray.
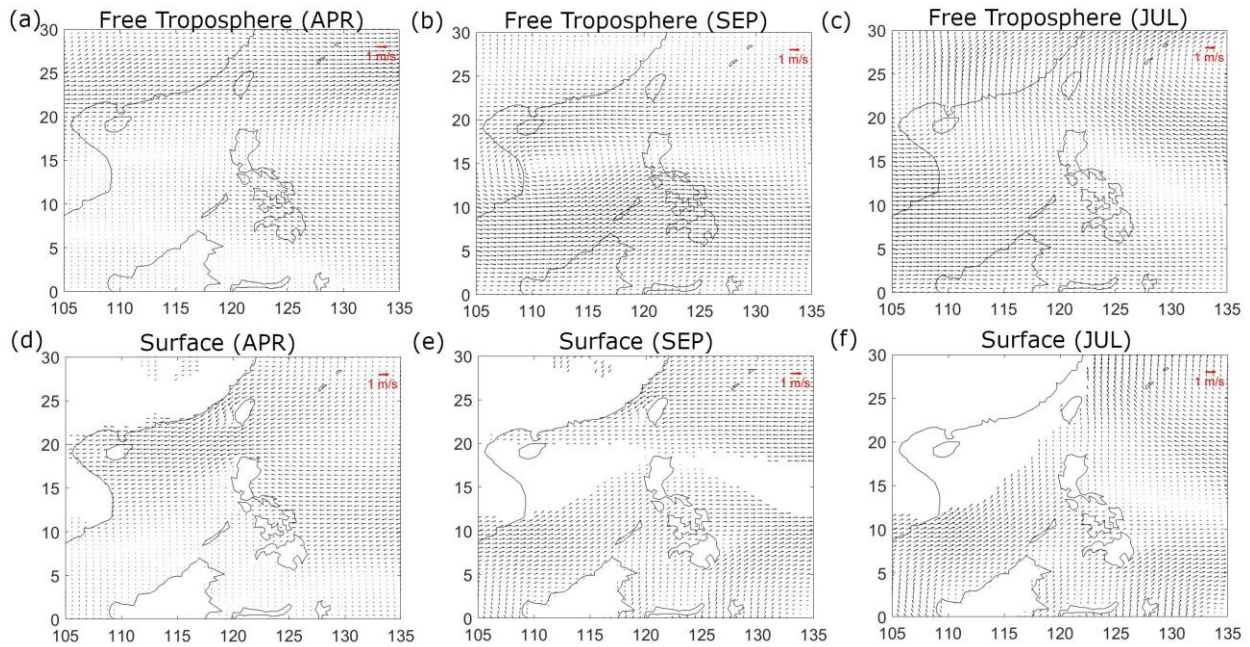
Figure 14: Monthly averaged winds for (a & d) April, (b & e) September, and (c & f) July from MERRA-2 at (725 hPa, a-c) the free troposphere approximate and at (1000 hPa, d-f) the surface.

The correlation maps of the second PC and the OC contribution to AOD (Fig. 13b and 13e) show high and statistically significant correlations from 0°N to 15°N. The large magnitude of the correlation coefficient (gray areas in Fig. 13b) stands out in ~~the~~ southern Southeast Asia and is the potential OC source. In this case, it is known that Indonesia is a major source of biomass burning during its fire season (Glover and Jessup, 1998), and thus the local significance established in the southern Southeast Asia is most likely due to the Indonesia biomass burning source. The burning season in Indonesia is from August to October, and that is the same time when the AOD values peak in the area (Fig. S3h, S3i, and S3j), as well as the peak of the second PC in the time series (Fig. S4). Winds are usually from the southwest and west due to the southwest monsoon from September to October, when the second PC peaked, and thus the second PC may be related to the southwest monsoon. During the same time the surface and free troposphere mean monthly winds (Fig. 14b and 14e) are from the southwest (in the general direction of Indonesia) towards the south portion of Southeast Asia and thus corroborate the observation that the second PC may be highlighting the regional effect of the Indonesia forest fires. Of interest is the line of separation of the northern and southern Southeast Asia in the principal component that is within the area of the monsoon trough (Wang et al., 2007). This line is also evident in the surface and the free troposphere maps where the southwest winds from the area of Indonesia meet the easterlies in north Southeast Asia (Fig. 14b and 14e) and which thus appears to be limiting the dispersion of the biomass burning emissions to southern Southeast Asia.

The third PC was also well correlated to the sulfate AOD fraction though, compared to the first PC correlation maps, there were distinctions between the northern and southern East Asia regions (Fig. 13c and 13f). The local Philippine source still came out in the correlation maps as a significant source. It was not clear from the PC time series (Fig. S4), which showed peaks in the third PC in February, how the dates were related to the PC profile. The free troposphere winds in

43

1034   July (Fig. 14c), as well as the AOD monthly mean map in July (Fig. 14c), however, showed
1035   more similarities to the third PC regression map. Both showed a delineation between the
1036   northern East Asia and southern East Asia (including Hong Kong) features. Mean winds (Fig.
1037   14c) in the free troposphere are from the west, due to the southwest monsoon, in the area around
1038   the Philippines, and they were from the northeast in north Southeast Asia. The interface of the
1039   winds is within the approximate location of the monsoon trough in July (Wang et al., 2007), and
1040   it is thus possible that the monsoon trough is causing the separation of the sulfate sources. This
1041   could be investigated further. The monsoon trough has been noted to scavenge aerosol particles
1042   from southern Southeast Asia (Reid et al., 2013). It is evident from the analysis that meteorology
1043   affects the transport and processing of aerosol particles in region which along with local sources
1044   contribute to the aerosol composition in Southeast Asia (Cruz et al., 2019; AzadiAghdam et al.,
1045   2019; Braun et al., 2020; Hilario et al., 2020b; Hilario et al., 2022).
1046
1047   **4.   Conclusion**

1048   Metro Manila has both urban and industrial local sources known to contribute to the dominance
1049   of fine mode particles in its air (Cruz et al., 2019). Ten years of AERONET data in Manila
1050   Observatory suggest that aerosol particles in Metro Manila were mixed in size but with a
1051   prevalent fine mode fraction (>50% FMF) throughout the year. Background clean marine aerosol
1052   particles (58% of the time) and fine polluted aerosol particles (20% of the time) were the most
1053   dominant clear sky day sources impacting the atmospheric column over Metro Manila based on
1054   cluster analysis of volume size distributions. The proximity of Metro Manila to the sea, both in
1055   the east and west, along with local sources, transportation being the most prominent, together
1056   contribute to the prevalence of the marine and fine particles. The prevalence of marine particles
1057   could explain the relatively small AOD values in Metro Manila compared to other Southeast
1058   Asian megacities (Reid et al., 2013).

1059   Regional sources and meteorology also impact monthly aerosol optical depth trends in Metro
1060   Manila from EOF analysis. Biomass burning from Borneo and Sumatra emerged in the study as
1061   the second most prevalent regional anthropogenic aerosol particle source in Southeast Asia.
1062   Though the monsoon trough limits the dispersion of aerosol particles throughout the entire
1063   Southeast Asia, biomass burning emissions impact southern Southeast Asia including Metro
1064   Manila during the southwest monsoon (July to September). The monsoon winds facilitate the
1065   transport of fine particles during the peak burning season in Borneo and Sumatra (August-
1066   September). This is experienced in Metro Manila as higher than usual aerosol particle loadings
1067   duringaround the same period. (August to October). Climatologically, August iswas also when
1068   aerosol optical depth peaked over Metro Manila, concurrentthere were particles with the greatest
1069   fine mode fractions that were relatively absorbing and non-hygroscopic possibly due to increased
1070   organic and elemental carbon fractional contributions. Though not as strong a source as the
1071   Borneo and Sumatra case, the peninsular Southeast Asia burning season (March-April) also
1072   contributed to extreme aerosol particle concentrations over Metro Manila.

1073   High aerosol particle loadings due to transported dust, probably from East Asia, were observed
1074   in Metro Manila during the transition period between the southwest and northeast monsoons and
1075   during the northeast monsoon (December to February). These extreme events are transient
1076   because the lowest median aerosol particle loadings of the year were observed during the
1077   northeast monsoon when annual wind speeds were highest. Particles then were observed to be

largest in diameter, with the greatest coarse fraction contribution, relatively high absorptivity, and most hygrosocopicity, compared to other months of the year. This is probably due to constituents other than soot, especially aged dust (Kim and Park, 2012; Geng et al., 2014) and sea salt which the northeast winds appear to be bringing in from the general direction of the Luzon Island and the Philippine Sea (West Pacific Ocean).

Cloud processing is one of the cases that were linked to very high aerosol particle loading in Metro Manila. This is associated with sulfate sources, which appear more localized in nature because of a power plant nearby. This sulfate source seems to be distinct from the industrial sulfate air mass from East Asia, which is the most dominant regional aerosol particle source in Southeast Asia (Li et al., 2013). Winds appear to limit the mixing of this notable East Asia air mass with local industrial sources in the region including the Philippines and Indonesia.

The formation of cloud systems in Southeast Asia is complex due to intersecting large- and small-scale mechanisms. Additionally, the interaction of particles and clouds in Southeast Asia is not yet well understood. In Metro Manila, both topography and meteorology affect aerosol particle distribution (Cruz et al., 2023). This baseline study on the aerosol particle characteristics in Metro Manila and in regional Southeast Asia shows how meteorology impacts varied aerosol particle sources (e.g., sulfate, elemental carbon, and organic carbon) and their distribution in the region. This can help in mitigating aerosol particle sources in the region and in the deepening of the understanding of the relationship of aerosol particles, meteorology, and clouds.

Data availability

Aerosol Robotic Network (AERONET) (2020), Version 3 Direct Sun Algorithm, Site: Manila Observatory, Philippines, Accessed: [*28 September 2020*], https://aeronet.gsfc.nasa.gov/cgi-bin/webtool_aod_v3?stage=3&region=Asia&state=Philippines&site=Manila_Observatory&place_code=10&if_polarized=0

Aerosol Robotic Network (AERONET) (2020), Version 3 Direct Sun and Inversion Algorithm, Site: Manila Observatory, Philippines, Accessed: [*28 September 2020*], https://aeronet.gsfc.nasa.gov/cgi-bin/webtool_inv_v3?stage=3&region=Asia&state=Philippines&site=Manila_Observatory&place_code=10&if_polarized=0

Multi-angle Imaging SpectroRadiometer (MISR) Jet Propulsion Laboratory (2018), Level 3 Component Global Aerosol product in netCDF format covering a month V004, Accessed: [*22 November 2021],* https://search.earthdata.nasa.gov/

Global Modeling and Assimilation Office (GMAO) (2015), MERRA-2 inst3_3d_asm_Np: 3d,3-Hourly,Instantaneous,Pressure-Level,Assimilation,Assimilated Meteorological Fields V5.12.4, Greenbelt, MD, USA, Goddard Earth Sciences Data and Information Services Center (GES DISC), Accessed: [*10 March 2021*], https://doi.org/10.5067/QBZ6MG944HW0

Global Modeling and Assimilation Office (GMAO) (2015), MERRA-2 tavg1_2d_flx_Nx: 2d,1-Hourly,Time-Averaged,Single-Level,Assimilation,Surface Flux Diagnostics V5.12.4, Greenbelt,

1117 MD, USA, Goddard Earth Sciences Data and Information Services Center (GES DISC),
1118 Accessed: **[*10 March 2021*]**, https://doi.org/10.5067/7MCPBJ41Y0K6

1119 Global Modeling and Assimilation Office (GMAO) (2015), MERRA-2 tavg1_2d_csp_Nx: 2d,1-
1120 Hourly,Time-averaged,Single-Level,Assimilation,COSP Satellite Simulator V5.12.4, Greenbelt,
1121 MD, USA, Goddard Earth Sciences Data and Information Services Center (GES DISC),
1122 Accessed: **[*13 July 2021*]**, https://doi.org/10.5067/H0VVAD8F6MX5

1123 Nguyen, P., E.J. Shearer, H. Tran, M. Ombadi, N. Hayatbini, T. Palacios, P. Huynh, G.
1124 Updegraff, K. Hsu, B. Kuligowski, W.S. Logan, and S. Sorooshian, The CHRS Data Portal, an
1125 easily accessible public repository for PERSIANN global satellite precipitation data, Nature
1126 Scientific Data, Vol. 6, Article 180296, 2019, Accessed: **[*11 March 2021*],**
1127 https://doi.org/10.1038/sdata.2018.296

1128
1129 Author contributions
1130 GRL and AS designed the experiment. NL, SNU, GRL, GFG, HJO, JBS, and MTC, carried out
1131 various aspects of the data collection. GRL, AS, JBS, MOC, MRH, CC, and CCLDG conducted
1132 analysis and interpretation of the data. GRL prepared the manuscript draft with contributions
1133 from the coauthors. AFA, LDG, MRH, GRL, and AS reviewed and edited the manuscript. AS
1134 led the management and funding acquisition. All authors approved the final version of the
1135 manuscript.

1136
1137 Competing interests
1138 We declare that Armin Sorooshian is a member of the editorial board of Atmospheric Chemistry
1139 and Physics. The peer-review process was guided by an independent editor, and the authors have
1140 also no other competing interests to declare.

1141
1142 Acknowledgements

1148

1149 References:

1150 AERONET Inversion Products (Version 3):
1151 https://aeronet.gsfc.nasa.gov/new_web/Documents/Inversion_products_for_V3.pdf, access: June
1152 25, 2021, 2019.

1153 Alas, H. D., Müller, T., Birmili, W., Kecorius, S., Cambaliza, M. O., Simpas, J. B. B., Cayetano,
1154 M., Weinhold, K., Vallar, E., and Galvez, M. C.: Spatial characterization of black carbon mass
1155 concentration in the atmosphere of a southeast asian megacity: an air quality case study for
1156 Metro Manila, Philippines, Aerosol Air Qual. Res., 18, 2301-2317,
1157 https://doi.org/10.4209/aaqr.2017.08.0281, 2018.

1158   Aldhaif, A. M., Lopez, D. H., Dadashazar, H., and Sorooshian, A.: Sources, frequency, and
1159   chemical nature of dust events impacting the United States East Coast, Atmos. Environ., 231,
1160   117456, https://doi.org/10.1016/j.atmosenv.2020.117456, 2020.

1161   Aldhaif, A. M., Lopez, D. H., Dadashazar, H., Painemal, D., Peters, A. J., and Sorooshian, A.:
1162   An Aerosol Climatology and Implications for Clouds at a Remote Marine Site: Case Study Over
1163   Bermuda, J. Geophys. Res.- Atmos., 126, e2020JD034038,
1164   https://doi.org/10.1029/2020JD034038, 2021.

1165   Alizadeh-Choobari, O., and Gharaylou, M.: Aerosol impacts on radiative and microphysical
1166   properties of clouds and precipitation formation, Atmos. Res., 185, 53-64,
1167   https://doi.org/10.1016/j.atmosres.2016.10.021, 2017.

1168   Andrews, E., Ogren, J. A., Kinne, S., and Samset, B.: Comparison of AOD, AAOD and column
1169   single scattering albedo from AERONET retrievals and in situ profiling measurements, Atmos.
1170   Chem. Phys., 17, 6041-6072, https://doi.org/10.5194/acp-17-6041-2017, 2017.
1171   Amnuaylojaroen, T.: Air Pollution Modeling in Southeast Asia—An Overview, Vegetation Fires
1172   and Pollution in Asia, 531-544, https://doi.org/10.1007/978-3-031-29916-2_31, 2023.

1173   Ångström, A.: On the atmospheric transmission of sun radiation and on dust in the air,
1174   Geografiska Annaler, 11, 156-166, 1929.

1175   Arthur, D., and Vassilvitskii, S.: k-means++: The advantages of careful seeding, Stanford, 2006.

1176   AzadiAghdam, M., Braun, R. A., Edwards, E.-L., Bañaga, P. A., Cruz, M. T., Betito, G.,
1177   Cambaliza, M. O., Dadashazar, H., Lorenzo, G. R., and Ma, L.: On the nature of sea salt aerosol
1178   at a coastal megacity: Insights from Manila, Philippines in Southeast Asia, Atmos. Environ., 216,
1179   116922, https://doi.org/10.1016/j.atmosenv.2019.116922, 2019.

1180   Bagtasa, G.: Contribution of tropical cyclones to rainfall in the Philippines, Journal of Climate,
1181   30, 3621-3633, 2017.

1182   Bañares, E. N., Narisma, G. T. T., Simpas, J. B. B., Cruz, F. A. T., Lorenzo, G. R. H.,
1183   Cambaliza, M. O. L., and Coronel, R. C.: Seasonal and diurnal variations of observed convective
1184   rain events in metro Manila, Philippines, Atmos. Res., 105646,
1185   https://doi.org/10.1016/j.atmosres.2021.105646, 2021.

1186   Barth, M., Rasch, P., Kiehl, J., Benkovitz, C., and Schwartz, S.: Sulfur chemistry in the National
1187   Center for Atmospheric Research Community Climate Model: Description, evaluation, features,
1188   and sensitivity to aqueous chemistry, J. Geophys. Res.- Atmos., 105, 1387-1415,
1189   https://doi.org/10.1029/1999JD900773, 2000.

1190   Bautista VII, A. T., Pabroa, P. C. B., Santos, F. L., Racho, J. M. D., and Quirit, L. L.:
1191   Carbonaceous particulate matter characterization in an urban and a rural site in the Philippines,
1192   Atmospheric Pollution Research, 5, 245-252, https://doi.org/10.5094/APR.2014.030, 2014.

1193   Bergstrom, R. W., Russell, P. B., and Hignett, P.: Wavelength dependence of the absorption of
1194   black carbon particles: Predictions and results from the TARFOX experiment and implications

1195   for the aerosol single scattering albedo, J. Atmos. Sci., 59, 567-577,
1196   https://doi.org/10.1175/1520-0469(2002)059<0567:WDOTAO>2.0.CO;2, 2002.

1197   Bergstrom, R. W., Pilewskie, P., Schmid, B., and Russell, P. B.: Estimates of the spectral aerosol
1198   single scattering albedo and aerosol radiative effects during SAFARI 2000, J. Geophys. Res.-
1199   Atmos., 108, https://doi.org/10.1029/2002JD002435, 2003.

1200   Bergstrom, R. W., Pilewskie, P., Russell, P. B., Redemann, J., Bond, T. C., Quinn, P. K., and
1201   Sierau, B.: Spectral absorption properties of atmospheric aerosols, Atmos. Chem. Phys., 7, 5937-
1202   5943, https://doi.org/10.5194/acp-7-5937-2007, 2007.

1203   Bi, J., Huang, J., Hu, Z., Holben, B., and Guo, Z.: Investigating the aerosol optical and radiative
1204   characteristics of heavy haze episodes in Beijing during January of 2013, J. Geophys. Res.-
1205   Atmos., 119, 9884-9900, https://doi.org/10.1002/2014JD021757, 2014.

1206   Björnsson, H., and Venegas, S.: A manual for EOF and SVD analyses of climatic data, CCGCR
1207   Report, 97, 112-134, 1997.

1208   Bohren, C. F., and Clothiaux, E. E.: Fundamentals of atmospheric radiation: an introduction with
1209   400 problems, John Wiley & Sons, 2006.

1210   Braun, R. A., Aghdam, M. A., Bañaga, P. A., Betito, G., Cambaliza, M. O., Cruz, M. T.,
1211   Lorenzo, G. R., MacDonald, A. B., Simpas, J. B., and Stahl, C.: Long-range aerosol transport
1212   and impacts on size-resolved aerosol composition in Metro Manila, Philippines, Atmos. Chem.
1213   Phys., 20, 2387-2405, https://doi.org/10.5194/acp-20-2387-2020, 2020.

1214   Buchard, V., Randles, C., Da Silva, A., Darmenov, A., Colarco, P., Govindaraju, R., Ferrare, R.,
1215   Hair, J., Beyersdorf, A., and Ziemba, L.: The MERRA-2 aerosol reanalysis, 1980 onward. Part
1216   II: Evaluation and case studies, Journal of Climate, 30, 6851-6872, https://doi.org/10.1175/JCLI-
1217   D-16-0613.1, 2017.

1218   Cahyono, W. E., Setyawati, W., Hamdi, S., Cholianawati, N., Kombara, P. Y., and Sari, W. J.:
1219   Observations of aerosol optical properties during tropical forest fires in Indonesia, Materials
1220   Today: Proceedings, 63, S445-S450, https://doi.org/10.1016/j.matpr.2022.04.113, 2022.

1221   Caido, N. G., Ong, P. M., Rempillo, O., Galvez, M. C., and Vallar, E.: Spatiotemporal analysis
1222   of MODIS aerosol optical depth data in the Philippines from 2010 to 2020, Atmosphere, 13, 939,
1223   https://doi.org/10.3390/atmos13060939, 2022.

1224   Chang, C.-P., Wang, Z., McBride, J., and Liu, C.-H.: Annual cycle of Southeast Asia—Maritime
1225   Continent rainfall and the asymmetric monsoon transition, Journal of climate, 18, 287-301,
1226   https://doi.org/10.1175/JCLI-3257.1, 2005.

1227   Che, H., Xia, X., Zhu, J., Wang, H., Wang, Y., Sun, J., Zhang, X., and Shi, G.: Aerosol optical
1228   properties under the condition of heavy haze over an urban site of Beijing, China, Environ. Sci.
1229   Pollut. R., 22, 1043-1053, https://doi.org/10.1007/s11356-014-3415-5, 2015.

1230   Chen, Q., McGowan, S., Gouramanis, C., Fong, L., Balasubramanian, R., and Taylor, D.:
1231   Rapidly rising transboundary atmospheric pollution from industrial and urban sources in

Southeast Asia and its implications for regional sustainable development, Environ. Res. Lett., 15, 1040a1045, https://doi.org/10.1088/1748-9326/abb5ce, 2020.

Choi, M., Lim, H., Kim, J., Lee, S., Eck, T. F., Holben, B. N., Garay, M. J., Hyer, E. J., Saide, P. E., and Liu, H.: Validation, comparison, and integration of GOCI, AHI, MODIS, MISR, and VIIRS aerosol optical depth over East Asia during the 2016 KORUS-AQ campaign, Atmos. Meas. Tech., 12, 4619-4641, https://doi.org/10.5194/amt-12-4619-2019, 2019.

Cohen, J. B.: Quantifying the occurrence and magnitude of the Southeast Asian fire climatology, Environmental Research Letters, 9, 114018, https://dx.doi.org/10.1088/1748-9326/9/11/114018, 2014.

Cohen, J. B., Lecoeur, E., and Hui Loong Ng, D.: Decadal-scale relationship between measurements of aerosols, land-use change, and fire over Southeast Asia, Atmos. Chem. Phys., 17, 721-743, https://doi.org/10.5194/acp-17-721-2017, 2017.

Coronas, J.: The Climate and Weather of the Philippines, 1903-1918, by Rev. José Coronas. SJ, Chief, Meteorological Division, Weather Bureau, Manila Observatory, Manila,: Bureau of Printing, 1920.

Crosbie, E., Sorooshian, A., Monfared, N. A., Shingler, T., and Esmaili, O.: A multi-year aerosol characterization for the greater Tehran area using satellite, surface, and modeling data, Atmosphere, 5, 178-197, https://doi.org/10.3390/atmos5020178, 2014.

Crosbie, E., Ziemba, L. D., Shook, M. A., Robinson, C. E., Winstead, E. L., Thornhill, K. L., Braun, R. A., MacDonald, A. B., Stahl, C., and Sorooshian, A.: Measurement report: Closure analysis of aerosol–cloud composition in tropical maritime warm convection, Atmos. Chem. Phys., 22, 13269-13302, https://doi.org/10.5194/acp-22-13269-2022, 2022.

Cruz, F., Narisma, G. T., Villafuerte II, M. Q., Chua, K. C., and Olaguera, L. M.: A climatological analysis of the southwest monsoon rainfall in the Philippines, Atmos. Res., 122, 609-616, https://doi.org/10.1016/j.atmosres.2012.06.010, 2013.

Cruz, M. T., Bañaga, P. A., Betito, G., Braun, R. A., Stahl, C., Aghdam, M. A., Cambaliza, M. O., Dadashazar, H., Hilario, M. R., Lorenzo, G. R., Ma, L., MacDonald, A. B., Pabroa, C., Yee, J. R., Simpas, J. B., and Sorooshian, A.: Size-resolved composition and morphology of particulate matter during the southwest monsoon in Metro Manila, Philippines, Atmos. Chem. Phys., 19, 10675–10696, https://doi.org/10.5194/acp-19-10675-2019, 2019.

Cruz, M. T., Simpas, J. B., Sorooshian, A., Betito, G., Cambaliza, M. O. L., Collado, J. T., Eloranta, E. W., Holz, R., Topacio, X. G. V., and Del Socorro, J.: Impacts of regional wind circulations on aerosol pollution and planetary boundary layer structure in Metro Manila, Philippines, Atmos. Environ., 293, 119455, https://doi.org/10.1016/j.atmosenv.2022.119455, 2023.

Deep, A., Pandey, C. P., Nandan, H., Singh, N., Yadav, G., Joshi, P., Purohit, K., and Bhatt, S.: Aerosols optical depth and Ångström exponent over different regions in Garhwal Himalaya,

India, Environmental Monitoring and Assessment, 193, 324, https://doi.org/10.1007/s10661-021-09048-4, 2021.

Di Girolamo, L., Holz, R., Reid, J., Tanelli, S., van den Heever, S., Narsma, G., and Simpas, J.: Cloud and aerosol monsoonal processes-Philippines experiment (CAMP2Ex), NASA White Paper, 2015.

Diner, D. J., Di Girolamo, L., and Nolin, A.: Preface to the MISR special issue, Remote Sens. Environ., 107, 1, https://doi.org/10.1016/j.rse.2006.11.001, 2007.

Dong, X., and Fu, J. S.: Understanding interannual variations of biomass burning from Peninsular Southeast Asia, part II: Variability and different influences in lower and higher atmosphere levels, Atmospheric Environment, 115, 9-18, https://doi.org/10.1016/j.atmosenv.2015.05.052, 2015.

Dorado, S. V., Holdsworth, J. L., Lagrosas, N. C., Villarin, J. R., Narisma, G., Ellis, J., and Perez, R.: Characterization of urban atmosphere of Manila with lidar, filter sampling, and radiosonde, Lidar Remote Sensing for Industry and Environment Monitoring, 2001, 591-598,

Dubovik, O., Holben, B., Kaufman, Y., Yamasoe, M., Smirnov, A., Tanré, D., and Slutsker, I.: Single-scattering albedo of smoke retrieved from the sky radiance and solar transmittance measured from ground, J. Geophys. Res.- Atmos., 103, 31903-31923, https://doi.org/10.1029/98JD02276, 1998.

Dubovik, O., and King, M. D.: A flexible inversion algorithm for retrieval of aerosol optical properties from Sun and sky radiance measurements, J. Geophys. Res.- Atmos., 105, 20673-20696, https://doi.org/10.1029/2000JD900282, 2000.

Dubovik, O., Holben, B., Eck, T. F., Smirnov, A., Kaufman, Y. J., King, M. D., Tanré, D., and Slutsker, I.: Variability of absorption and optical properties of key aerosol types observed in worldwide locations, J. Atmos. Sci., 59, 590-608, https://doi.org/10.1175/1520-0469(2002)059<0590:VOAAOP>2.0.CO;2, 2002.

Eck, T., Holben, B., Reid, J., O'neill, N., Schafer, J., Dubovik, O., Smirnov, A., Yamasoe, M., and Artaxo, P.: High aerosol optical depth biomass burning events: A comparison of optical properties for different source regions, Geophys. Res. Lett., 30, https://doi.org/10.1029/2003GL017861, 2003.

Eck, T., Holben, B., Dubovik, O., Smirnov, A., Goloub, P., Chen, H., Chatenet, B., Gomes, L., Zhang, X. Y., and Tsay, S. C.: Columnar aerosol optical properties at AERONET sites in central eastern Asia and aerosol transport to the tropical mid-Pacific, J. Geophys. Res.- Atmos., 110, https://doi.org/10.1029/2004JD005274, 2005.

Eck, T., Holben, B., Reid, J., Mukelabai, M., Piketh, S., Torres, O., Jethva, H., Hyer, E., Ward, D., and Dubovik, O.: A seasonal trend of single scattering albedo in southern African biomass-burning particles: Implications for satellite products and estimates of emissions for the world's largest biomass-burning source, J. Geophys. Res.- Atmos., 118, 6414-6432, https://doi.org/10.1002/jgrd.50500, 2013.

1307 Eck, T. F., Holben, B., Reid, J., Dubovik, O., Smirnov, A., O'neill, N., Slutsker, I., and Kinne, S.:
1308 Wavelength dependence of the optical depth of biomass burning, urban, and desert dust aerosols,
1309 J. Geophys. Res.- Atmos., 104, 31333-31349, https://doi.org/10.1029/1999JD900923, 1999.

1310 Eck, T. F., Holben, B. N., Reid, J., Giles, D., Rivas, M., Singh, R. P., Tripathi, S., Bruegge, C.,
1311 Platnick, S., and Arnold, G.: Fog-and cloud-induced aerosol modification observed by the
1312 Aerosol Robotic Network (AERONET), J. Geophys. Res.- Atmos., 117,
1313 https://doi.org/10.1029/2011JD016839, 2012.

1314 Ervens, B., Sorooshian, A., Aldhaif, A. M., Shingler, T., Crosbie, E., Ziemba, L., Campuzano-
1315 Jost, P., Jimenez, J. L., and Wisthaler, A.: Is there an aerosol signature of chemical cloud
1316 processing?, Atmos. Chem. Phys., 18, 16099-16119, https://doi.org/10.5194/acp-18-16099-2018,
1317 2018.

1318 Faloona, I.: Sulfur processing in the marine atmospheric boundary layer: A review and critical
1319 assessment of modeling uncertainties, Atmos. Environ., 43, 2841-2854,
1320 https://doi.org/10.1016/j.atmosenv.2009.02.043, 2009.

1321 Feingold, G.: Modeling of the first indirect effect: Analysis of measurement requirements,
1322 Geophys. Res. Lett., 30, https://doi.org/10.1029/2003GL017967, 2003.

1323 Flores, J.: Climate of the Philippines, Climates of the Northern and Eastern Asia, 159-213, 1969.

1324 Formenti, P., Andreae, M. O., and Lelieveld, J.: Measurements of aerosol optical depth above
1325 3570 m asl in the North Atlantic free troposphere: results from ACE-2, Tellus B, 52, 678-693,
1326 https://doi.org/10.1034/j.1600-0889.2000.00006.x, 2000.

1327 Garay, M. J., Bull, M. A., Nastan, A. M., Witek, M. L., Seidel, F. C., Diner, D. J., Kahn, R. A.,
1328 Limbacher, J. A., and Kalashnikova, O. V.: Data Product Specification for the MISR Level 2
1329 Aerosol Product, Jet Propulsion Laboratory, California Institute of Technology. JPL D-100649.
1330 https://asdc.larc.nasa.gov/documents/misr/DPS_AEROSOL_V023.20180125.pdf, 2018.

1331 Gautam, R., Hsu, N. C., Eck, T. F., Holben, B. N., Janjai, S., Jantarach, T., Tsay, S.-C., and Lau,
1332 W. K.: Characterization of aerosols over the Indochina peninsula from satellite-surface
1333 observations during biomass burning pre-monsoon season, Atmos. Environ., 78, 51-59,
1334 https://doi.org/10.1016/j.atmosenv.2012.05.038, 2013.

1335 Gelaro, R., McCarty, W., Suárez, M. J., Todling, R., Molod, A., Takacs, L., Randles, C. A.,
1336 Darmenov, A., Bosilovich, M. G., and Reichle, R.: The modern-era retrospective analysis for
1337 research and applications, version 2 (MERRA-2), J. Climate, 30, 5419-5454,
1338 https://doi.org/10.1175/JCLI-D-16-0758.1, 2017.

1339 Geng, H., Hwang, H., Liu, X., Dong, S., and Ro, C.-U.: Investigation of aged aerosols in size-
1340 resolved Asian dust storm particles transported from Beijing, China, to Incheon, Korea, using
1341 low-Z particle EPMA, Atmos. Chem. Phys., 14, 3307-3323, https://doi.org/10.5194/acp-14-
1342 3307-2014, 2014.

1343   Giles, D. M., Holben, B. N., Eck, T. F., Sinyuk, A., Smirnov, A., Slutsker, I., Dickerson, R.,
1344   Thompson, A., and Schafer, J.: An analysis of AERONET aerosol absorption properties and
1345   classifications representative of aerosol source regions, J. Geophys. Res.- Atmos., 117,
1346   https://doi.org/10.1029/2012JD018127, 2012.

1347   Giles, D. M., Sinyuk, A., Sorokin, M. G., Schafer, J. S., Smirnov, A., Slutsker, I., Eck, T. F.,
1348   Holben, B. N., Lewis, J. R., and Campbell, J. R.: Advancements in the Aerosol Robotic Network
1349   (AERONET) Version 3 database–automated near-real-time quality control algorithm with
1350   improved cloud screening for Sun photometer aerosol optical depth (AOD) measurements,
1351   Atmos. Meas. Tech., 12, 169-209, https://doi.org/10.5194/amt-12-169-2019, 2019.

1352   Glover, D., and Jessup, T.: The Indonesian fires and haze of 1997: the economic toll, Economy
1353   and Environment Program for SE Asia (EEPSEA) Singapore and the World Wildlife Fund
1354   (WWF) Indonesia, Jakarta, 1998.

1355   Guyon, P., Boucher, O., Graham, B., Beck, J., Mayol-Bracero, O. L., Roberts, G. C., Maenhaut,
1356   W., Artaxo, P., and Andreae, M. O.: Refractive index of aerosol particles over the Amazon
1357   tropical forest during LBA-EUSTACH 1999, J. Aerosol Sci., 34, 883-907,
1358   https://doi.org/10.1016/S0021-8502(03)00052-1, 2003.

1359   Hartley, W. S., and Hobbs, P. V.: An aerosol model and aerosol-induced changes in the clear-sky
1360   albedo off the east coast of the United States, J. Geophys. Res.- Atmos., 106, 9733-9748,
1361   https://doi.org/10.1029/2001JD900025, 2001.

1362   Haywood, J., and Boucher, O.: Estimates of the direct and indirect radiative forcing due to
1363   tropospheric aerosols: A review, Rev. Geophys., 38, 513-543,
1364   https://doi.org/10.1029/1999RG000078, 2000.

1365   Hendrickson, B. N., Brooks, S. D., Thornton, D. C., Moore, R. H., Crosbie, E., Ziemba, L. D.,
1366   Carlson, C. A., Baetge, N., Mirrielees, J. A., and Alsante, A. N.: Role of sea surface microlayer
1367   properties in cloud formation, Frontiers in Marine Science, 7, 596225,
1368   https://doi.org/10.3389/fmars.2020.596225, 2021.

1369   Herber, A., Thomason, L. W., Gernandt, H., Leiterer, U., Nagel, D., Schulz, K. H., Kaptur, J.,
1370   Albrecht, T., and Notholt, J.: Continuous day and night aerosol optical depth observations in the
1371   Arctic between 1991 and 1999, J. Geophys. Res.- Atmos., 107, AAC 6-1-AAC 6-13,
1372   https://doi.org/10.1029/2001JD000536, 2002.

1373   Hilario, M. R. A., Cruz, M. T., Bañaga, P. A., Betito, G., Braun, R. A., Stahl, C., Cambaliza, M.
1374   O., Lorenzo, G. R., MacDonald, A. B., AzadiAghdam, M., Pabroa, P. C., Yee, J. R., Simpas, J.
1375   B., and Sorooshian, A.: Characterizing weekly cycles of particulate matter in a coastal megacity:
1376   The importance of a seasonal, size-resolved, and chemically-speciated analysis, J. Geophys.
1377   Res.- Atmos., 125, e2020JD032614, https://doi.org/10.1029/2020JD032614, 2020a.

1378   Hilario, M. R. A., Cruz, M. T., Cambaliza, M. O. L., Reid, J. S., Xian, P., Simpas, J. B.,
1379   Lagrosas, N. D., Uy, S. N. Y., Cliff, S., and Zhao, Y.: Investigating size-segregated sources of

1380 elemental composition of particulate matter in the South China Sea during the 2011 Vasco
1381 cruise, Atmos. Chem. Phys., 20, 1255-1276, https://doi.org/10.5194/acp-20-1255-2020, 2020b.

1382 Hilario, M. R. A., Crosbie, E., Shook, M., Reid, J. S., Cambaliza, M. O. L., Simpas, J. B. B.,
1383 Ziemba, L., DiGangi, J. P., Diskin, G. S., and Nguyen, P.: Measurement report: Long-range
1384 transport patterns into the tropical northwest Pacific during the CAMP 2 Ex aircraft campaign:
1385 chemical composition, size distributions, and the impact of convection, Atmos. Chem. Phys., 21,
1386 3777-3802, https://doi.org/10.5194/acp-21-3777-2021, 2021a.

1387 Hilario, M. R. A., Olaguera, L. M., Narisma, G. T., and Matsumoto, J.: Diurnal characteristics of
1388 summer precipitation over Luzon Island, Philippines, Asia-Pacific Journal of Atmospheric
1389 Sciences, 57, 573-585, https://doi.org/10.1007/s13143-020-00214-1, 2021b.

1390 Hilario, M. R. A., Bañaga, P. A., Betito, G., Braun, R. A., Cambaliza, M. O., Cruz, M. T.,
1391 Lorenzo, G. R., MacDonald, A. B., Pabroa, P. C., and Simpas, J. B.: Stubborn aerosol: why
1392 particulate mass concentrations do not drop during the wet season in Metro Manila, Philippines,
1393 Environmental Science: Atmospheres, 2, 1428-1437, https://doi.org/10.1039/D2EA00073C,
1394 2022.

1395 Hogan, T. F., Liu, M., Ridout, J. A., Peng, M. S., Whitcomb, T. R., Ruston, B. C., Reynolds, C.
1396 A., Eckermann, S. D., Moskaitis, J. R., and Baker, N. L.: The navy global environmental model,
1397 Oceanography, 27, 116-125, https://doi.org/10.5670/oceanog.2014.73, 2014.

1398 Holben, B. N., Eck, T. F., Slutsker, I. a., Tanre, D., Buis, J., Setzer, A., Vermote, E., Reagan, J.
1399 A., Kaufman, Y., and Nakajima, T.: AERONET—A federated instrument network and data
1400 archive for aerosol characterization, Remote Sens. Environ., 66, 1-16,
1401 https://doi.org/10.1016/S0034-4257(98)00031-5, 1998.

1402 Holben, B. N., Tanre, D., Smirnov, A., Eck, T., Slutsker, I., Abuhassan, N., Newcomb, W.,
1403 Schafer, J., Chatenet, B., and Lavenu, F.: An emerging ground-based aerosol climatology:
1404 Aerosol optical depth from AERONET, J. Geophys. Res.- Atmos., 106, 12067-12097,
1405 https://doi.org/10.1029/2001JD900014, 2001.

1406 Hong, Y., and Di Girolamo, L.: Cloud phase characteristics over Southeast Asia from A-Train
1407 satellite observations, Atmos. Chem. Phys., 20, 8267-8291, https://doi.org/10.5194/acp-20-8267-
1408 2020, 2020.

1409 Hong, Y., and Di Girolamo, L.: An overview of aerosol properties in clear and cloudy sky based
1410 on CALIPSO observations, Earth and Space Science, 9, e2022EA002287,
1411 https://doi.org/10.1029/2022EA002287, 2022.

1412 Hoppel, W., Frick, G., Fitzgerald, J., and Larson, R.: Marine boundary layer measurements of
1413 new particle formation and the effects nonprecipitating clouds have on aerosol size distribution,
1414 J. Geophys. Res.- Atmos., 99, 14443-14459, https://doi.org/10.1029/94JD00797, 1994.

1415 Huang, C., Li, J., Sun, W., Chen, Q., Mao, Q.-J., and Yuan, Y.: Long-Term Variation
1416 Assessment of Aerosol Load and Dominant Types over Asia for Air Quality Studies Using

Multi-Sources Aerosol Datasets, Remote Sensing, 13, 3116, https://doi.org/10.3390/rs13163116, 2021.

Hyer, E. J., Reid, J. S., Prins, E. M., Hoffman, J. P., Schmidt, C. C., Miettinen, J. I., and Giglio, L.: Patterns of fire activity over Indonesia and Malaysia from polar and geostationary satellite observations, Atmos. Res., 122, 504-519, https://doi.org/10.1016/j.atmosres.2012.06.011, 2013.

Jamora, J. B., Gudia, S. E. L., Go, A. W., Giduquio, M. B., and Loretero, M. E.: Potential CO2 reduction and cost evaluation in use and transport of coal ash as cement replacement: A case in the Philippines, Waste Manage., 103, 137-145, https://doi.org/10.1016/j.wasman.2019.12.026, 2020.

Jose, S., Gharai, B., Niranjan, K., and Rao, P.: Investigation on seasonal variations of aerosol properties and its influence on radiative effect over an urban location in central India, Atmos. Environ., 133, 41-48, https://doi.org/10.1016/j.atmosenv.2016.03.029, 2016.

Kaskaoutis, D., Kosmopoulos, P., Kambezidis, H., and Nastos, P.: Aerosol climatology and discrimination of different types over Athens, Greece, based on MODIS data, Atmos. Environ., 41, 7315-7329, https://doi.org/10.1016/j.atmosenv.2007.05.017, 2007.

Kaskaoutis, D., Badarinath, K., Kumar Kharol, S., Rani Sharma, A., and Kambezidis, H.: Variations in the aerosol optical properties and types over the tropical urban site of Hyderabad, India, Journal of Geophysical Research: Atmospheres, 114, https://doi.org/10.1029/2009JD012423, 2009.

Kiely, L., Spracklen, D. V., Wiedinmyer, C., Conibear, L., Reddington, C. L., Archer-Nicholls, S., Lowe, D., Arnold, S. R., Knote, C., and Khan, M. F.: New estimate of particulate emissions from Indonesian peat fires in 2015, Atmospheric Chemistry and Physics, 19, 11105-11121, https://doi.org/10.5194/acp-19-11105-2019, 2019.

Kim, J.-S., and Park, K.: Atmospheric aging of Asian dust particles during long range transport, Aerosol Sci. Tech., 46, 913-924, https://doi.org/10.1080/02786826.2012.680984, 2012.

Kirchstetter, T. W., Novakov, T., and Hobbs, P. V.: Evidence that the spectral dependence of light absorption by aerosols is affected by organic carbon, J. Geophys. Res.- Atmos., 109, https://doi.org/10.1029/2004JD004999, 2004.

Koven, C. D., and Fung, I.: Inferring dust composition from wavelength-dependent absorption in Aerosol Robotic Network (AERONET) data, J. Geophys. Res.- Atmos., 111, https://doi.org/10.1029/2005JD006678, 2006.

Kudo, R., Nishizawa, T., and Aoyagi, T.: Vertical profiles of aerosol optical properties and the solar heating rate estimated by combining sky radiometer and lidar measurements, Atmos. Meas. Tech., 9, 3223-3243, https://doi.org/10.5194/amt-9-3223-2016, 2016.

Kumar, K. R., Sivakumar, V., Reddy, R. R., Gopal, K. R., and Adesina, A. J.: Identification and classification of different aerosol types over a subtropical rural site in Mpumalanga, South

1453   Africa: seasonal variations as retrieved from the AERONET Sunphotometer, Aerosol Air Qual.
1454   Res., 14, 108-123, https://doi.org/10.4209/aaqr.2013.03.0079, 2014.

1455   Kumar, K. R., Yin, Y., Sivakumar, V., Kang, N., Yu, X., Diao, Y., Adesina, A. J., and Reddy,
1456   R.: Aerosol climatology and discrimination of aerosol types retrieved from MODIS, MISR and
1457   OMI over Durban (29.88 S, 31.02 E), South Africa, Atmos. Environ., 117, 9-18,
1458   https://doi.org/10.1016/j.atmosenv.2015.06.058, 2015.

1459   Kuttippurath, J., and Raj, S.: Two decades of aerosol observations by AATSR, MISR, MODIS
1460   and MERRA-2 over India and Indian Ocean, Remote Sens. Environ., 257, 112363,
1461   https://doi.org/10.1016/j.rse.2021.112363, 2021.

1462   Lee, H.-H., Iraqui, O., Gu, Y., Yim, S. H.-L., Chulakadabba, A., Tonks, A. Y.-M., Yang, Z., and
1463   Wang, C.: Impacts of air pollutants from fire and non-fire emissions on the regional air quality in
1464   Southeast Asia, Atmos. Chem. Phys., 18, 6141-6156, https://doi.org/10.5194/acp-18-6141-2018,
1465   2018.

1466   Lee, J., Kim, J., Song, C., Kim, S., Chun, Y., Sohn, B., and Holben, B.: Characteristics of aerosol
1467   types from AERONET sunphotometer measurements, Atmospheric Environment, 44, 3110-
1468   3117, https://doi.org/10.1016/j.atmosenv.2010.05.035, 2010.

1469   Li, G., Bei, N., Cao, J., Huang, R., Wu, J., Feng, T., Wang, Y., Liu, S., Zhang, Q., and Tie, X.: A
1470   possible pathway for rapid growth of sulfate during haze days in China, Atmos. Chem. Phys., 17,
1471   3301-3316, https://doi.org/10.5194/acp-17-3301-2017, 2017.

1472   Li, J., Carlson, B. E., and Lacis, A. A.: Application of spectral analysis techniques in the
1473   intercomparison of aerosol data: 1. An EOF approach to analyze the spatial-temporal variability
1474   of aerosol optical depth using multiple remote sensing data sets, J. Geophys. Res.- Atmos., 118,
1475   8640-8648, https://doi.org/10.1002/jgrd.50686, 2013.

1476   Li, Z., Niu, F., Fan, J., Liu, Y., Rosenfeld, D., and Ding, Y.: Long-term impacts of aerosols on
1477   the vertical development of clouds and precipitation, Nat. Geosci., 4, 888-894,
1478   https://doi.org/10.1038/ngeo1313, 2011.

1479   Lin, N.-H., Sayer, A. M., Wang, S.-H., Loftus, A. M., Hsiao, T.-C., Sheu, G.-R., Hsu, N. C.,
1480   Tsay, S.-C., and Chantara, S.: Interactions between biomass-burning aerosols and clouds over
1481   Southeast Asia: Current status, challenges, and perspectives, Environ. Pollut., 195, 292-307,
1482   https://doi.org/10.1016/j.envpol.2014.06.036, 2014.

1483   Lloyd, S.: Least squares quantization in PCM, IEEE T. Inform. Theory, 28, 129-137,
1484   https://doi.org/10.1109/TIT.1982.1056489, 1982.

1485   Lynch, P., Reid, J. S., Westphal, D. L., Zhang, J., Hogan, T. F., Hyer, E. J., Curtis, C. A., Hegg,
1486   D. A., Shi, Y., and Campbell, J. R.: An 11-year global gridded aerosol optical thickness
1487   reanalysis (v1. 0) for atmospheric and climate sciences, Geosci. Model Dev., 9,
1488   https://doi.org/10.5194/gmd-9-1489-2016, 2016.

1489 Matsumoto, J., Olaguera, L. M. P., Nguyen-Le, D., Kubota, H., and Villafuerte, M. Q.:
1490 Climatological seasonal changes of wind and rainfall in the Philippines, Int. J. Climatol., 40,
1491 4843-4857, https://doi.org/10.1002/joc.6492, 2020.

1492 Moosmüller, H., and Sorensen, C.: Small and large particle limits of single scattering albedo for
1493 homogeneous, spherical particles, J. Quant. Spectrosc. Ra., 204, 250-255,
1494 https://doi.org/10.1016/j.jqsrt.2017.09.029, 2018.

1495 Mora, M., Braun, R. A., Shingler, T., and Sorooshian, A.: Analysis of remotely sensed and
1496 surface data of aerosols and meteorology for the Mexico Megalopolis Area between 2003 and
1497 2015, J. Geophys. Res.- Atmos., 122, 8705-8723, https://doi.org/10.1002/2017JD026739, 2017.

1498 Nakata, M., Mukai, S., and Yasumoto, M.: Seasonal and regional characteristics of aerosol
1499 pollution in east and southeast Asia, Frontiers in Environmental Science, 6, 29,
1500 2018 https://doi.org/10.3389/fenvs.2018.00029, 2018.

1501 Fires and Smoke in Borneo: https://earthobservatory.nasa.gov/images/40182/fires-and-smoke-in-
1502 borneo), 2009.

1503 Nguyen, P., Shearer, E. J., Tran, H., Ombadi, M., Hayatbini, N., Palacios, T., Huynh, P.,
1504 Braithwaite, D., Updegraff, G., and Hsu, K.: The CHRS Data Portal, an easily accessible public
1505 repository for PERSIANN global satellite precipitation data, Scientific Data, 6, 1-10,
1506 https://doi.org/10.1038/sdata.2018.296, 2019 2019a.

1507 Nguyen, T. T., Pham, H. V., Lasko, K., Bui, M. T., Laffly, D., Jourdan, A., and Bui, H. Q.:
1508 Spatiotemporal analysis of ground and satellite-based aerosol for air quality assessment in the
1509 Southeast Asia region, Environmental Pollution, 255, 113106,
1510 https://doi.org/10.1016/j.envpol.2019.113106, 2019b.

1511 North, G. R., Bell, T. L., Cahalan, R. F., and Moeng, F. J.: Sampling errors in the estimation of
1512 empirical orthogonal functions, Mon. Weather Rev., 110, 699-706, https://doi.org/10.1175/1520-
1513 0493(1982)110<0699:SEITEO>2.0.CO;2, 1982.

1514 O'Neill, N., Eck, T., Smirnov, A., Holben, B., and Thulasiraman, S.: Spectral discrimination of
1515 coarse and fine mode optical depth, J. Geophys. Res.- Atmos., 108,
1516 https://doi.org/10.1029/2002JD002975, 2003.

1517 Oanh, N. K., Upadhyay, N., Zhuang, Y.-H., Hao, Z.-P., Murthy, D., Lestari, P., Villarin, J.,
1518 Chengchua, K., Co, H., and Dung, N.: Particulate air pollution in six Asian cities: Spatial and
1519 temporal distributions, and associated sources, Atmospheric environment, 40, 3367-3380,
1520 https://doi.org/10.1016/j.atmosenv.2006.01.050, 2006.

1521 Oanh, N. T. K., Permadi, D. A., Hopke, P. K., Smith, K. R., Dong, N. P., and Dang, A. N.:
1522 Annual emissions of air toxics emitted from crop residue open burning in Southeast Asia over
1523 the period of 2010–2015, Atmos. Environ., 187, 163-173,
1524 https://doi.org/10.1016/j.atmosenv.2018.05.061, 2018.

Ong, H. J. J., Lagrosas, N., Uy, S. N., Gacal, G. F. B., Dorado, S., Tobias Jr, V., and Holben, B.:
Determination of Monthly Aerosol Types in Manila Observatory and Notre Dame of Marbel
University from Aerosol Robotic Network (AERONET) measurements, AGU Fall Meeting
Abstracts, 2016, A54E-03,

Pace, G., Sarra, A. d., Meloni, D., Piacentino, S., and Chamard, P.: Aerosol optical properties at
Lampedusa (Central Mediterranean). 1. Influence of transport and identification of different
aerosol types, Atmos. Chem. Phys., 6, 697-713, https://doi.org/10.5194/acp-6-697-2006, 2006.

Pandolfi, M., Alados-Arboledas, L., Alastuey, A., Andrade, M., Angelov, C., Artiñano, B.,
Backman, J., Baltensperger, U., Bonasoni, P., and Bukowiecki, N.: A European aerosol
phenomenology–6: scattering properties of atmospheric aerosol particles from 28 ACTRIS sites,
Atmos. Chem. Phys., 18, 7877-7911, https://doi.org/10.5194/acp-18-7877-2018, 2018.

Petters, M. D., Carrico, C. M., Kreidenweis, S. M., Prenni, A. J., DeMott, P. J., Collett Jr, J. L.,
and Moosmüller, H.: Cloud condensation nucleation activity of biomass burning aerosol, J.
Geophys. Res.- Atmos., 114, https://doi.org/10.1029/2009JD012353, 2009.

Plymale, N. T., Szekely, J. E., and Rubinstein, A. H.: Statistical Cluster Analysis of Global
Aerosol Optical Depth for Simplified Atmospheric Modeling, J. Appl. Meteorol. Clim.,
https://doi.org/10.1175/JAMC-D-21-0150.1, 2021.

PSA: Highlights of the Philippine population 2015 census of population, Philippine Statistics
Authority, 2016.

Qi, Y., Ge, J., and Huang, J.: Spatial and temporal distribution of MODIS and MISR aerosol
optical depth over northern China and comparison with AERONET, Chinese science bulletin,
58, 2497-2506, https://doi.org/10.1007/s11434-013-5678-5, 2013.

Ramage, C. S.: Monsoon meteorology, Academic Press, New York, 1971.

Randles, C., Da Silva, A., Buchard, V., Colarco, P., Darmenov, A., Govindaraju, R., Smirnov,
A., Holben, B., Ferrare, R., and Hair, J.: The MERRA-2 aerosol reanalysis, 1980 onward. Part I:
System description and data assimilation evaluation, J. Climate, 30, 6823-6850,
https://doi.org/10.1175/JCLI-D-16-0609.1, 2017.

Reid, J., Koppmann, R., Eck, T., and Eleuterio, D.: A review of biomass burning emissions part
II: intensive physical properties of biomass burning particles, Atmos. Chem. Phys., 5, 799-825,
https://doi.org/10.5194/acp-5-799-2005, 2005.

Reid, J., Xian, P., Hyer, E., Flatau, M., Ramirez, E., Turk, F., Sampson, C., Zhang, C., Fukada,
E., and Maloney, E.: Multi-scale meteorological conceptual analysis of observed active fire
hotspot activity and smoke optical depth in the Maritime Continent, Atmos. Chem. Phys., 12,
2117, https://doi.org/10.5194/acp-12-2117-2012, 2012.

Reid, J., Maring, H., Narisma, G., van den Heever, S., Di Girolamo, L., Ferrare, R., Holz, R.,
Lawson, P., Mace, G., and Simpas, J.: The coupling between tropical meteorology, aerosol
lifecycle, convection, and radiation, during the Cloud, Aerosol and Monsoon Processes

1562 Philippines Experiment (CAMP 2 Ex), B. Am. Meteorol. Soc., https://doi.org/10.1175/BAMS-
1563 D-21-0285.1, 2023.

1564 Reid, J. S., Hobbs, P. V., Liousse, C., Martins, J. V., Weiss, R. E., and Eck, T. F.: Comparisons
1565 of techniques for measuring shortwave absorption and black carbon content of aerosols from
1566 biomass burning in Brazil, J. Geophys. Res.- Atmos., 103, 32031-32040,
1567 https://doi.org/10.1029/98JD00773, 1998.

1568 Reid, J. S., Hyer, E. J., Johnson, R. S., Holben, B. N., Yokelson, R. J., Zhang, J., Campbell, J. R.,
1569 Christopher, S. A., Di Girolamo, L., and Giglio, L.: Observing and understanding the Southeast
1570 Asian aerosol system by remote sensing: An initial review and analysis for the Seven Southeast
1571 Asian Studies (7SEAS) program, Atmos. Res., 122, 403-468,
1572 https://doi.org/10.1016/j.atmosres.2012.06.005, 2013.

1573 Reid, J. S., Lagrosas, N. D., Jonsson, H. H., Reid, E. A., Sessions, W. R., Simpas, J. B., Uy, S.
1574 N., Boyd, T., Atwood, S. A., and Blake, D. R.: Observations of the temporal variability in
1575 aerosol properties and their relationships to meteorology in the summer monsoonal South China
1576 Sea/East Sea: the scale-dependent role of monsoonal flows, the Madden–Julian Oscillation,
1577 tropical cyclones, squall lines and cold pools, Atmos. Chem. Phys., 15, 1745-1768,
1578 https://doi.org/10.5194/acp-15-1745-2015, 2015.

1579 Rizza, U., Mancinelli, E., Morichetti, M., Passerini, G., and Virgili, S.: Aerosol optical depth of
1580 the main aerosol species over Italian cities based on the NASA/MERRA-2 model reanalysis,
1581 Atmosphere, 10, 709, https://doi.org/10.3390/atmos10110709, 2019.

1582 Rolph, G., Stein, A., and Stunder, B.: Real-time environmental applications and display system:
1583 READY, Environ. Modell. Softw., 95, 210-228, https://doi.org/10.1016/j.envsoft.2017.06.025,
1584 2017.

1585 Ross, J. L., Hobbs, P. V., and Holben, B.: Radiative characteristics of regional hazes dominated
1586 by smoke from biomass burning in Brazil: Closure tests and direct radiative forcing, J. Geophys.
1587 Res.- Atmos., 103, 31925-31941, https://doi.org/10.1029/97JD03677, 1998.

1588 Saleh, R., Hennigan, C., McMeeking, G., Chuang, W., Robinson, E., Coe, H., Donahue, N., and
1589 Robinson, A.: Absorptivity of brown carbon in fresh and photo-chemically aged biomass-
1590 burning emissions, Atmos. Chem. Phys., 13, 7683-7693, https://doi.org/10.5194/acp-13-7683-
1591 2013, 2013.

1592 Schlosser, J. S., Braun, R. A., Bradley, T., Dadashazar, H., MacDonald, A. B., Aldhaif, A. A.,
1593 Aghdam, M. A., Mardi, A. H., Xian, P., and Sorooshian, A.: Analysis of aerosol composition
1594 data for western United States wildfires between 2005 and 2015: Dust emissions, chloride
1595 depletion, and most enhanced aerosol constituents, J. Geophys. Res.- Atmos., 122, 8951-8966,
1596 https://doi.org/10.1002/2017JD026547, 2017.

1597 Schuster, G., Dubovik, O., and Arola, A.: Remote sensing of soot carbon–Part 1: Distinguishing
1598 different absorbing aerosol species, Atmos. Chem. Phys., 16, 1565-1585,
1599 https://doi.org/10.5194/acp-16-1565-2016, 2016.

Schuster, G. L., Dubovik, O., ~~Holben, B. N., and Clothiaux, E. E.: Inferring black carbon content and specific absorption from Aerosol Robotic Network (AERONET) aerosol retrievals, J. Geophys. Res.- Atmos., 110, https://doi.org/10.1029/2004JD004548, 2005.~~
~~Schuster, G. L., Dubovik, O.,~~ and Holben, B. N.: Angstrom exponent and bimodal aerosol size distributions, J. Geophys. Res.- Atmos., 111, https://doi.org/10.1029/2005JD006328, 2006.

Sharma, M., Kaskaoutis, D. G., Singh, R. P., and Singh, S.: Seasonal variability of atmospheric aerosol parameters over Greater Noida using ground sunphotometer observations, Aerosol Air Qual. Res., 14, 608-622, https://doi.org/10.4209/aaqr.2013.06.0219, 2014.

Shen, Z., Liu, J., Horowitz, L., Henze, D., Fan, S., Mauzerall, D. L., Lin, J.-T., and Tao, S.: Analysis of transpacific transport of black carbon during HIPPO-3: implications for black carbon aging, Atmos. Chem. Phys., 14, 6315-6327, https://doi.org/10.5194/acp-14-6315-2014, 2014.

Sinyuk, A., Holben, B. N., Eck, T. F., Giles, D. M., Slutsker, I., Korkin, S., Schafer, J. S., Smirnov, A., Sorokin, M., and Lyapustin, A.: The AERONET Version 3 aerosol retrieval algorithm, associated uncertainties and comparisons to Version 2, Atmospheric Measurement Techniques, 13, 3375-3411, https://doi.org/10.5194/amt-13-3375-2020, 2020.

Smirnov, A., Holben, B. N., Dubovik, O., O'Neill, N. T., Eck, T. F., Westphal, D. L., Goroch, A. K., Pietras, C., and Slutsker, I.: Atmospheric aerosol optical properties in the Persian Gulf, J. Atmos. Sci., 59, 620-634, https://doi.org/10.1175/1520-0469(2002)059<0620:AAOPIT>2.0.CO;2, 2002.

Smith, S. J., Aardenne, J. v., Klimont, Z., Andres, R. J., Volke, A., and Delgado Arias, S.: Anthropogenic sulfur dioxide emissions: 1850–2005, Atmos. Chem. Phys., 11, 1101-1116, https://doi.org/10.5194/acp-11-1101-2011, 2011.

Sorooshian, A., Wang, Z., Feingold, G., and L'Ecuyer, T. S.: A satellite perspective on cloud water to rain water conversion rates and relationships with environmental conditions, J. Geophys. Res.- Atmos., 118, 6643-6650, https://doi.org/10.1002/jgrd.50523, 2013.

Stahl, C., Cruz, M. T., Bañaga, P. A., Betito, G., Braun, R. A., Aghdam, M. A., Cambaliza, M. O., Lorenzo, G. R., MacDonald, A. B., and Hilario, M. R. A.: Sources and characteristics of size-resolved particulate organic acids and methanesulfonate in a coastal megacity: Manila, Philippines, Atmos. Chem. Phys., 20, 15907-15935, https://doi.org/10.5194/acp-20-15907-2020, 2020.

Stahl, C., Crosbie, E., Bañaga, P. A., Betito, G., Braun, R. A., Cainglet, Z. M., Cambaliza, M. O., Cruz, M. T., Dado, J. M., and Hilario, M. R. A.: Total organic carbon and the contribution from speciated organics in cloud water: airborne data analysis from the CAMP 2 Ex field campaign, Atmos. Chem. Phys., 21, 14109-14129, https://doi.org/10.5194/acp-21-14109-2021, 2021.

Stein, A., Draxler, R. R., Rolph, G. D., Stunder, B. J., Cohen, M., and Ngan, F.: NOAA's HYSPLIT atmospheric transport and dispersion modeling system, B. Am. Meteorol. Soc., 96, 2059-2077, https://doi.org/10.1175/BAMS-D-14-00110.1, 2015.

1637 Stevens, B., and Feingold, G.: Untangling aerosol effects on clouds and precipitation in a
1638 buffered system, Nature, 461, 607-613, https://doi.org/10.1038/nature08281, 2009.

1639 Sullivan, R. C., Levy, R. C., da Silva, A. M., and Pryor, S. C.: Developing and diagnosing
1640 climate change indicators of regional aerosol optical properties, Scientific Reports, 7, 1-13,
1641 https://doi.org/10.1038/s41598-017-18402-x, 2017.

1642 Tao, W. K., Chen, J. P., Li, Z., Wang, C., and Zhang, C.: Impact of aerosols on convective
1643 clouds and precipitation, Rev. Geophys., 50, https://doi.org/10.1029/2011RG000369, 2012.

1644 Tsay, S.-C., Hsu, N. C., Lau, W. K.-M., Li, C., Gabriel, P. M., Ji, Q., Holben, B. N., Welton, E.
1645 J., Nguyen, A. X., and Janjai, S.: From BASE-ASIA toward 7-SEAS: A satellite-surface
1646 perspective of boreal spring biomass-burning aerosols and clouds in Southeast Asia,
1647 Atmospheric environment, 78, 20-34, 2013.https://doi.org/10.1016/j.atmosenv.2012.12.013,
1648 2013.

1649 Van Beelen, A., Roelofs, G., Hasekamp, O., Henzing, J., and Röckmann, T.: Estimation of
1650 aerosol water and chemical composition from AERONET Sun–sky radiometer measurements at
1651 Cabauw, the Netherlands, Atmos. Chem. Phys., 14, 5969-5987, https://doi.org/10.5194/acp-14-
1652 5969-2014, 2014.

1653 Wall, C. J., Norris, J. R., Possner, A., McCoy, D. T., McCoy, I. L., and Lutsko, N. J.: Assessing
1654 effective radiative forcing from aerosol–cloud interactions over the global ocean, Proceedings of
1655 the National Academy of Sciences, 119, e2210481119,
1656 https://doi.org/10.1073/pnas.2210481119, 2022.

1657 Wang, L., Lau, K.-H., Fung, C.-H., and Gan, J.-P.: The relative vorticity of ocean surface winds
1658 from the QuikSCAT satellite and its effects on the geneses of tropical cyclones in the South
1659 China Sea, Tellus A, 59, 562-569, https://doi.org/10.1111/j.1600-0870.2007.00249.x, 2007.

1660 Wang, S.-H., Welton, E. J., Holben, B. N., Tsay, S.-C., Lin, N.-H., Giles, D., Stewart, S. A.,
1661 Janjai, S., Nguyen, X. A., and Hsiao, T.-C.: Vertical distribution and columnar optical properties
1662 of springtime biomass-burning aerosols over Northern Indochina during 2014 7-SEAS
1663 campaign, Aerosol and Air Quality Research, 15, 2037-2050,
1664 https://doi.org/10.4209/aaqr.2015.05.0310, 2015.

1665 Wu, M.-c., and Choy, C.-w.: An Observational Study of the Changes in the Intensity and Motion
1666 of Tropical Cyclones crossing Luzon, Tropical Cyclone Research and Review, 4, 95-109,
1667 https://doi.org/10.6057/2015TCRRh3.01, 2016.

1668 Xian, P., Reid, J. S., Atwood, S. A., Johnson, R. S., Hyer, E. J., Westphal, D. L., and Sessions,
1669 W.: Smoke aerosol transport patterns over the Maritime Continent, Atmos. Res., 122, 469-485,
1670 https://doi.org/10.1016/j.atmosres.2012.05.006, 2013.

1671 Xiao, N., Shi, T., Calder, C. A., Munroe, D. K., Berrett, C., Wolfinbarger, S., and Li, D.: Spatial
1672 characteristics of the difference between MISR and MODIS aerosol optical depth retrievals over
1673 mainland Southeast Asia, Remote Sensing of Environment, 113, 1-9,
1674 https://doi.org/10.1016/j.rse.2008.07.011, 2009.

1675 Xie, Y., Li, Z., Zhang, Y., Zhang, Y., Li, D., Li, K., Xu, H., Zhang, Y., Wang, Y., and Chen, X.:
1676 Estimation of atmospheric aerosol composition from ground-based remote sensing
1677 measurements of Sun-sky radiometer, J. Geophys. Res.- Atmos., 122, 498-518,
1678 https://doi.org/10.1002/2016JD025839, 2017.

1679 Yang, S., Lau, W. K., Ji, Z., Dong, W., and Yang, S.: Impacts of radiative effect of pre-monsoon
1680 biomass burning aerosols on atmospheric circulation and rainfall over Southeast Asia and
1681 southern China, Climate Dynamics, 59, 417-432, https://doi.org/10.1007/s00382-021-06135-7,
1682 2022.

1683 Yumul Jr, G. P., Cruz, N. A., Dimalanta, C. B., Servando, N. T., and Hilario, F. D.: The 2007 dry
1684 spell in Luzon (Philippines): its cause, impact and corresponding response measures, Climatic
1685 change, 100, 633-644, https://doi.org/10.1007/s10584-009-9677-0, 2010.

1686 Zhao, G., Di Girolamo, L., Dey, S., Jones, A. L., and Bull, M.: Examination of direct cumulus
1687 contamination on MISR-retrieved aerosol optical depth and angstrom coefficient over ocean,
1688 Geophysical Research Letters, 36, https://doi.org/10.1029/2009GL038549, 2009.

1689 Zhao, G., Zhao, C., Kuang, Y., Bian, Y., Tao, J., Shen, C., and Yu, Y.: Calculating the aerosol
1690 asymmetry factor based on measurements from the humidified nephelometer system, Atmos.
1691 Chem. Phys., 18, 9049-9060, https://doi.org/10.5194/acp-18-9049-2018, 2018.